LBL-26381 c.2

RECEIVED
LAWRENCE
BERKELEY LABORATORY

MAY 17 1989

LIBRARY AND
DOCUMENTS SECTION

Center for Advanced Materials

CAM

Characterization of Nb-Al Superconducting Materials

Y. Im
(Ph.D. Thesis)

December 1988

TWO-WEEK LOAN COPY

This is a Library Circulating Copy which may be borrowed for two weeks.

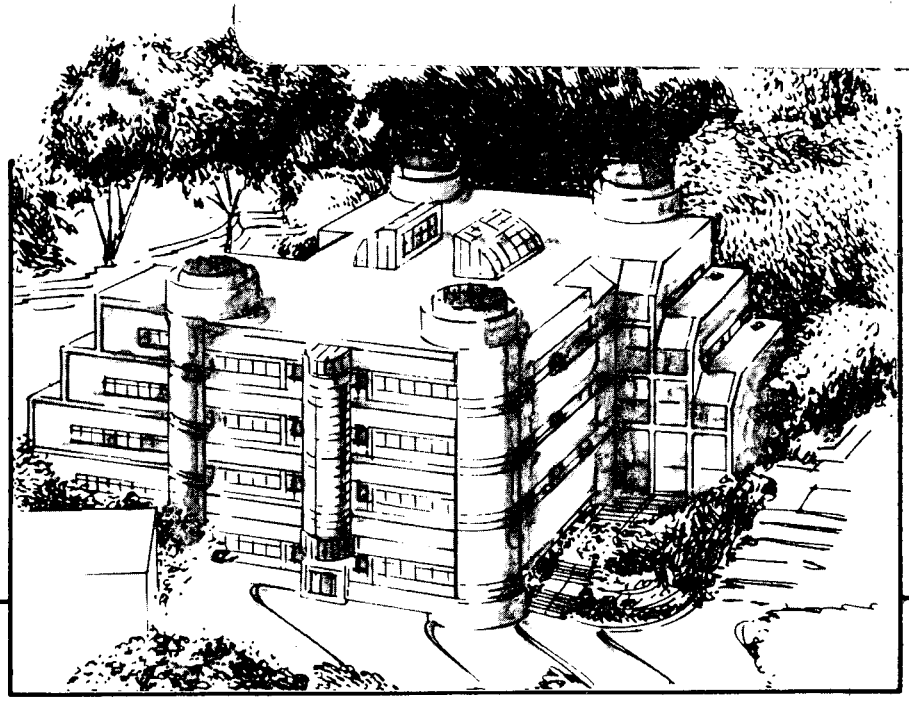

Materials and Chemical Sciences Division

Lawrence Berkeley Laboratory • University of California

ONE CYCLOTRON ROAD, BERKELEY, CA 94720 • (415) 486-4755

Prepared for the U.S. Department of Energy under Contract DE-AC03-76SF00098

LBL-26381 c.2

DISCLAIMER

This document was prepared as an account of work sponsored by the United States Government. While this document is believed to contain correct information, neither the United States Government nor any agency thereof, nor the Regents of the University of California, nor any of their employees, makes any warranty, express or implied, or assumes any legal responsibility for the accuracy, completeness, or usefulness of any information, apparatus, product, or process disclosed, or represents that its use would not infringe privately owned rights. Reference herein to any specific commercial product, process, or service by its trade name, trademark, manufacturer, or otherwise, does not necessarily constitute or imply its endorsement, recommendation, or favoring by the United States Government or any agency thereof, or the Regents of the University of California. The views and opinions of authors expressed herein do not necessarily state or reflect those of the United States Government or any agency thereof or the Regents of the University of California.

LBL 26381

Characterization of Nb-Al Superconducting Material

Yoonsoon Im

Ph.D. Dissertation

Department of Materials Science and Mineral Engineering
University of California at Berkeley

and

Center for Advanced Materials
Materials and Chemical Sciences Division
Lawrence Berkeley Laboratory
1 Cyclotron Road
Berkeley, CA 94720

December 1988

This work is supported by the Director, Office of Energy Research,
Office of Development and Technology, Office of Magnetic Systems, Base Technique
Division of the U. S. Department of Energy under Contract No. *DE-AC03-76SF00098*

Characterization of Nb-Al Superconducting Material

Yoonsoon Im

ABSTRACT

The superconducting A15 phase formation in the Nb/Al binary system was studied in order to provide a systematic approach toward achieving optimum processing conditions for Nb/Al superconducting wires. A series of Nb/Al multi-layered thin-film samples was made to simulate reactions in powder metallurgy (P/M) processed wires while a Nb-Al bulk sample was made by an arc-welding technique to study reactions in the bulk. It was found that the reactions in P/M wires and multi-layered thin-film samples were governed by kinetics while those in the bulk sample were governed by thermodynamics.

Using knowledge about the crystal structures of the reacted compound phases, three reaction controlling mechanisms were proposed to explain the sequence of phase formation in Nb/Al multi-layered samples: the activation energy barrier for nucleation, the energy barrier associated with short range order, and the diffusion barrier controlled mechanism. The proposed reaction mechanisms were consistent with observations in P/M processed wires.

The optimum Al/Nb layer configuration to avoid remaining Nb or Nb_2Al was qualitatively calculated to be 1100Å ~ 1260Å for Nb and 290Å ~ 330Å for Al. The average Nb filament thickness and the critical current densities of various superconducting wires showed good correlation in spite of the differences in processing and the microstructural inhomogeneity. It was shown that the critical current density of a superconducting wire increased by improving its Nb/Al filament distribution.

It is concluded that the critical current density of a Nb/Al superconducting wire can be maximized if Nb and Al filaments are reduced to the optimum thickness range and homogeneously distributed.

ACKNOWLEDGEMENT

This is it! Yes, the moment has come at last. How relieved I am. Yet I feel more apprehensive than ever. I am like a bird whose wings have just become strong enough to fly solo. Now I am leaving the nest where I have learned to unfold my wings and to fly. I am going to miss everyone around me.

A very special thanks to my research advisor, Prof. J. W. Morris, Jr., who so generously helped me physically and mentally throughout my Ph D program. My thanks are extended to Dr. J. Kortright who made sputter-deposited samples for me, and to Mr. J. Holthuis, Mr. P. Ruegg and Mr. J. Wu for technical support. My heart will remember the beautiful friendship I proudly shared with my co-workers.

It was my honor to have Prof. L. DeJonghe, Prof. A. Stacy, Prof. R. Gronsky and Prof. E. Weber as my Qualifying Exam committee. I am indebted to Prof. J. W. Morris, Jr., Prof. A. Stacy and Prof. R. Gronsky for reading my thesis patiently in spite of their busy schedules.

This is a good time for me to thank those who have helped me become what I am now. My parents, brother and sisters have always been the strongest support behind me. Mrs. Agnes Davis Kim has been my spiritual lift. I am thankful of my parents-in-law for trusting me. I would like to share this happy moment with my wife Haesoo who has encouraged me through good and bad days in Berkeley.

This work was supported by the Director, Office of Energy Research, Office of Development and Technology, Office of Magnetic systems, Base Technique Division of the U. S. Department of Energy under contract # *DE-AC03-76SF00098.*

TABLE OF CONTENTS

	Page
I. INTRODUCTION	1
II. BACKGROUND	6
A. Basic Theory:	6
(1) Penetration Depth and Coherence Length	6
(2) Thermodynamics of Superconductivity	7
(3) Ginzberg-Landau Theory	8
(4) The Upper Critical Field	10
(5) Some Results of BCS Theory	12
(6) Theories of Flux Pinning	12
B. Metallurgy of A15 Superconductors:	15
(1) Structure	15
(2) Physical Metallurgy	16
(3) Fabrication of Nb_3Al Superconductors	20
(4) Addition of a Third Element to Nb/Al Material System	21
(5) Thin Film study of Nb_3Al	22
III. OBJECTIVES	24
IV. EXPERIMENTAL APPROACH	26
(1) Powder Metallurgy Processed Wire Samples	26
(2) Multi-layered Samples	26
(3) Bulk Nb-Al Samples	27
A. TEM Sample Preparation	28

Page

(1) Chemical Thinning Technique 28

(2)Mechanical Technique: Dimpling and Ion-milling 30

B. Optical and SEM Sample Preparation 32

C. Indexing Microdiffraction Patterns 32

V. RESULTS 36

A. P/M Processed Wire Samples 36

B. Multi-layered Samples 37

C. Bulk samples 38

VI. DISCUSSION 40

A. Reactions in Bulk Samples 40

B. Reactions in P/M Processed Wire Samples 40

C. Reactions in Multi-layered Samples 41

D. Reaction Controlling Mechanisms in Multi-layered Samples 44

(1) The Activation Energy for Nucleation 44

(2) The Energy Barrier associated with Short Range Order 45

(3) The Diffusion Barrier by the Nb_3Al Layer 46

E. Primary Diffusing Element in Nb_3Al 47

F. Optimum Layer Configuration for Nb_3Al Formation 48

G. Optimum Processing Conditions for Superconducting Wires 49

VII. SUMMARY 51

VIII. CONCLUDING REMARKS 54a

IX. REFERENCES 55

	Page
X. FIGURE CAPTIONS	61
XI. FIGURES	70
XII. APPENDIX	116
A. Computer-generated Microdiffraction Patterns	117
B. The Listing of the Computer Program	120

I. INTRODUCTION

Superconductivity has two distinctive characteristics: the zero electrical resistance and the exclusion of magnetic field inside the superconducting material in its superconducting state. In 1911, Kamerlingh Onnes first discovered the loss of electrical resistance in mercury below some finite but low temperature[1]. A consequence of zero resistivity is that everywhere within a superconductor the electric field E is zero. In 1933 Meissner and Ochsenfeld[2] were able to show that the magnetic induction B was also zero inside the superconducting material. This is known as the Meissner effect.

Superconductivity appears below a temperature that is characteristic of each superconductor; this is called the critical temperature T_c. At T_c, the resistance drops sharply to zero and remains zero at all temperatures below T_c. Almost immediately after the discovery of superconductivity, Onnes found that superconductivity was destroyed by the passage of a transport current density greater than a certain critical value J_c[3] or by the application of an external magnetic field greater than a critical value H_c[4]. These three parameters, T_c, H_c and J_c, are interrelated forming a three-dimensional critical surface, shown schematically in Fig. 1. The critical temperature and the critical magnetic field are characteristic of the material. For a given temperature and field, for instance, the conductor has a definite critical current density $J_c(T,H)$.

Superconductors are divided into two classes called type I and type II. An important difference between the two types is seen in the magnetization curve, a plot of $-4\pi M$, where M is the magnetization inside the superconductor, as a function of the applied magnetic field B_a.

The magnetization curve for type I superconductors is shown in Fig. 2. Consider applying a magnetic field to the superconductor by increasing B from zero to a value B_a

($=H_a$) of magnitude less than the critical field. The result may be viewed as follows. The time-varying magnetic flux induces a surface screening current in the superconductor via Faraday's law. This current persists in the superconductor after the applied field has reached a constant value B_a, and (neglecting demagnetizing effects) produces a field $-B_a$ inside the sample. The induced field $-B_a$ just cancels the applied field B_a, resulting in a net magnetic induction of zero within the superconductor; this is called a complete Meissner effect. When the applied magnetic field exceeds the critical value, the induced field disappears and the material becomes normal.

The second class of superconductors, known as type II, exhibits a magnetization curve of the kind shown in Fig. 3. At values of the applied magnetic field below a value H_{c1}, the specimen (assumed to be a long cylinder parallel to B_a) is superconducting, and magnetic flux is completely excluded. The value H_{c1} is called the lower critical field, and is the value at which flux begins to penetrate the sample. For values of the applied field between Hc1 and the upper critical field H_{c2}, the flux density B is not zero within the superconductor and the Meissner effect is said to be incomplete. The sample is threaded by flux lines and is said to be in the mixed state or the vortex state; this state contains both superconducting and normal regions. Finally, when the applied field exceeds H_{c2}, the sample becomes a normal conductor. All superconductors with critical fields large enough to be of interest for practical applications are of type II.

More than 27 elements and a few thousands alloys and compounds have been found to be superconducting[5]. Metals that are not superconductors are usually either good electrical conductors at normal temperatures, such as the alkali and noble metals, or transition metals with strong magnetic moments. A number of transition-metal dichalcogenides (e.g.,TaS_2, $NbSe_2$) have a crystal structure composed of layers of atoms[17]. These materials have rather low ($T_c \leq 4$ K) critical temperatures, but very high

(about 15 Tesla) values of H_{c2} for magnetic fields oriented parallel to the plane of the layers. The Chevrel phases are compounds of the type $M Mo_6 X_8$, where M is a metal (e.g. Pb,Sn) and X is either S, Sn or Te. A well studied member of this group is $PbMo_6S_8$, with a T_c of 12 ~ 15 K[18]. The critical fields of some Chevrel compounds are approaching 60 Tesla.

Among alloys of the transition metals (Nb-Ti[6], Nb-Zr[7], Mo-Re[8] etc.), $Nb_{38}Ti_{62}$[9] may be presently the most widely used material for magnets. NbTi superconducting wires are flexible enough to be wound into a magnet with a magnetic field up to 8 Tesla. NbN, discovered in 1941[10], has a critical temperature of 15 K and an upper critical field of 15 Tesla. The intermetallic compounds with the A15 structure, such as Nb_3Sn[11], $Nb_3(Al,Ge)$[12],[13], Nb_3Al[14] and Nb_3Ge[15],[16], are thought to be the next generation materials for magnets with critical fields above 8 Tesla because of their excellent superconducting properties.

After many years of search for superconductors with transition temperatures significantly higher than 20 K, a literal explosion of success has occurred in past few years. Beginning with the discovery by Bednorz and Müller[19] of a 30 K transition in $La_{2-x}Ba_xCuO_{4-\delta}$, a rapid series of advances has occurred culminating in recent reports by Wu et al.[20], Chu et al.[21], Tarascon et al.[22] and Zhongxian et al.[23] of an onset temperature greater than 90 K in Y-Ba-Cu-O compounds. In spite of the continuous discovery and improvement of various 'high T_c' oxide superconductors, it is not likely that these compounds will be used for construction of high fields magnets in the near future due to their inherently weak mechanical strength. Superconducting wires made from 'conventional' metallic superconductors can endure the elastic strain caused by the Lorentz force in large magnets; an important consideration for practical devices.

Superconductors are employed in large-scale electrical devices mainly because they can be constructed with extremely high overall current densities[24]. The critical current density of the superconductor itself lies in the range $10^{10} \sim 10^{13}$ A/m^2. These figures are reduced by a factor of up to 10 for the overall current density in the conductor because of the necessity of providing a normal conductor (Al or Cu) for stability, and reinforcement (stainless steel) for mechanical strength. This current density compares very favorably with the maximum allowable current density in force-cooled copper of 2×10^7 A/m^2. These high current densities allow the construction of smaller, lighter, and more compact machines. Compactness is aided by the fact that the lack of power dissipation consequent upon the absence of electrical resistivity reduces the necessity for internal cooling. It is the reduction in size that largely accounts for the economic attractiveness of superconducting machinery, lowering capital, installation, maintenance, and running costs. The reduced power requirements are an added attraction, though they must be balanced against the power consumed by refrigeration.

It is obvious therefore that the most important requirement of a bulk superconductor is that it be able to allow the highest possible current density. Because the superconductor invariably operates in a high-field environment, due to the self-field of the current it is carrying if to nothing else, a high value of the upper critical field H_{c2} is essential. If the conductor is to experience alternating currents, as it will in some of the transmission line proposals, or ripple fields, as may happen in some of the alternator designs, then ac losses must be low. Resistance to radiation damage may be a requirement for superconductors in controlled thermonuclear fusion reactor magnet applications. The superconductor must be mechanically strong and able to withstand forces imposed by current and field (Lorentz forces). It must be stable against flux jumps and sudden changes in current, field, or temperature. It must also be possible to fabricate the conductor in long lengths(i.e. greater

than a few km). This means that at some stage during processing the conductor must be ductile. Commercial availability of the chemical constituents is also important. And finally, the cost must be kept as low as possible.

A15 superconductors, such as Nb_3Sn, Nb_3Al and $Nb_3(Al,Ge)$, are best qualified for these requirements. Among these, Nb_3Sn has been commercialized mainly because it can be relatively easily fabricated into a long multi-filamentary wire. Nb_3Al is another candidate for high field superconductors. It has the A15 structure and an upper critical field of ~30 Teslas at 4.2 K, which is well above the values of the superconductors currently in commercial use: Nb_3Sn (H_{c2} = 24 Teslas), and NbTi (H_{c2} = 19 Teslas).

Nb_3Al has a potential of carrying higher current densities in high magnetic fields than Nb_3Sn and NbTi. The superconducting properties of Nb_3Al are known to be improved by adding Ge, but the effect of Ge addition on the superconducting A15 phase formation is not yet understood. The commercialization of Nb_3Al (or $Nb_3(Al,Ge)$) has been delayed because of difficulty in fabrication and lack of understanding of superconducting phase formation.

II. BACKGROUND

A. Basic Theory

(1) Penetration Depth and Coherence Length

A superconductor exhibits zero resistivity at temperatures below the critical temperature T_c. Even below T_c, however, the application of a sufficiently strong magnetic field (H_c) or strong current density (J_c), will destroy the superconductivity. On cooling below T_c, magnetic flux is expelled from a superconductor (Meissner effect), so that the magnetic induction becomes equal to zero within the superconductor. The magnetic induction does not fall abruptly to zero at the surface of the superconductor, but decreases exponentially over a characteristic distance, the penetration depth λ, from the surface. The London equation[25]

$$\mathbf{J} = \left(\frac{-c}{4\pi\lambda_L^2}\right)\mathbf{A}$$

relates the current density **J** in a superconductor to the magnetic vector potential **A**. The penetration depth λ_L is defined as

$$\lambda_L^2 = \frac{mc^2}{4\pi\rho q^2}$$

$$\{1\}$$

for particles of mass m, charge q, and concentration ρ. The London theory is a "local" theory in that the current density $J_c(r)$ at the point r is determined by $A(r)$, the value of the vector potential at the same point r. For pure metal superconductors, the penetration depth is typically 500Å. The flux is excluded by supercurrents that flow in the penetration layer so as to produce a magnetic field within the superconductor that exactly cancels any externally applied field.

A similar effect occurs within the skin depth of a normally conducting metal when subjected to a changing magnetic field, but once the field is held constant the normal resistance causes the skin depth current to decay. In a superconductor the lack of resistance allows the current to persist, and flux is permanently excluded from the bulk. This, however, is not the complete explanation of the Meissner effect, since flux is excluded whenever a superconductor goes from the normal to the superconducting state by lowering the temperature in a constant applied magnetic field. Herein lies the difference between a superconductor, in which E = B = 0, and a perfect conductor, in which only E = 0.

Pippard[26] argued that an electron traveling from a normal region of a metal into a superconducting region cannot change its wave function from that of the normal state to that of the superconducting state abruptly, but that this change must take place over a distance ξ, the "range of coherence". Pippard estimated that $\xi \approx 1$ μm for pure metals. He then proposed a "nonlocal" variation of the London theory, in which $J_c(r)$ is now determined by the value of A averaged over a sphere of radius ξ centered at *r*. A similar situation exists for normal metals, e.g. in the anomalous skin effect, in which averaging must take place over the normal electron mean free path *l*. In fact, later work on superconductors showed that λ increased and ξ decreased in a superconductor as the normal electron mean free path decreased.

(2) Thermodynamics of Superconductivity

The Gibbs function of a magnetic system is given by

$$G_s(H) = G_s(0) - \mu \int_0^{H_c} M dH$$

For a type I pure metal superconductor, between H = 0 and H = H_c, B = 0 and M = - H. Thus,

$$G_s(h) = G_s(0) + \frac{1}{2}\mu_o H^2$$

In the normal state, ignoring small diamagnetic or paramagnetic effects,

$$G_n(H) = G_n(0)$$

and at H_c, the Gibbs functions of the normal and superconducting states are equal:

$$G_n(0) = G_n(H_c) = G_s(H_c) = G_s(0) + \frac{1}{2}\mu_o H_c^2$$

or

$$\Delta G_{ns} = G_n(0) - G_s(0) = \frac{1}{2}\mu_o H_c^2 \qquad \{2\}$$

The Gibbs function of the superconducting state at zero field is lower than that of the normal state by an amount $\frac{1}{2}\mu_o H_c^2$ per unit volume. This quantity is often referred to as the superconducting condensation energy. In equation {2}, the magnetic properties of the normal state have been ignored, it being assumed that the free energy of the normal state is unaffected by any magnetic field. This assumption is reasonable at low fields since superconductors in the normal state are either diamagnetic or paramagnetic, with very small susceptibilities. These small susceptibilities, however, give rise to a very large effect as the high critical fields, of the order of tens of teslas, found in some type II superconductors are approached.

If the normal state has a susceptibility χ, then in a magnetic field H the Gibbs function per unit volume is changed by $-\frac{1}{2}\chi H^2$. The high-field superconductors are based on transition metal alloys or compounds, with a noneven number of electrons per atom. They will, therefore, be paramagnetic rather than diamagnetic, and their susceptibility χ will be positive. In a magnetic field the Gibbs function of the normal state will be lowered and there will be a field H_p given by

$$\frac{1}{2}\chi H_p^2 = \Delta G_{ns}$$

above which the normal state always has a lower Gibbs function than the superconducting state in zero field. The Gibbs function of the superconducting state increases as a field is

applied, and H_p thus, if it is lower than H_{c2}, represents the maximum field at which superconductivity will persist.

(3) Ginzberg-Landau Theory

The Ginzberg-Landau theory was developed in 1950[27] to give a more adequate description of the behavior of a superconductor in a magnetic field. The normal-to-superconducting transition was thought of as an ordering process, describable in terms of an order parameter ψ. In the normal state, $\psi = 0$; in the superconducting state ψ has a value between 0 and 1. $|\psi|^2$ represents the fraction of conduction electrons that are in the superconducting momentum state, and are described by the single superconducting wave function. In the fully superconducting state $|\psi|^2 = \psi = 1$. In the presence of an externally applied magnetic field, $H_a = B_a / \mu_o$, two extra terms are required. The first represents the energy arising from the work done in expelling the magnetic field from the superconductor. In addition, if there is a spatial variation in ψ within the superconductor, i.e. $\nabla\psi \neq 0$, then the superelectrons are given a momentum $-i\hbar\nabla\psi - e\mathbf{A}\psi$ and an increase in kinetic energy $(1/2m)\,|-i\hbar\,\nabla\psi - 2e\mathbf{A}\psi\,|^2$.

For the case of a superconductor that fills all the space to one side of the x=0 plane, with a magnetic field along the z direction, independent of y and z coordinates, the Ginzberg-Landau equation can be solved to yield

$$A(x) = A(0)\, e^{-x/\lambda}$$

from which

$$B(x) = B_a\, e^{-x/\lambda}$$

where $\lambda = (m/4|\psi|^2\mu_o e^2)^{1/2}$ equal to the London penetration depth.

The Ginzberg-Landau equations also predict the Meissner effect. Ginzberg-Landau introduce a new parameter:

$$\kappa = \lambda/\xi = 2\sqrt{2}\,\lambda^2 e\mu_o H_c/\hbar \qquad \{3\}$$

Superconducting and normal regions can exist side by side in the same piece of metal. This happens, for instance, in a specimen with a nonzero demagnetization coefficient at a field below H_c, when the superconductor breaks up into a mixture of superconducting and normal regions called the intermediate state. An extra energy term must be associated with the boundaries between the normal and superconducting states. This boundary energy, α_{ns} per unit area, can be estimated as follows: imagine two pieces of identical superconductor, each with a large plane boundary, held some distance apart. One is supposed to be in the normal state and penetrated by a magnetic field $H_a < H_c$; the other is in the superconducting state with $H = 0$. The two pieces are brought together so that their plane faces are in contact along the plane x=0. Because ψ cannot change abruptly, but now does so over a distance equal to ξ, this is equivalent to a volume (superconductor area) X ξ becoming normal, and thus there is an increase in energy of $(1/2)\mu_o H_c^2 \xi$ X area. At the same time the magnetic field penetrates into the superconductor over a distance λ, lowering the energy by an amount $(1/2)\mu_o H_a^2$ X area(Fig 4)[24]. The surface energy is therefore

$$\alpha_{ns} = \frac{1}{2}\mu_o(H_c^2\xi - H_a^2\lambda) \qquad \{4\}$$

For pure metals $\xi >> \lambda$, and the equation is often written

$$\alpha_{ns} = \frac{1}{2}\mu_o \Delta H_c^2$$

where $\Delta = 1.89\xi$ for $\kappa << 1$ (i.e., $\xi >> \lambda$) using the Ginzberg-Landau equations. Much more interesting is the result that for $\kappa >> 1$, $\Delta \approx -\lambda$; i.e., the surface energy is negative. The possibility of negative energy also follows from Eq. {4} when $\lambda > \xi$. Since α is positive value of κ at which $\alpha = 0$. This is found, in the Ginzberg-Landau theory, to be when $\kappa = 1/\sqrt{2}$.

(4) The Upper Critical Field

The consequences of a superconductor with $\kappa > 1/\sqrt{2}$ have been considered by Abrikosov[28] in his theoretical paper published in 1957. He showed that for large κ superconductivity could exist up to a field, called the upper critical field, given by

$$H_{c2} = \sqrt{2}\kappa H_c \qquad \{5\}$$

Referring back to Eq. {4}, it can be seen that for $\lambda > \xi$ ($\kappa > 1$), the surface energy is still positive at low values of the external applied field H_a, but goes negative as H_a exceeds $H_c(\xi/\lambda)^{1/2} = H_c/(\kappa)^{1/2}$, a value known as the lower critical field H_{c1}. A more accurate estimate by Abrikosov, for $\kappa >> 1$, is

$$H_{c1} = (H_c/\sqrt{2}\kappa)\ (\ln \kappa + 0.08)$$

Numerical calculations show this to be valid for $\kappa > 20$.

When a superconductor with $\kappa > 1/\sqrt{2}$ is subjected to an externally applied field, it shows a Meissner effect up to H_{c1}. At this field normal regions are nucleated at the surface of the superconductor. The superconductor is now said to be in the mixed state. As the external field is raised, more of these normal regions are nucleated; the induction B within the superconductor rises, until their mutual repulsion makes it increasingly difficult for more normal regions to enter. At some sufficiently high field the normal regions are so densely packed within the superconductor that they begin to overlap and the normal state is achieved. This field is the upper critical field H_{c2} given by Eq. {5}. Provided that the motion of these normal regions is in no way hindered, reduction of the magnetic field allows them to move back out of the superconductor. The magnetization and induction curves, shown in Fig.'s 2 and 3, are reversible. Superconductors that show this behavior, with $\kappa > 1/\sqrt{2}$, are type II, in contrast to type I with $\kappa < 1/\sqrt{2}$.

The normal regions are continuous in the direction parallel to the field since flux must be continuous, and these regions may be thought of as flexible rods of normal material. The flux within one of these normal regions is quantized, as first suggested by

London, into units of the flux quantum $\phi_0 = (h/2e)$ ($=2 \times 10^{-15}$ Wb). It can be shown that the energy of one of these normal regions, or flux lines, is proportional to $\Phi_c^2 = n^2\phi_0^2$, and it is therefore energetically favorable for a multiquanta flux line of $n\phi_0$ to break up into n single-quantum flux lines. The mixed state of a type II superconductor consists of a lattice of single-quantum flux lines. Abrikosov originally postulated a square array; it is now known from both theory and direct observation that the flux-line lattice is a triangular array (Fig. 5) Each flux line may be regarded as having a core of normal electrons, ξ in diameter, the flux quantum being supported by circulating supercurrents that decay over a radius λ from the core (Fig. 6). The magnetic induction in the mixed state B is $n\phi_0$, where n is the area density (number crossing unit area normal to B) of flux lines.

(5) Some results of the BCS Theory

In most superconductors, the attractive interaction between the members of a pair is via the intermediary of a phonon, the quantum of lattice vibration. Superconductors are those materials in which the electron-phonon interaction is strong; it is for this reason that superconductors have lower electrical conductivity in the normal state than most nonsuperconductors since the largest contribution to normal resistivity is from scattering by phonons.

The theory of Bardeen, Cooper and Schriefer (BCS theory) assumes that the interaction potential V is constant and isotropic for all electrons within the Cooper shell and zero for all other electrons. The condensation of electrons into Cooper pairs causes an alteration of the energy levels near the Fermi surface in the superconducting state, leading to an energy gap E_g between the ground state of the superconductor and the lowest excited state (Fig. 7). The energy gap E_g is the binding energy of a Cooper pair in which two electrons occupy states of opposite wave vector and spin. One may show[30] that the energy gap $E_g(0)$ and the gap parameter $\Delta(0)$, both at 0 K, are given by

$$E_g(0) = 2\Delta(0) \approx 3.52\ k_B T_c$$

(6) Theories of Flux Pinning

The most important parameter of a superconductor that is to be used in a magnet of large-scale device is the critical current density J_c. It is the high values of current density that make the employment of superconductors instead of conventional conductors an attractive proposition.

Silsbee[31] hypothesized that the critical current in a type I superconductor is that current which just produces the critical field at the surface of the superconductor. The critical current is reduced by the application of an external field since the field it now has to produce is the difference between the critical field and the applied field. the critical currents of type II superconductors below H_{c1} agree with the Silsbee hypothesis, with H_c replaced by H_{c1}, but above H_{c1} they are much lower than would be expected by inserting H_{c2} in the Silsbee rule, and the variation with an applied field can be quite complicated. For fully reversible type II superconductors the critical current above H_{c1} is practically zero.

Flux lines in the mixed state of a type II superconductor experience a Lorentz force F_L whenever a current flows in the superconductor, given by

$$\mathbf{F}_{L(v)} = \mathbf{J} \times \mathbf{B} \text{ per unit volume of superconductor}$$

where **J** is the current density and **B** the flux density (= $n\,\phi_o$, where n is the number of flux lines per unit area). The force acts in a direction normal to both the flux lines and the current. Unless otherwise prevented, the flux lines will move in the direction of this force, and in so doing induce an electric field $\mathbf{E} = \mathbf{V} \times \mathbf{B}$ where **V** is the velocity of the flux lines; the superconductor now shows an induced resistance whose value approaches that of the normal state resistance as **B** gets close to $\mu_o H_{c2}$.

The critical current is that current which just produces a detectable voltage across the specimen, and is therefore that current which first causes the flux lines to move. If there is no hindrance to the motion of flux lines, then the critical current above H_{c1} is zero and the superconductor is "reversible". It is possible to "pin" flux lines and prevent them from moving by interaction with microstructural features of the material, and a pinning force F_p is exerted on the flux lines that opposes the Lorentz force. The critical current density J_c is determined by the magnitude of the pinning force:

$$J_c \times B = F_{p(v)} \text{ per unit volume}$$

Pinning is due to crystal lattice defects, such as dislocations found in heavily cold-worked materials, grain boundaries, impurities, or precipitates of a second phase. Flux lines interact with pinning centers because the superconducting properties of the latter differ from those of the bulk of the superconductor. The strength of the interaction is related to the magnitude of this difference. Strong pinning materials are metallurgically dirty and by analogy with mechanically strong or magnetically hard materials, irreversible superconductors are called hard superconductors. The critical current is not a property of a particular composition, but of a particular sample of superconductor, and is strongly influenced by the sample's metallurgical history; just as for mechanical strength, its value cannot be predicted with any accuracy.

A problem essential to the proper understanding of flux pinning in practical materials lies in explaining the difference in behavior between the two materials, NbTi and Nb_3Sn, commonly available as commercial superconductors. Both materials have similar values of κ, namely about 20 ~ 40. Their microstructures are on a comparable scale. The cell size in NbTi is in the range 25 ~ 100 nm; the grain size in Nb_3Sn lies in the range 20 ~ 100 nm. In both cases precipitation may be present in the boundaries. Despite these similarities, the flux-pining behavior is very different.

NbTi is a ductile bcc alloy. It is processed by the conventional metallurgical techniques of extrusion and drawing, to fine wire. Pinning is due to dislocation cell structures of subgrain boundaries, reinforced by precipitation of α titanium. The scaling law for the pinning forces is very close to $B_{c2}^2\, b(1-b)$ for a wide range of compositions[32] where b is the reduced induction ($=B/\mu_o H_{c2}$). Nb_3Sn is a brittle intermetallic compound with the A15 crystal structure. Pinning in this material is attributed to grain boundaries, and the pinning strength is inversely proportional to the grain diameter. The scaling law for a wide range of Nb_3Sn materials produced by the bronze process or its variations is very close to $B_{c2}^{5/2}\, b^{1/2}\, (1-b)^2$ [33].

$F_p \propto b(1-b)$, with a maximum at $b = 0.5$, is often said to be indicative of a 'pin-breaking' mechanism because many types of interactions between individual flux lines and strong pinning centers can be shown theoretically to have a field variation of the form b(1-b), and because pins must be broken before flux can move. The shear modulus C_{66} for the flux-line lattice at high fields is $\propto (1-b)^2$ [34][35], and the proportionality $F_p \propto b^{1/2}(1-b)^2$, with a maximum $b = 0.2$, is described as being due to 'pin avoidance' by a flux-lattice shearing mechanism[36]. At high fields, b(1-b) is always larger than $b^{1/2}(1-b)^2$. If the former type of pinning behavior could be induced in Nb_3Sn, with a critical field about twice that of NbTi, this would lead to an extremely valuable advance in magnet design, with superconducting magnets readily producing 20 Tesla[37].

B. Metallurgy of A15 Superconductors

(1) Structure

A15 structure, shown in Fig. 8, is crystallographically classified as the Cr_3Si structure. It has a primitive cubic cell of eight atoms, and belongs to the space group O_h^3-Pm3n. The cubic unit cell has six A atoms at $\frac{1}{4}0\frac{1}{2}$, $\frac{1}{2}\frac{1}{4}0$, $0\frac{1}{2}\frac{1}{4}$, $\frac{3}{4}0\frac{1}{2}$, $\frac{1}{2}\frac{3}{4}0$, $0\frac{1}{2}\frac{3}{4}$; and

two B atoms at 000, $\frac{1}{2}\frac{1}{2}\frac{1}{2}$. The conspicuous feature of the A15 structure is the chains of A atoms parallel to the 3 ⟨100⟩ directions. The interatomic spacing along these chains is 10 ~ 15 % less than the distance of closest approach in a pure A crystal.

At least 46 of the 76 known A15 compounds are superconductors. It generally occurs, with some exceptions, close to the A_3B stoichiometric ratio. The A atoms are group IV-A, V-A and VI-A transition metals Ti, Zr, V, Nb, Ta, Cr, Mo and W; the B atoms come mainly from periodic groups III-B and IV-B, and the precious metals Os, Ir, Pt and Au.

The A15 structure requires that the radius ratio, based on the Goldschmidt CN 12 radii of the constituent atoms, must be close to unity[38]. The tendency of A element to form the A15 phase is found to decrease in the order V, Nb, Cr, Ti, Mo, Zr, Ta, W and Hf. The radius ratio r_A/r_B, expressed in terms of the Goldschmidt CN 12 radii, lies between 0.84 and 1.12, with a most probable value of 0.94. The electron-to-atom ratio (e/a) influences the composition at which the A15 phase is most likely to occur, the most probable values of the ratio being 4.75 or 7.0.

The A15 phases usually exist over a range of composition. The homogeneity range often includes the composition at high temperatures, but falls to the A-rich side at lower temperatures. Several compounds do not form the ideal composition ratio at any temperature range.

(2) Physical Metallurgy

Only 6 of the superconducting A15 compounds are of actual or potential interest as conductors on the basis of their superconducting properties. V_3Si, V_3Ga and Nb_3Sn have a range of homogeneity that includes the stoichiometric A_3B composition. Maximum T_c is readily obtainable in bulk samples of these compounds. Nb_3Al and Nb_3Ga include the ideal stoichiometric composition only at temperatures so high that thermal disorder is

excessive. Nb_3Ge does not exist in equilibrium at the stoichiometric ratio. These last three compounds, all with potentially higher values of T_c and H_{c2} than the first three, normally contain excess Nb and their T_c's are, as a consequence, degraded from the optimum values.

Hanak et al.[39] were the first to suggest that T_c could be affected by long-range crystallographic order (LRO) in the Nb_3Sn compound. Reed et al.[40] suggested that it was most deleterious to have Sn atoms in the Nb sites and that it was important not to disrupt the continuity of chains of Nb atoms along the ⟨100⟩ direction. An extensive determination of the effect of LRO on T_c of 26 binary A15 compounds was carried out by Blaugher et al.[41]. They showed that for compounds in which the B atom is not a transition element, T_c is maximized when all the A atoms are on A sites, all the B atoms are on B sites, and the LRO parameter S† approaches 1. When the B atom is a transition element, the compounds do not have the same sensitivity to ordering. The effects of composition upon T_c can not be unambiguously separated from those of LRO, as it is not possible to have S = 1 unless the composition of the compound corresponds to the ideal 3:1 ratio. S decreases automatically with any departure from stoichiometry.

A third element added to the A15 structure may substitute for the A element, substitute for the B element or form a pseudobinary (a mixture of A_3B and A'_3B') with either A = A' or B = B'. In the typical A15 compounds, the substitution of an A atom by a third element, even one in the same periodic group, invariably results in a decrease in T_c. Thus, once again, the importance of A-chain integrity in conferring a high T_c on the material is highlighted. The substitution of some of the B atoms by a third element is

---

† The positions of the atoms in the unit cell can be described by the Bragg-Williams long range order parameter $S = (P - r) / (1 - r)$, where $0 \leq S \leq 1$, P is the probability of an A site being occupied by an A atom, and r is the fraction of A atoms in the binary alloy.

usually not so deterrent, and may even result in a slight increase in T_c. The addition of a third element may enable a closer approach to perfect stoichiometry or perfect LRO. Neither Nb_3Ge nor Nb_3Al can be formed at the stoichiometric composition in the bulk. However, at compositions close to $Nb_3(Al_{0.8}Ge_{0.2})$, the perfect stoichiometry can be just achieved at high temperatures in the Nb-Al-Ge ternary system. Subsequent heat treatment produces specimens with critical temperatures close to 21 K[12].

The A15 compounds are 'dirty' type II superconductors in that their BCS coherence length ξ_o is very much greater than their normal mean free path l [42]. The upper critical fields of the A15 compounds are a few tens of Teslas. Because of the high fields involved, direct measurement of H_{c2} at temperatures well below T_c is difficult, and $H_{c2}(0)$ is often calculated from other data. Low-field, high-temperature (near to T_c) data can be extrapolated to give $H_{c2}(0)$, as follows

$$H_{c2}(0) = -\,0.693\, T_c \left[\frac{dH_{c2}(T)}{dT} \right]_{T \approx T_c}$$

Using the above equation ignores the possibility of paramagnetic limitation of the upper critical field. If a compound is strongly paramagnetic in the normal state, then superconductivity is unlikely to exist beyond a field $H_p(0)$ given by

$$H_p(0) = 1.84\, T_c$$

For the two vanadium-based compounds V_3Ga and V_3Si and for the ternary $Nb_3(Al_{0,7}Ge_{0.3})$, $H_p(0)$ is less than $H_{c2}(0)$, and these compounds are expected to be paramagnetically limited. For other compounds, $H_p(0)$ is greater than $H_{c2}(0)$ by 2~4 Teslas. The effect of electron spin-flip scattering process is to increase the paramagnetism of the superconducting state and counteract the limiting effect of normal-state paramagnetism.

Little can be done to raise the upper critical field of A15 compounds by the manipulation of the normal-state resistivity. Because of their intrinsic brittleness, they

cannot be deformed as can the ductile alloys. The addition of alloying elements or impurities in sufficient quantities to have significant effect on the normal-state resistivity will almost certainly result in a reduction in T_c. Radiation damage can produce an initial increase in H_{c2} through an increase in the normal-state resistance, but this is ultimately counteracted by the drastic decrease in T_c. It is suggested that T_c is the most important factor in determining H_{c2} and a significant increase in H_{c2} can only be achieved by an increase in T_c[24].

The excellent critical current densities in A15 compound superconductors are attributed to the defects that pin flux lines such as precipitates, grain boundaries, and radiation-induced defects. The effect of precipitates on J_c is not clearly understood. The precipitates themselves may act as flux-pinning centers, or they may cause grain refinement, which gives rise to higher J_c values. Nembach and Tachikawa[43] and Nembach[44] showed that precipitates in V_3Ga and Nb_3Sn refine grain size and increase J_c. J_c is raised when precipitates are introduced into Nb_3Sn. Flux pinning in Nb_3Ge prepared by chemical vapor deposition is attributed to precipitates of the Nb_5Ge_3 phase[45],[46]. It is believed that maximum flux pinning is obtained with precipitates ~ 50Å in diameter at a spacing of ~ 200Å. This is on a finer scale than the most effective grain size, ~ 800Å.

It has been shown that the J_c of Nb_3Sn superconductors increased by grain refinement[47]~[50]. The current density increases linearly with decreasing grain size, reaching a maximum value at a grain diameter ~ 800Å, and then decreases. The microstructure of Nb_3Sn wires are such that the grains are elongated in the direction parallel to the Lorentz force (Fig. 9), resulting in the 'pin avoidance' mechanism with the flux pinning force $F_p \propto b^{1/2}(1-b)^2$. In the case of Nb_3Al, the grains are elongated in the direction normal to the Lorentz force (Fig. 10), making the flux lines more difficult to

shear. It is more likely that, in Nb_3Al, the flux pinning force may be proportional to b(1-b) as in the case of NbTi, which is always larger than $b^{1/2}(1-b)^2$ at high fields.

As with the upper critical field, many of the practices that can be used to enhance J_c in ductile alloys, such as alloying, deformation, and irradiation, cannot be readily applied to the A15 compounds because of the greater degradation of T_c. The compounds must be prepared in such a manner as to give the smallest possible grain size, or to induce a fine dispersion of a second phase, in order to maximize J_c.

(3) Fabrication of Nb_3Al Superconductors

Of the many known superconducting A15 compounds, only two, V_3Ga and Nb_3Sn, have been developed as commercial conductors. The necessity of using high reaction temperatures, combined with the inherent brittleness of the A15 compounds, put severe limitations on the manufacture and use of these conductors. Some of the problems were overcome using the "wind and react" technique; the conductors were first wound into a solenoid and then converted to the A15 superconducting compounds by heat treatment of the entire solenoid. However, these early 'wind and react' A15 wire conductors were unacceptable commercially since they suffered from severe flux jumping and damage during quenching to the normal state.

Toward the latter half of the 1960s it was shown both theoretically and experimentally that flux jumping is absent in superconductors that are less than about 50μm in diameter[51][52]. This work provided the incentive for Kauffman and Pickett[53] (Nb_3Sn) and Tachikawa and Tanaka[54][55] (V_3Ga) to develop a solid state diffusion technique that eventually led to the commercial production of fine-filament A15 conductors. Even though a number of manufacturing techniques[56]-[64] have been developed for laboratory use of commercial application, only powder metallurgical[65],[66] and jelly-roll[67] techniques have been successful for Nb_3Al.

A powder metallurgy (P/M) technique has been widely investigated as a possible processing method of Nb_3Al superconductors[68]-[74]. In this technique, elemental powders of Nb and Al are mixed and compacted into a monel tube, swaged and drawn into a fine wire (Fig. 11). The wire is then heat treated to form the superconducting A15 phase. Since the A15 compound is brittle, only very limited plastic deformation is possible after the phase is formed.

The superconducting properties of P/M processed wires are affected by parameters such as area reduction ratio (R), starting Nb and Al powder size and shape, overall composition and heat treatment conditions. Using larger powder sizes ensures better drawing because of smaller surface-oxidation to volume ratio, but creates less Nb/Al interface for the same reduction ratio, resulting in less A15 phase formation. Because the A15 phase is believed to form only in the vicinity of the Nb/Al interface during heat treatments, the wires are made with extremely high area reductions in order to increase the amount of Nb/Al interface[71][72].

A heat treatment at high temperatures improves the stoichiometry of the A15 phase (higher T_c & H_c) but results in the excessive grain growth (lower J_c). A lower temperature heat treatment has the opposite effect. It has been reported that heat treatments between 900°C ~ 1100°C result in best superconducting properties[71][90]. The long range order of the A15 phase is optimized by an additional annealing heat treatment at 700 ~ 750°C.

The superconducting Nb_3Al is not the only stable phase in the Nb/Al system. The Nb/Al equilibrium phase diagram[75] indicates that Nb_2Al and $NbAl_3$ can also be stable at the reaction temperature range (Fig. 12). Because Nb_2Al, $NbAl_3$ and remaining Nb are not useful superconductors, they reduce the effective cross-section of the superconducting wire, lowering the critical current density.

(4) Addition of a Third Element to Nb/Al Material System

There are three possibilities of thermodynamic stabilities of the A15 phase with respect to other Nb_a-X_b phases ($\frac{a}{b} < 3$) as illustrated in Fig. 13[24]. In the case of Nb-Al system, the tetragonal Nb_2Al phase is more stable than the superconducting Nb_3Al phase. Because the Gibbs free energy ΔG of Nb_2Al is lower than that of Nb_3Al, the composition range of the A15 phase is restricted to the Nb-rich side and the formation of the stoichiometric Nb_3Al is prevented.

Addition of a third element (Si, Ge) creates a miscibility gap between Nb_2Al and Nb_3Al which allows the A15 phase boundary to advance to the stoichiometric composition at the appropriate Al-to-Ge (or Si) ratio. As yet, the factors that influence phase stability are insufficiently understood and thus little progress has been made in achieving the proper processing conditions.

(5)Thin Film Study of Nb_3Al

The A15 superconducting phase is believed to form only in the vicinity of Nb/Al interface. In P/M wires, the Nb and Al powders are drawn into thin filaments forming alternating layers of Nb and Al, which are very inhomogeneously distributed. Therefore, P/M wires are not suitable for studying reactions at the Nb/Al interface. The reactions in the bulk[76]-[78] or thin films made by liquid-quenching[79]-[82], co-sputtering[83] or laser beam irradiation[84][85] technique have been extensively studied, but they do not represent those in the P/M wire. In those samples, the A15 phase forms from the supersaturated bcc Nb-Al solid solution. The reactions at the Nb/Al interface can be better simulated using Nb/Al multi-layered samples with uniform layers of known thickness. Bormann et al. studied the effect of Nb/Al layer thickness on the reactions using multi-layered Nb/Al samples by an X-ray diffraction technique[86]. Since their work was based solely on indirect observations, the results yielded no microstructural information about the reactions.

A transmission electron microscopy study on these multi-layered samples would provide direct information about the reactions at the Nb/Al interface.

III. OBJECTIVES

Magnetically confined plasma fusion reactors will be operated under very high magnetic fields. Superconductors are considered to be more economical than normal conductors mainly because they can be constructed with extremely high current densities. The conductors must be mechanically strong enough to withstand the Lorentz forces at the high fields. The A15 superconductors are best qualified for these requirements.

Among the few A15 superconducting compounds that are of actual or potential interest as high field superconductors, only two, V_3Ga and Nb_3Sn, have been developed commercially. Nb_3Al has been widely studied because of its superior superconducting properties and is considered as one of the candidates to replace Nb_3Sn. Although a substantial amount of processing and property data has been obtained in the past decade, a comprehensive understanding of the processing-microstructure-property relationship for Nb_3Al has been lacking.

Nb_3Al superconducting wires have been made by a powder metallurgical or a jelly-roll technique. The critical current density of a powder metallurgy processed wire is determined by the volume fraction, grain morphology, long range order and stoichiometry of the A15 phase. The stoichiometry, long range order and grain morphology have been extensively studied to obtain the optimum processing conditions.

The critical current density of the wire is also affected by the amount of the superconducting Nb_3Al phase. The microstructure of a reacted P/M wire is composed of three different phases: the superconducting Nb_3Al, the tetragonal Nb_2Al phase and Nb which remained after reaction. It is believed that Nb_3Al forms only at the vicinity of the Nb/Al interface during heat treatments. But the reaction mechanism at the Nb/Al interface

has not been understood. It is not yet known how to suppress the formation of Nb_2Al kinetically by manipulating the microstructure.

It has been known that an addition of third elements (Ge, Si) allows the stoichiometric A15 compound to form at the appropriate Al-to-Ge (or Si) ratio. But, it would be logical to study the relationship of the microstructure and reactions in the binary Nb-Al system before advancing to a ternary system (Nb-Al-Ge, Nb-Al-Si) which is more complicated than the binary one.

The purpose of this research is to develop a systematic approach toward achieving optimum processing conditions for Nb_3Al superconducting wires by understanding reaction mechanisms in the binary Nb-Al system. The fundamental information thus obtained may be used as a stepping stone to more complicated material systems. The relationships between processing, microstructure and properties of the P/M processed Nb/Al wires will also be discussed using various types of samples and techniques.

IV. EXPERIMENTAL APPROACH

Nb/Al superconducting wires made by a powder metallurgy (P/M) technique were used to characterize the microstructures with relation to their superconducting properties and processing conditions. The P/M processed wires, however, are not adequate to monitor reactions at the Nb/Al interface because of their inhomogeneous morphology. Nb/Al multi-layered samples with uniform layers of known thickness and distribution are better for studying reaction mechanisms at the Nb/Al interface. A bulk sample was also made as a reference to compare reactions at the interface with those in the bulk.

(1) Powder Metallurgy Processed Wire Samples

Niobium powders of 65 μm size and aluminum powders of 20 μm size were used. The chemical composition of wires was 3 ~ 5 weight % Al. A set of wire samples was made using 65 μm Nb powders which were coated with 5 weight % Al in total. Various area reduction ratios (R) with the maximum of 10,000 were obtained by stopping drawing at successive stages. The details of wire processing are explained elsewhere[68].

(2) Multi-layered Samples

Two sets of Nb/Al thin film multi-layered samples were made by sputtering Nb and Al alternatively on Nb, Si wafer and quartz substrates. A custom-built magnetron sputtering machine with separate 4' diameter source targets of 99.9% purity Al and Nb were used for the experiment. The basic vacuum of 10^{-7} Torr and an Ar pressure of 0.002 Torr was used. The distance between the sample and the source target was 100 mm. The sputtered thickness ratios of Nb and Al layers were intended to correspond to the proper stoichiometry of the superconducting phase. One set of the thin films was coated with 20

pairs of 300Å Nb/90Å Al layers, and the other with 10 pairs of 1000Å Nb/300Å Al layers. A similar layer configurations were used by Bormann et al. in their X-ray diffraction study[86].

Samples with thicker layers were prepared using a cold-rolling technique. Several Nb plates were polished and cleaned before Al was coated in a vacuum chamber. The thickness of the Al-coat was controlled by varying coating time at constant current. The Al-coated Nb plates were then stacked and cold-rolled into a multi-layered tape or ribbon. This procedure is illustrated in Fig. 14. The whole stack of Nb plates was placed in an Al tube before cold-rolling in order to ensure bonding between Al-coated Nb plates and to protect the sample from oxidation during heat treatments. It was not possible to control the Al thickness precisely in this way, but it was a straightforward method of producing Nb/Al/Nb layers with Al layers of a few hundred Å to several μm thickness.

(3) Bulk Nb-Al Sample

A Nb-Al bulk sample was made by plasma welding Nb and Al plates in a isolated chamber. The chamber was mechanically pumped to 10^{-3} Torr and then a continuous flow of 99.9% Ar gas was introduced during welding. The molten Nb-Al mixture was rapidly solidified on the remaining Nb plate which did not melt during welding, producing a very inhomogeneous morphology and composition gradient throughout the sample.

All samples were heat treated at temperature ranges between 300°C ~ 900°C for various lengths of time in a quartz tube. The quartz tube was first pumped down to 10^{-6} Torr and then back-filled with 99.9% Ar. The samples were characterized using a variety of techniques. X-ray diffractometry, differential scanning calorimetry, optical microscopy, S.E.M. and T.E.M. with the convergent beam micro-diffraction and the

energy dispersive X-ray spectroscopy capabilities were employed to study the microstructures and to identify compounds.

A. TEM Sample Preparation

(1) Chemical Thinning Technique

A special chemical thinning technique was developed to make longitudinal TEM samples of thin wire samples whose diameter was as small as 10 mil (254 μm). A 6 mm-long wire sample was ground down on a 340-mesh abrasive paper until its thickness was less than 2 mil (51 μm). Then the sample was polished on a 600-mesh abrasive paper. A rubber bottle plug served as a good sample holder for grinding the small wire sample. The sample was cut to two pieces and pasted with silver epoxy on a 3 mm Cu disc grid. After the epoxy was hardened at 70°C for several hours, the Cu grid was clamped using a sharp-point tweezer and an enamel coat was applied on both the grid and the tip of the tweezer except for the wire region so that only the sample would be electropolished during chemical thinning (Fig. 15).

A least two different chemical solutions have been suggested for polishing Nb or Nb-based alloys. Kestel[87] developed a jet electropolishing solution, designated BK-1, which was prepared by mixing 500 ml CH_3OH, 100 ml butyl cellosolve, 90 ml H_2SO_4, and 30 ml HF. Schober and Sorajic[88] developed a noncorrosive electrolyte for electropolishing Nb for TEM. They used the electrolyte of 0.05 mol/liter $Mg(ClO_4)_2$ in CH_3OH with the following conditions for best results: (Samples: 3 mm Nb discs, 25 μm thick)

Electrolyte: 0.05 mol/liter $Mg(ClO_4)_2$ in CH_3OH

Voltage: 50 ~ 70 V

Bath temperature: - 5°C

Flow rate: medium

Polishing time: ~ 30 sec.

Total current: ~ 90 mA

Since the wire samples were too small to make a 3 mm disk, the jet polishing solution could not be used. An alternative chemical thinning method was developed for the small wire sample. A beaker containing about 50 ml electrolyte was cooled by iced water while the electrolyte was gently agitated by a magnetic stirrer. A 5 mm x 15 mm fine net made by stainless steel was used for the cathode electrode, and the anode was directly connected to the tweezer which clamped the sample. The chemical thinning apparatus is shown in Fig. 16. The condition which gave best results for small wire samples is described below:

Electrolyte: 0.1 mol/liter $Mg(ClO_4)_2$ in CH_3OH

Voltage: 30 ~ 33 V

Bath temperature: 0°C

Flow rate: slow

Polishing time: 3 ~ 5 sec.

The polishing time was a critical factor: the sample must be quickly removed from the electrolyte as soon as it perforated. A viscous layer formed on the sample surface was easily removed by washing in a running water for 20 seconds and cleaning with CH_3OH. The surface of the electropolished sample was mirror-smooth and an additional ion-mill was not necessary. Finally the enamel coat on the sample was removed by acetone. The stainless steel electrode was regularly cleaned in acetone for a better result. The shelf-life of the $Mg(ClO_4)_2$ solution was at least a few months.

Transverse TEM samples were made using a different technique which is explained in section (B).

(2) Mechanical Technique: Dimpling and Ion-milling

The structure and chemistry of thin films are best studied by TEM when they are viewed in cross-section. A technique for TEM sample preparation that can be viewed in cross-section has been developed for silicon-based materials[89].

Cross-sectional TEM samples of sputtered Nb/Al multi-layered samples were made in a similar way. A sputtered sample sheet was cut into pieces which were 2.2 mm wide and 15 mm long by a diamond saw. Two pieces were then glued together with "Devcon 2-ton epoxy" so that multi-layer sides faced each other. It was critical to minimize the thickness of the glue layer using a small vise in this stage. The "M-Bond 610 Adhesive", used by Bravman et al.[89] for Si-based materials, did not give good results for samples with the Nb substrate because it ion-milled faster than Nb. When the epoxy hardened, the sample was put into a brass tube (2.8 mm ID, 3 mm OD, 20 mm long) and the gap was filled with epoxy. After the epoxy hardened, the tube was sliced into 0.5 mm-thick discs by the diamond saw. As many as 10 ~ 15 discs could be made from one tube. The brass tube (or ring) provided extra strength and safety in handling samples for the following stages. The procedure is illustrated in Fig. 17.

At this point, the process of thinning began. The thinning and the dimpling were done using a dimpler[1]. A sample disc was mounted on a sample holder of the dimpler using "Crystal-Bond[2]" wax which has a good strength and a low melting temperature. The sample was mechanically ground by hand on a 340-grit sand paper until its thickness was approximately 3 mil (100 μm). In order to control the sample thickness, a piece of 3 mil-thick self-adhesive tape was put on near each side of the sample before grinding started: the grinding stopped when the tape started to wear away. The sample was then polished

[1] Dimpler: Model D500 made by VCR Group, San Fransisco, CA 94312
[2] Crystal Bond: Ramco Products, P.O.Box 429 Ossining, NY 10562

flat using a flattening wheel. A well-polished surface was obtained using the "Cyton[3]" solution.

When one side of the sample was polished to the mirror-surface, a 3 mm oval Cu grid was glued on it using the "Devcon 2-ton epoxy". The epoxy was cured at room temperature for 24 hours. Curing at higher temperatures in this stage was not desirable: the viscosity of the epoxy became so low before hardening that the surface tension of the epoxy displaced the Cu disc. After the epoxy was hardened, the sample was removed from the holder on a hot plate. Remaining wax on the sample surface was removed by soaking the sample in acetone. The sample was then remounted on the holder with the polished side down this time.

At this point, the processing of dimpling began. By dimpling, the outer perimeter of the disc remains thick, but the center is thinned with a concave impression. The sample was dimpled until the center was thinner than 20 μm. The dimple-depth measurement by a micrometer gauge attached to the dimpler was not dependable because of a layer of crystal bond wax between the sample and the holder. In this experiment, the dimple-depth was determined by measuring the diameter of the dimple. The conversion between the dimple-depth and the dimple-diameter was plotted on a graph for convenience (Fig. 18). The dimpled surface was polished with the "Cyton" solution. Finally the sample was removed from the holder as explained previously.

Prior to ion milling, the sample was cleaned by soaking in acetone once again. The sample was ion milled from both sides. During milling, the sample was force-cooled by liquid-nitrogen cold-trap. The following milling conditions gave good results:
6 KV, 18°, 1.0 mA until perforation followed by 4 KV, 12°, 0.4 mA for 2 hrs.

[3] Cyton: VCR Group, San Fransisco, CA 94312

The transverse TEM sample of wires were prepared using a similar technique. A 15 mm long wire sample was put into a 3 mm OD brass tube and the gap was filled with epoxy. When the epoxy was hardened, the tube was sliced to 0.5 mm thick discs and ground, dimpled and ion-milled the same way as the multi-layered samples. The same technique was used to make TEM samples out of the bulk Nb-Al material. The bulk was sliced with 0.5 mm thickness by a diamond saw, ground by hand on a sand paper, dimpled and ion-milled.

B. Optical and SEM Sample Preparation

Samples were ground flat by hand on 600-mesh sand paper, and polished on a "Buehler" polishing wheel using 1μm and 0.3 μm Al_2O_3 powder abrasives. When mirror-surface was obtained, the sample was chemically etched to reveal the microstructure. A mixture of HNO_3, HF and/or H_2SO_4 was used as described below.

* Chemical Polishing Solution for Nb-based materials: 2 ~ 3 seconds at 0°C

H_2SO_4	(1.84)	50		HF	(40 %)	20
HNO_3	(1.40)	20	or	HNO_3	(1.40)	20
HF	(40 %)	20		H_2O		20

C. Indexing Microdiffraction Patterns Obtained by TEM

The crystal structures and the lattice constants of Nb_3Al , Nb_2Al and $NbAl_3$ are listed in Table 1.

Table 1.

Compound	Crystal Structure	Lattice Parameters (Å)
Nb	bcc	$a_o=b_o=c_o=3.30$
Al	fcc	$a_o=b_o=c_o=4.049$
Nb_3Al	A15	$a_o=b_o=c_o=5.187$
Nb_2Al	Sigma	$a_o=b_o=9.923$, $c_o=5.171$
$NbAl_3$	$D0_{22}$	$a_o=b_o=3.845$ $c_o=8.601$

In spite of apparent differences in the crystal structures and lattice parameters of these compounds, it was not easy to identify phases by indexing diffraction patterns because of their similar interplanar angles and d_{hkl} values, where d_{hkl} is the interplanar spacing. The d_{hkl}'s for the phases of the Nb-Al system are listed in Table 2.

Table 2.

Nb		Al		Nb_3Al		Nb_2Al		$NbAl_3$	
hkl indices	d_{hkl}	hkl indices	d_{hkl}	hkl indices	d_{hkl}	hkl indices	d_{hkl}	hkl indices	d_{hkl}
110	2.333	111	2.338	110	3.668	101	4.543	002	4.310
200	1.650	200	2.025	200	2.594	210	4.403	101	3.510
211	1.347	220	1.432	210	2.320	111	4.137	110	2.715
220	1.167	113	1.221	211	2.118	220	3.480	112	2.298
310	1.044	222	1.169	220	1.834	211	3.346	103	2.298
222	0.953	400	1.012	310	1.640	310	3.120	004	2.152
321	0.882	133	0.929	222	1.497	301	2.769	200	1.920
400	0.825	420	0.906	320	1.439	320	2.737	202	1.753
				321	1.386	311	2.669	211	1.687
				400	1.297	002	2.571	105	1.573
						400	2.467	213	1.474
						112	2.445	204	1.433
						410	2.397	006	1.433
						330	2.331	220	1.358
						202	2.281	222	1.293
						212	2.222		
						411	2.172		

Procedure of indexing diffraction patterns involves two stages[91]: "(1) the determination of the general {hkl} indices of the spot, that is the combination of h,k and l without definite values and signs; (2) assignment of specific (hkl) indices to the individual spots and the determination of the beam direction **B**". For stage (1), 'camera constant method' was used because the camera constant of the microscope was known. A list of d_{hkl} spacings were obtained by measuring the distance R of the spot from the center spot and dividing the camera constant by R. For stage (2), the closest spot to the center ($h_1k_1l_1$) was arbitrarily indexed for a given combination of h,k and l, and then other spots were indexed so that the indices can be added vectorically, that is

$$h_1 = h_2 + h_3$$

$$k_1 = k_2 + k_3$$

$$l_1 = l_2 + l_3$$

The angles between lines from the center spot to the two spots were also measured and the correct combination of ($h_1k_1l_1$),($h_2k_2l_2$),($h_3k_3l_3$) was confirmed.

These repetitive calculations and comparisons can be systematically performed using a computer. Using the graphic capability of 'Microsoft BASIC' language and an 'Apple Macintosh' personal computer, I developed a computer program which not only calculates d_{hkl}'s and angles but also finds the zone axis of the diffraction pattern of interest. The program can also generate and display the diffraction pattern of given zone axis on the computer screen. Examples of computer generated microdiffraction patterns for Nb_3Al, Nb_2Al and $NbAl_3$ are shown in Appendix A. Using this computer program, indexing diffraction patterns became a routine work which took less than 20 minutes for each pattern. The listing of the program is placed in Appendix B.

V. RESULTS

Variation of heat treatment conditions in an experiment can be minimized if the phase formation temperature ranges are known. A differential scanning calorimeter (D.S.C.) was used for such a purpose in this research. A powder metallurgy processed Nb/Al wire sample was heated with a 20.0°C / min. ramp from 225°C to 725°C where the temperature was held for 5 minutes, while the heat transfer in and out of the sample was monitored. 725°C was the maximum operating temperature of the D.S.C.. Then the sample was furnace-cooled to 225°C and heated back to 725°C with the same 20.0°C / min. ramp, where the temperature was held for 15 minutes. The plot of heat flow vs. temperature/time is shown in Fig. 19. The heat-flow 1 represents the first run and the heat-flow 2 is for the second run. The heat-flow 1 curve shows an exotherm at the temperature range between 300°C and 600°C with its peak at around 550°C. The curve then showed a steep endotherm from 680°C up to 725°C. A large dip in the curve was recorded while holding at the temperature, indicating another exothermic reaction. When the sample underwent the second run, no exotherm was found until about 680°C: a large exothermic reaction was recorded above that temperature.

A. P/M processed wire samples

Fig. 20 is a TEM micrograph of the longitudinal section of an unreacted P/M processed wire with the reduction ratio R = 5000. Nb and Al powders have been drawn down to form thin irregular ribbons or layers. Regions exist where some Nb powders have agglomerated during drawing to form superlayers much wider than the nominal value. In Fig. 20 the Nb layer thickness appears to vary from 250 Å to 2500 Å. The inhomogeneity of Nb layers is better revealed in a transverse TEM micrograph shown in Fig. 21.

Reacted compound phases were identified by both microdiffraction and energy dispersive X-ray spectrometry using TEM. When the wire samples were heat treated below 700°C, the formation of $NbAl_3$ was observed. Fig. 22 shows a TEM micrograph of a wire sample heat treated at 650°C for 2 hrs. The $NbAl_3$ grains were equiaxed and relatively defect-free. Some Nb remained after reaction but Al or Nb-Al solid solution was not detected. The chemical composition of the $NbAl_3$ phase was found to be approximately 75 atomic % Al. A longer heat treatment only resulted in the coarsening of $NbAl_3$ grains (Fig. 23).

Fig. 24 shows a TEM micrograph of a wire sample heat treated at 700°C for 24 hrs. $NbAl_3$ disappeared and elongated Nb_3Al grains are shown as well as some remaining Nb. The tetragonal Nb_2Al phase was also found in the sample. The Nb_3Al phase did not form when the sample was heat treated for a short period of time (<1 hr.) at 700°C. However, the formation of Nb_3Al and Nb_2Al did not require a long reaction time above 700°C.

There were regions with very thick remaining Nb (Fig. 25) or regions with thick superconducting Nb_3Al layers (Fig. 26) in a wire sample heat treated at 900°C for 20 min.. A Nb_3Al / Nb_2Al / Nb_3Al configuration, shown in Fig. 27, was frequently observed in reacted wire samples. The superconducting Nb_3Al grains are relatively defect-free while the Nb_2Al grains are heavily faulted and smaller than Nb_3Al (Fig. 28). The chemical composition of Nb_3Al was measured to be 21 ~ 23 atomic % Al while that of Nb_2Al was 33 ~ 39 atomic % Al.

B. Multi-layered samples

Cross-sectional views of sputtered multi-layered samples were observed using a Philips 400 EM. Fig. 29 shows the uniform thickness and distribution of the multi-layers. When heat treated at 600°C for 100 hrs, both thin and thick multi-layers reacted to form the

$NbAl_3$ phase with the composition being about 75 atom% Al (Fig. 30). The remaining Nb layers contained no measurable Al in solid solution. $NbAl_3$ was found to form at temperatures as low as 300°C. The $NbAl_3$ phase reacted with the remaining Nb to form Nb_3Al after heat treatments above 700°C. Fig. 31 shows the Nb_3Al formation from a 1000Å Nb / 300Å Al multi-layered sample heat treated at 900°C / 20 min. The same result was obtained for thin multi-layered sample. The Nb-Al solid solution and Nb_2Al were reported to form in the thick multi-layered sample by Bormann et al.[86] but were not seen in this work.

Reactions at the Nb/Al interface with thicker Al layers (> 300Å) were studied using the cold-rolled samples. When a multi-layered sample with 630Å thick Al layers were heat treated at 900°C for 20 minutes, a $Nb_3Al/Nb_2Al/Nb_3Al$ layer configuration was found (Fig. 32). The $Nb_3Al/Nb_2Al/Nb_3Al$ layer configuration was frequently found in P/M superconducting wires[72]. When there was a sufficient Al supply, $NbAl_3$ was found regardless of heat treatment conditions as long as both the Nb and Al layers remained. Fig. 33 shows a sample heat treated at 600°C for 100 hrs. Nucleated $NbAl_3$ grains were detached from the Nb/Al interface as they grew larger and new $NbAl_3$ grains grew at the fresh Nb/Al interface. This $NbAl_3$ formation stopped when all Nb was consumed (Fig. 34). When a similar sample was heat treated at 900°C for 20 minutes, neither Nb_3Al or Nb_2Al was found to form: only $NbAl_3$ formed. The $NbAl_3$ layer was found to grow thicker than 100 μm as shown in Fig. 35, even though it was not as porous as that found at lower temperatures.

C. Bulk samples

The Nb-Al bulk sample was composed of two regions of different microstructures. Region I is shown in Fig. 36. A layer of a Nb-Al solid solution grew from the remaining Nb, and a mixture of the solid solution and Nb_3Al was present above it. Transmission

electron microscope study revealed that the Nb_3Al phase nucleated and grew from the Nb-Al solid solution (Fig. 37). The Nb-Al solid solution was highly dislocated and had an Al concentration gradient which was increasing toward the Nb_3Al-solid solution peritectic. The Al solubility in Nb was measured to be 5 ~ 15 atomic % by energy dispersive X-ray spectroscopy on TEM. The chemical composition of the Nb_3Al phase was 21 ~ 23 atomic% Al.

Region II did not contain Nb_3Al or a Nb-Al solid solution. Instead, a layer of Nb_2Al phase grew on the remaining Nb. The Nb_2Al-$NbAl_3$ eutectic structure was found on top of it. A typical microstructure of the region is shown in Fig. 38. A TEM photo of a eutectic of Nb_2Al and $NbAl_3$ is shown in Fig. 39. TEM with microdiffraction and energy dispersive X-ray spectroscopy were used for phase identification. The chemical composition of $NbAl_3$ was about 75 atomic % Al and that of Nb_2Al phase was 33 ~ 39 atomic % Al.

The microstructures for both regions did not change noticeably even after the sample was heat treated at 900°C for 24 hrs.

VI. DISCUSSION

A. Reactions in Bulk Samples

The Nb/Al binary phase diagram[75] indicates that all three compounds (Nb_3Al, Nb_2Al and $NbAl_3$) and the Nb-Al solid solution are thermodynamically stable over a large temperature range. All three compounds and the Nb-Al solid solution were found in the bulk sample made by plasma welding method. The bulk sample contained two regions of different microstructures caused by chemical inhomogeneity.

In region I, Nb and Al solidified as a Nb-Al solid solution on top of the remaining Nb plate. The superconducting Nb_3Al was found to form from the Nb-Al solid solution. The Nb peaks in the X-ray diffraction data were split into two (Fig. 40), indicating the existence of pure Nb and a Nb-Al solid solution. The difference in lattice parameters was 0.01 ~ 0.02 Å, which corresponded to a solid solution of about 10 atomic % Al[92].

In region II, however, columnar grains of Nb_2Al grew from the remaining Nb plate which were followed by the eutectic of Nb_2Al and $NbAl_3$. Nb_3Al or the Nb-Al solid solution was not found in this region. It is believed that the inhomogeneity of the microstructure was caused by a steep chemical composition gradient in the sample: the local chemical composition determines which phases form in a particular region. Since Nb and Al reacted at a very high temperature in the molten state, diffusion was fast enough for the system to reach the thermodynamic equilibrium.

B. Reactions in P/M Processed Wire Samples

In P/M processed Nb/Al wire samples, phase formation was affected by heat treatment temperatures. Only $NbAl_3$ formed by at heat treatment temperature below 700°C while Nb_3Al and Nb_2Al were found after heat treatment above 700°C. Nb-Al solid

solution was not found in any case. The phases formed in the wire samples were studied by combining D.S.C., X-ray diffractometry and TEM.

The first exotherm found below 600°C in the D.S.C. curve is attributed to the formation of $NbAl_3$. Fig. 41 shows the microstructure of a wire sample which suffered from a 20°C / min. heating ramp to 700°C in the D.S.C.. Only $NbAl_3$ was found to form: Nb_3Al, Nb_2Al and Nb-Al solid solution were not found in this sample. The second exotherm detected around 725°C was found to be due to the formation of Nb_3Al and Nb_2Al.

A steep endotherm between 680°C ~ 725°C that appeared in the first run was not understood. The sharp endotherm could be caused either by Ar gas absorption into the sample, by the dissolution of $NbAl_3$ (e.g., formation of a Nb-Al solid solution) before formation of Nb_3Al and/or Nb_2Al, by change in the specific heat of the sample, or by melting of a phase. But none of these were observed experimentally. The specific heat of the sample was not measured in this experiment. Since the formations of Nb_3Al and Nb_2Al could not be separately observed in the wire sample, information about the competition between Nb_3Al and Nb_2Al could not be obtained.

C. Reactions in Multi-layered Samples

It has been believed that reactions in the wires are limited to the vicinity of the Nb/Al interface. The study of reactions at the Nb/Al interface required transmission electron microscopy because of its high spatial resolution. But it was not possible to monitor the reactions in the P/M processed wire samples because of the irregular morphology of Nb/Al interface. Therefore, reactions in the vicinity of Nb/Al interface were studied using Nb/Al multi-layered samples.

Reactions in multi-layered samples were not only affected by heat treatment conditions but also by Nb/Al layer configuration. As summarized in Table 3, different

sequences of phase formation were observed from samples with different layer configurations. Reactions at the interface (or in thin films) have been extensively studied in various material systems such as Ni/Si[93], Co/Si[94], Pd/Al[95], Pt/Al[96], Au/In[97] and Cu/Al[98][99]. A sequence of phase formation has been frequently found from many of these thin film material systems.

Table 3.

	< 650°C	> 700°C	Al layer thickness
Nb + Al	$NbAl_3$	$NbAl_3$	>> 1μm
Nb + Al	$NbAl_3$	Nb_3Al	≤ 300Å
Nb + Al	$NbAl_3$	Nb_3Al+Nb_2Al*	intermediate

* Nb_3Al / Nb_2Al / Nb_3Al Layer Configuration

There have been efforts to predict phase formations in thin films using equilibrium phase diagrams[100]-[102]. Kirkadly[103] argued that a condition of (near-) equilibrium must exist at phase interfaces. Eifert[104] suggested that the interface compositions were essentially time constant although they might not be those predicted by the equilibrium tie-lines. However, formation of amorphous phases during solid state reactions has been observed, which indicates that kinetics is responsible for the early state of reactions[105]-[107]. d'Heurle and Gas[108] divided the reactions in thin films into three categories: diffusion-controlled, nucleation-controlled and reaction-rate-controlled. Gösele and Tu[109] have demonstrated that the competition between interface-controlled and diffusion-controlled phenomena has specific effects on the sequence of phase formation. But no model was successful to predict which compound was kinetically favorable in the competition in nucleation between compounds. Most of the work on thin film reactions concerned the

controlling mechanisms that were related to the growth of *already* nucleated phases rather than the nucleation itself of the phases which formed in sequence.

Gösele and Tu[109] termed the "thin film case" when the thickness of compound layers was on the order of a few hundred to several thousand Å in contrast to the "bulk case" for much thicker diffusion couples with layer thickness above ~ 10μm. In the "thin film case", not all of the compound phases predicted by the equilibrium phase diagram may be present simultaneously. In the case of silicides it is even more common to see only one compound phase between the silicon and the metal.

In the Nb-Al system, only $NbAl_3$ was found in thick (> 1000μm) multi-layered samples regardless of heat treatment conditions. This should belong to the category of the "thin film case" because Nb_3Al and Nb_2Al were missing. Nb-Al thin films (< 100μm) with 25 atomic % Al which were made by rapid quenching[79]-[81] or laser irradiation techniques[84][85], however, contained a mixture of a Nb-Al solid solution and Nb_3Al, which is similar to the region I of the bulk sample. In some silicon-metal diffusion couples with very thick layers, all of the compound phases predicted by the equilibrium phase diagram were found, but they did not form simultaneously but sequentially. Therefore, it is not adequate to distinguish reactions by the thickness of layers.

Meng et al.[110] suggested that differences in the relative ease of nucleation and differences in diffusivities are factors which determine the formation of the particular phases at Ni/Ti and Ni/Zr interface. In the bulk case, on the contrary, diffusion is not a reaction-controlling factor and the reaction would occur in the direction to minimize the Gibbs free energy of the system. Therefore, the criterion between the "thin film case" (or the "interface case") and the "bulk case" should be whether the reactions are governed by kinetics or thermodynamics. Reactions at the interface would be governed by kinetics

while those in the bulk would be governed by thermodynamics. The thickness of layers would only affect the sequence of phase formation in the thin films.

D. Reaction Controlling Mechanisms in Nb/Al Multi-layered Samples

If the reactions in thin films (or at the interface) are controlled by the kinetics, then the atoms at the vicinity of the interface would rearrange themselves to form a phase which is kinetically most favorable rather than thermodynamically most stable. The relative ease of nucleation and diffusion at the interface would be closely related to the crystal structures of the competing phases. Therefore, an effort was made to explain the sequence of phase formations in the Nb/Al thin films using knowledge about the crystal structure of each compound.

The crystal structures of three compound phases in Nb/Al system are illustrated in Fig. 42. $NbAl_3$ has the DO_{22} tetragonal structure and can easily form by substitutionally replacing 2 Al atoms with Nb atoms in 2 fcc Al unit cells. Fig. 42 a) illustrates the structural similarity between $NbAl_3$ and Al. The superconducting Nb_3Al phase has the A15 type cubic structure, with 2 Al atoms at the corners and the center and 2 Nb atoms on each face of the unit cell (Fig. 42 b)). The formation of the A15 structure might be viewed such that the fcc Al is bain-strained into the bcc structure by 6 interstitial Nb atoms in the tetrahedral sites. The Nb_2Al phase has the tetragonal sigma structure, containing 30 atoms in a unit cell as shown in Fig. 42 c).

Using knowledge about the crystal structures of the compound phases, three reaction controlling mechanisms are proposed to explain the reactions at the Nb/Al interface.

(1) The Activation Energy for Nucleation:

For heat treatments below 700°C, $NbAl_3$ formed regardless of holding time at the temperature and Nb/Al layer configuration. This indicates that Nb_3Al and Nb_2Al could not

overcome the activation energy for nucleation at this low temperature. According to the classical nucleation theory, the competition between the volume free energy ΔG and the surface energy σ gives rise to the activation energy for nucleation which is proportional to $\sigma^3/\Delta G^2$. Since the structure of $NbAl_3$ is similar to that of Al, the interfacial free energy between Al and $NbAl_3$ is thought to be very low. Thus the nucleation of $NbAl_3$ at the Nb/Al interface is kinetically favored, and $NbAl_3$ can nucleate at relatively low temperatures (< 700°C) regardless of Nb/Al layer configuration as illustrated in Fig. 43.

(2) The Energy Barrier associated with Short Range Order:

At reaction temperatures above 700°C, reactions were affected by the Al layer thickness provided that there were sufficient Nb supply. The first phase formed was $NbAl_3$ regardless of layer configuration because of the nucleation controlled mechanism. The $NbAl_3$ phase continued to grow as long as both Nb and Al layers remained. Nb_3Al and Nb_2Al were found only after all Al was consumed to form $NbAl_3$.

It is proposed that this stage of the reactions is governed by the energy barrier associated with short range order to form an ordered state. Formation of the $NbAl_3$ phase requires less rearrangement of atoms than that of Nb_3Al. The largest rearrangement of Nb and Al atoms is required to form the Nb_2Al phase whose unit cell is composed of 30 atoms. Therefore, the energy barrier associated with short range order would be smallest for $NbAl_3$ formation, larger for Nb_3Al formation and largest for Nb_2Al formation. Consequently, the kinetically favorable $NbAl_3$ phase will grow continuously as long as both Nb and Al layers remain. When all the Al is consumed to form the $NbAl_3$ phase, the next favorable Nb_3Al will start to form at the remaining Nb/$NbAl_3$ interface (Fig. 44). If the reacted $NbAl_3$ layer is sufficiently thin, all the $NbAl_3$ phase will react with remaining Nb to form the superconducting Nb_3Al phase as observed in the sputter-deposited samples.

(3) The Diffusion Barrier Controlled Mechanism:

When the Al layers were thicker than 300Å but thin enough to be fully consumed to form $NbAl_3$ during heat treatments, Nb_2Al formed between two Nb_3Al phase layers at reaction temperatures above 700°C. The average grain size of Nb_2Al was much smaller than that of Nb_3Al.

Formation of the Nb_2Al phase can be explained by a diffusion-barrier controlled mechanism. Diffusion through the Nb_3Al phase is expected to be very limited because of the strong strain in the A15 structure. Therefore, Nb_3Al grains will grow faster laterally along the Nb/$NbAl_3$ boundaries than to the perpendicular direction. The resulting Nb_3Al grains tend to have elongated shapes. When Nb_3Al grains grow to form a continuous layer, further diffusion is allowed only through the Nb_3Al grain boundaries and further growth of Nb_3Al will slow down. Since $NbAl_3$ is closer to Nb_2Al than to Nb_3Al in chemical composition, the formation of Nb_2Al would require less diffusion than that of Nb_3Al. The diffusion barrier allows the formation of Nb_2Al kinetically favorable over that of Nb_3Al. This sequence of phase formation results in the Nb_3Al / Nb_2Al / Nb_3Al layer configuration as shown in Fig. 45.

It has been observed experimentally that the thickness of a single Nb_3Al layer is about 700Å-800Å regardless of initial Nb/Al layer configuration. Heat treatments of samples with thicker layers only resulted in thicker Nb_2Al layers. If Nb_2Al formed by consuming Nb_3Al and $NbAl_3$, then the thickness of the resultant Nb_3Al layers would be dependent on the thickness of Nb_2Al layers. Therefore we concluded that Nb_3Al phase did not dissolve after it formed. However, it is not yet understood why Nb_3Al does not react with $NbAl_3$ to form the Nb_2Al phase as expected from the Nb/Al equilibrium phase diagram.

In Fig. 46, the Nb_3Al grains already formed a layer of 700Å ~ 800Å thickness and small Nb_2Al grains began to form between Nb_3Al and $NbAl_3$ layers. If the sample was heat treated for a longer period of time, the remaining $NbAl_3$ would be consumed to result in the $Nb_3Al/Nb_2Al/Nb_3Al$ configuration.

E. Primary diffusing element in Nb_3Al

If Nb_3Al does not dissolve once it forms, Nb_2Al must form from the remaining Nb and $NbAl_3$ which are separated by the Nb_3Al layer. There may be two possibilities to continue reactions: either excess Al diffuses out of $NbAl_3$, or Nb diffuses into $NbAl_3$ from the remaining Nb layer. In both cases, diffusion will occur through the Nb_3Al layer. If Al is the primary diffuser in the Nb_3Al layer, then more Nb_3Al will form at the Nb/Nb_3Al interface. This will result in the thickening of the Nb_3Al layer. If, on the contrary, Nb is the primary diffuser in the Nb_3Al layer, then Nb_2Al will grow from the $Nb_3Al/NbAl_3$ interface. In this case, the thickness of the Nb_3Al layer will not be changed during the reaction. Both possibilities are illustrated in Fig. 47.

It has not yet been verified which is the primary diffusing element in the Nb_3Al phase. Until present time, Al has been regarded as the primary diffusing element[86][111] in the formation of Nb_3Al. But the observation that the Nb_3Al layers do not grow more than a certain thickness is an indirect evidence that Nb is the primary diffusing element in Nb_3Al. This is a rather unexpected result since Al is the primary diffusing element in many material systems[112][113].

Maas et. al.[112] showed that Al is the primary diffusing element in the formation of $NbAl_3$. Colgan and Mayer[113] found that Al was the dominant moving element for the growth of many Al-rich compound phases while Ni was the dominant moving element for the growth of the Ni-rich phase, Ni_3Al. It has been suggested that the species the compound is richer in is likely to be the dominant diffusing element because there is a

higher probability of a continuous sublattice of that species to exchange with[113][114]. Exchanges between different atomic species are less likely because of the disorder produced and increase in energy involved.

In the Nb/Sn system, Sn is the primary diffusing element in the Nb_3Sn superconducting phase. In this case, the A15 (Nb_3Sn) layer continuously grows at the Nb/Nb_3Sn interface by the grain boundary diffusion of Sn through the A15 layer without forming a Nb-depleted phase as in Nb/Al system[115][116]. Further investigation is required before a conclusion can be reached.

F. Optimum layer configuration for Nb_3Al formation

The critical current density of the Nb/Al superconductor will be improved if the volume fraction of the superconducting Nb_3Al phase is maximized by avoiding Nb_2Al and excess Nb. It has been shown that Nb_3Al layers do not grow more than a certain thickness in multi-layered samples. Any remaining Nb and $NbAl_3$ would be used to form the non-superconducting Nb_2Al. The unwanted phases, remaining Nb and Nb_2Al, can be avoided only if the Nb/Al layers have an appropriate configuration.

The optimum layer configuration is qualitatively calculated as follows. The average thickness of Nb_3Al layers is about 700Å ~ 800Å. Assuming the chemical composition of Nb_3Al is approximately 22 atomic % Al, a 550Å~ 630Å thick Nb layer and a 145Å ~ 165Å thick Al layer would react to form a 700Å ~ 800Å thick Nb_3Al layer. Since each Al (or Nb) layer in the multi-layered sample has a pair of Nb/Al interfaces, the optimum layer thickness to avoid remaining Nb and Nb_2Al becomes 1100Å ~ 1260Å for Nb and 290Å ~ 330Å for Al. If Nb layers were thicker than this optimum value, some Nb would remain after heat treatments. If Al layers were thicker than this optimum value, Nb_2Al would form between Nb_3Al layers.

G. Optimum processing conditions for superconducting wires

The proposed reaction mechanisms are consistent with observations in powder metallurgy processed Nb/Al superconducting wires:

1] $NbAl_3$ forms below 650°C while Nb_3Al and Nb_2Al form above 700°C.

2] The $Nb_3Al/Nb_2Al/Nb_3Al$ configuration is observed.

3] Nb-Al solid solution is not observed.

4] A high reduction ratio (ie. thinner Al layers) yields more Nb_3Al.

Therefore we concluded that reactions in the P/M processed Nb/Al superconducting wires were successfully simulated by the Nb/Al multi-layered samples.

The calculated optimum Nb/Al layer thickness may be qualitatively used to estimate the volume fraction of Nb_3Al phase in Nb/Al superconducting wires. The average thickness of filaments (T_{Nb} or T_{Al}) was calculated by the following equation[68].

$$T_{Nb,Al} = \frac{\text{(Nb,Al powder size)}}{\text{(reduction ratio)}^{1/2}}$$

King et al.[71] made a series of P/M processed wires using 75μm ~ 100μm Nb and < 5μm Al powders. For the reduction ratio of $R = 10^5$, the average thickness of Nb filaments (T_{Nb}) was calculated to be 2370Å ~ 3160Å and that of Al (T_{Al}) < ~ 160Å. Almost 50% of Nb was expected to be either remained after heat treatments or inefficiently consumed to form Nb_2Al. In fact, 1000Å ~ 2000Å thick Nb layers were observed in their wire sample. Thieme et al.[117] showed that the critical current density of their wire samples increased nearly proportionally as the reduction ratio increased to $R = 1.8 \times 10^5$ and to $R = 3.4 \times 10^5$. For $R = 1.8 \times 10^5$, T_{Nb} was calculated to be 1770Å ~ 2360Å and T_{Al} < ~ 120Å. And for $R = 3.4 \times 10^5$, T_{Nb} was calculated to be 1290Å ~ 1720Å and T_{Al} < ~ 85Å. If the P/M processed wires had a homogeneous microstructure, the formation of Nb_2Al would be avoided with T_{Al} < 290Å ~ 330Å. However, 2500Å ~ 1μm thick Nb_2Al layers were

observed in the wires whose T_{Al} was only 160Å[71]. It is believed that the formation of Nb_2Al was caused by an inhomogeneous distribution of Nb/Al filaments.

Bruzzere et al.[118] obtained a high critical current density from Nb/Al single-core superconducting wires produced by a jelly-roll technique. They obtained T_{Nb} of 1400Å with R = 1.9 x 10^4. They reported that the J_c was greatly improved when T_{Al} decreased from ≥ 2000Å to 350Å. In spite of the relatively low reduction ratio, their J_c value (1.8 x 10^5 A/cm^2 at 4.2 K and 11 Tesla) was comparable to those with much higher R's as shown in Fig. 48. It is calculated that the optimum layer thickness may be achieved by a reduction ratio of R = 2.5 x 10^4 ~ 3.3 x 10^4 if 20μm Nb and 4.9μm Al foils are used as starting materials.

The jelly-roll technique has an advantage over the P/M process in the distribution of Nb/Al filaments. An attempt was made to demonstrate the effect of the distribution of Nb/Al filaments in P/M processed wires. A series of wires was made using 65 μm Nb powders which were precoated with Al by evaporation in order to improve the distribution of Nb/Al filaments. The amount of Al-coat was measured to be 5 weight % of the total weight of the powders. Johnson[68] showed that the critical current density of the Al-precoated P/M wire sample was approximately 15 % superior to that of a reference P/M wire sample which was made using 65μm Nb powders and 20μm Al powders of 5 weight %. It was suspected that the difference in J_c's of two wires would be more apparent if the wires were further reduced.

From the results of multi-layered samples and analysis of various superconducting wires, it was concluded that the volume fraction of the superconducting Nb_3Al phase may be maximized if Nb and Al filaments are homogeneously distributed and as thin as the optimum thickness.

VII. SUMMARY

Reaction mechanisms in the Nb-Al binary system were studied in order to provide a systematic approach toward achieving optimum processing conditions for Nb_3Al superconducting wires. The relationships between processing, microstructure and properties of the P/M processed Nb/Al wires were also discussed using experimental results from various types of samples and techniques.

Not only powder metallurgy processed superconducting wires but also various multi-layered samples and bulk samples were studied using conventional and analytical electron microscopy, X-ray diffractometry and differential scanning calorimetry. TEM sample preparation techniques were developed for P/M processed wires and the cross-section of multi-layered thin films. The reacted phases were identified by energy dispersive X-ray spectroscopy and microdiffraction using a convergent electron-beam probe. A computer program was developed specifically for indexing microdiffraction patterns of Nb-Al compound phases.

The bulk sample made by plasma welding method contained all three compound phases (Nb_3Al, Nb_2Al and $NbAl_3$) and the Nb-Al solid solution as predicted from the Nb/Al equilibrium phase diagram. Since reactions occurred in the molten state (high temperature), diffusion was fast enough for the system to reach the thermodynamic equilibrium.

In P/M processed Nb/Al wire samples, phase formations were affected by heat treatment temperatures. Phase formation temperatures were studied using D.S.C., X-ray diffractometry and TEM. Only $NbAl_3$ formed by a heat treatment below 700°C while Nb_3Al and Nb_2Al were found by a heat treatment above 700°C. Nb-Al solid solution was not found in any cases. Since the formations of Nb_3Al and Nb_2Al could not be separately

observed in wire samples, information about the competition between Nb_3Al and Nb_2Al could not be obtained.

Since P/M processed wire samples had an inhomogeneous filament morphology, reactions at the Nb/Al interface were studied using Nb/Al multi-layered samples. Reactions in multi-layered samples were not only affected by heat treatment conditions but also by Nb/Al layer configuration. It was found that phase formation occurred in sequence, which was frequently observed in many other thin-film material systems. It is suggested that the term "thin film case" should be used when reactions are governed by kinetics in contrast to the "bulk case" which is governed by thermodynamics, regardless of film thickness.

Using knowledge about the crystal structures of each compound phase, three reaction controlling mechanisms were proposed to explain the sequence of phase formation in Nb/Al multi-layered samples. At lower temperatures (<700°C), *the activation energy barrier for nucleation* allows the formation of $NbAl_3$ only regardless of layer configuration. At higher temperatures (>700°C), reaction is governed by *the energy barrier associated with short range order* to form an ordered state. Since the formation of Nb_3Al requires more rearrangement of atoms than that of $NbAl_3$, the Nb_3Al phase will not form until $NbAl_3$ formation is completed by exhausting Al supply. Nb_2Al requires the most arrangement of atoms to form, and does not form until the Nb_3Al blocks further diffusion by forming a continuous layer at the Nb/$NbAl_3$ interface. *The diffusion barrier* allows the formation of Nb_2Al kinetically favorable over Nb_3Al since Nb_2Al requires less Nb diffusion to form than that of Nb_3Al. Since the thickness of a single Nb_3Al layer was independent of Nb_2Al layer thickness, it was concluded that Nb_3Al did not dissolve during Nb_2Al formation.

Two possibilities of reactions between Nb and $NbAl_3$ were discussed: either excess Al diffused out of $NbAl_3$ or the remaining Nb diffused into $NbAl_3$. If Al was the primary diffuser, more Nb_3Al would form at the Nb/Nb_3Al interface. If Nb was the primary diffusing element, Nb_2Al would form at the $Nb_3Al/NbAl_3$ interface. The observation that the thickness of a single Nb_3Al layer was constant indicated that Nb might be the primary diffusing element in Nb_3Al, but it was not verified experimentally.

Since Nb_3Al layers did not grow more than 700Å ~ 800Å, any excess Nb and Al would either remain or form Nb_2Al after reaction. The optimum Al/Nb layer configuration to avoid remaining Nb or Nb_2Al was qualitatively calculated to be 1100Å ~ 1260Å for Nb and 290Å ~ 330Å for Al. If Nb layers were thicker than this optimum value, some Nb would remain after heat treatments. If Al layers were thicker than this optimum value, Nb_2Al would form between Nb_3Al layers.

The proposed reaction mechanisms for the multi-layered samples were consistent with observations in P/M processed wires. Therefore it was concluded that reactions in the P/M processed Nb/Al superconducting wires were successfully simulated by the Nb/Al multi-layered samples. Average filament thicknesses (T_{Nb} and T_{Al}) of various superconducting wires were calculated and compared with the optimum Nb/Al layer thickness for multi-layered samples in order to estimate the volume fraction of Nb_3Al phase in the wires qualitatively. The T_{Nb}'s and the critical current densities of the superconducting wires showed a good correlation in spite of the microstructural inhomogeneity.

The effect of the distribution of Nb/Al filaments on the critical current densities of P/M processed superconducting wires were demonstrated by comparing two sets of wires of different filament distribution. It is concluded that the critical current density of a Nb/Al

superconducting wire can be maximized if Nb and Al filaments are reduced to the optimum thickness range and homogeneously distributed.

VIII. CONCLUDING REMARKS

More than 2 hrs of heat treatment was required before Nb_3Al formed in a P/M processed wire sample at 700°C. For heat treatments above 800°C, it took less than 30 min to form Nb_3Al. If the time required to form Nb_3Al at various temperatures is measured, one may get qualitative thermodynamic data on the nucleation of Nb_3Al.

An interesting question is whether Nb_3Al (and/or Nb_2Al) will grow or dissolve at a temperature lower than 700°C if the phase is allowed to nucleate at a higher temperature (>700°C) and then cooled down to the low temperature. The phase will dissolve if it is thermodynamically unstable at the low temperature and the Nb/Al phase diagram must be modified accordingly. The difficulty of finding the heat treatment condition for nucleation of Nb_3Al may be overcome by using the D.S.C..

It has been reported that the Nb_3Al phase formation is affected by the presence of oxygen. It is inevitable that some oxygen is introduced into the P/M processed wires from the surface of Nb/Al powders. The multi-layered samples made by cold-rolling technique should also contain oxygen in the vicinity of the Nb/Al interface. Therefore I believe that the reactions in the P/M processed wires might be better simulated by the cold-rolled samples than the sputtered multi-layered samples. If one could make two sets of multi-layered samples with different oxygen content, then the affect of oxygen on the reactions at the Nb/Al interface could be investigated more precisely.

The effect of third element addition was not studied in this project partly because of the difficulties of sample preparation. Since Ge and Si are inherently brittle, samples containing elemental Ge or Si powders could not be plastically deformed successfully. The ternary multi-layered samples may be made by sputtering technique using Al-Ge eutectic alloy as a source target. The eutectic Al-Ge alloy has already been made. It is

expected that knowledge obtained from the binary Nb/Al system may be used to understand the effect of Ge or Si addition on the reactions at the Nb/Al(Ge or Si) interface.

IX. REFERENCES

1. H. K. Onnes, *Commun. Phys. Lab. Univ. Leiden* Nos. 119b, 120b, 122b (1911)

2. W. Meissner and R. Ochenfeld, *Naturwissenschaften* **21**, 787 (1933)

3. H. K. Onnes, *Commun. Phys. Lab. Univ. Leiden Suppl.* **34** No. 133d (1913)

4. H. K. Onnes, *Commun. Phys. Lab. Univ. Leiden* No. 139f (1914)

5. B. W. Roberts, *J. phys. Chem. Ref. Data* **5**, 581 (1976); B. W. Roberts, *Natl. Bur. Stand. (U.S.) Tech. Note* 983 (1978)

6. J. E. Kunzler, *Rev. Mod. Phys.* **33**, 501 (1961)

7. B. T. Matthias, *Phys. Rev.* **92**, 874 (1953)

8. J. E. Kunzler, E. Buehler, F. S. Hsu, B. T. Matthias and C. Wahl, *J. Appl. Phys.* **32**, 325 (1961)

9. T. H. Geballe and M. R. Beasley, *Mat. Sci. Energy Tech.* edited by G. G. Libowitz and M. S. Wittingham, Chap. 10 (1979)

10. G. Ascherman, E. Frederik, E. Just and J. Kramer, *Phys. Z.* **42**, 349 (1941)

11. B. T. Matthias, T. H. Geballe, S. Geller and E. Corenzwit, *Phys. Rev.* **95**, 1435 (1954)

12. B. T. Matthias, et al., *Science* **156**, 645 (1967)

13. G. Arrhenius et. al., *Proc. Natl. Acad. Sci. U. S. A.* **61**, 261, (1968)

14. P. R. Sahm and T. V. Pruss, *Phys. Lett.* **23A**, 707 (1969)

15. J. R. Gavaler, *Appl. Phys. Lett.* **23**, 480 (1973)

16. L.R. Testardi, J. H. Warnick and W. A. Royer, *Solid State Commun.* **15**, 1 (1974)

17. R. Dalven, *Am. J. Phys.* **52**, 11 (1984)

18. S. Foner, E. J. McNiff, Jr., and E. J. Alexander, *Appl. Supercon. Conf., Oakbrook* 1974; *IEEE Trans. on Mag.* **Mag-11**, 155 (1975)

19. J. G. Bednorz and K. A. Müller, *Z. Phys.* **B64**, 189 (1986)

20. M. K. Wu, J. R. Ashburn, C. J. Torng, P. H. Hor, R. L. Meng, L. Gao, Z. J. Huang, Y. Q. Wang, and C. W. Chu, *Phys. Rev. Lett.* (1987)

21. C. W. Chu, P. H. Hor, R. L. Meng, L. Gao, Z. J. Huang, Y. Q. Wang, M. K. Wu, J. R. Ashburn, and C. Y. Huang, *Phys. Rev. Lett.* (1987)

22. J. M. tarascon, L. H. Greene, W. R. McKinnon and G. W. Hull, *Phys. Rev. Lett.* (1987)

23. Z. Zhongxian, C. Liquan, C. Changgeng, H. Yuzhen, L. jinxiang, C. Genghua, T. Ruming, L. Guirong, C. Changgeng, C. Lie, W. Lianzhong, G. Shuquan, L. Shanlin and B. Jianqing, *Kexue Tongbao*, No. **6**, (1987)

24. D. Dew-hughes, *Treatise on Materials Science and Technology* Vol **14**, edtied by T. Luhman and D. Dew-Hughes (1979)

25. F. London and H. London, *Proc. R. Soc. london Ser. A* **149**, 71 (1935); *Physica* **2**, 963 (1935)

26. A. B. Pippard, *Proc. R. Soc. london Ser. A* **216**, 547 (1953)

27. V. L. Ginzberg and L. D. Landou, *JETP USSR* **20**, 1064 (1950)

28. A. A. Abrikosov, *Sov. Phys. JETP* **5**, 1174 (1957)

29. W. H. Kleiner, L. H. Roth and S. H. Autler, *Phys. Rev.* **133**, A1226 (1964)

30. M. Tinkham, *Introduction to Superconductivity* McGraw-Hill, New York (1975)

31. F. B. Silsbee, *J. Wash. Acad. Sci.* **6**, 597 (1916)

32. D. C. Larbalestier, *Superconductor Materials Science*, edited by S. Foner and B. B. Schwartz (New York: Plenum Press) 133 (1981)

33. M. Suenaga, *Superconductor Materials Science*, edited by S. Foner and B. B. Schwartz (New York: Plenum Press) 201 (1981)

34. R. Labusch, *Phys. Stat. Sol.* **32**, 439 (1969)

35. E. H. Brandt, *Phys. Stat. Sol.* **36**, 381 (1969)

36. E. J. Kramer, *J. Appl. Phys.* **44**, 1360 (1973)

37. D. Dew-Hughes, *Phil. Mag.* **B 55**, No 4, 459 (1987)

38. F. Laves, *Theory of Alloy Phases* American Society of Metals, Cleveland Ohio 183 (1956)

39. J. J. Hanak, G. D. Cody, P. R. Aron and H. C. Hitchcock, *High Magnetic Fields* edited by B. Lax et al., Wiley, New York 592 (1961)

40. T. B. Reed, H. C. Gatos, W. J. LaFleur and T. J. Roddy, *Metallurgy of Advanced Electronic Materials* edited by G. E. Brock , Wiley, New York 71 (1963)

41. R. D. Blaugher, R. A. Hein, J. E. Cox and R. M. Waterstrat, *J. Low Temp. Phys.* **1**, 531 (1969)

42. K. Hechler, G. Horn, G. Otto and E. Saur, *J. Low Temp. Phys.* **1**, 29 (1969)

43. E. Nambach and K. Tachikawa, *J. Less-Common Met.* **19**, 359 (1969)

44. E. Nambach, *Z. Metallkd.* **61**, 734 (1970)

45. A. I. Braginski, et al., *IEEE Trans. Mag.* **Mag-13**, 300 (1977)

46. R. V. carlson, R. J. Barlett, L. R. Newkirk and F. A. Valencia, *IEEE Trans. Mag.* **Mag-13**, 648 (1977)

47. J. S. Caslaw, *Cryogenics* **11**, 57 (1971)

48. R. M. Scanlan, W. A. Fietz and E. F. Koch, *J. Appl. Phys.* **46**, 2244 (1975)

49. A. W. West and R. D. Rawlings, *J. Mat. Sci.* **12**, 1862 (1977)

50. J. D. Livingston, *Phys. Stat. Sol.* (a) **44**, 295 (1978)

51. R. Hancox, *Phys. Lett.* **16**, 208 (1965)

52. R. Hancox, *Proc. Int. Conf. Low Temp. Phys.*, 10th Moscow **2B**, 45 (1966)

53. A. R. Kauffman and J. J. Pickett, *J. Appl. Phys.* **42**, 58 (1971)

54. K. Tachikawa and T. Tanaka, *Jpn. J. Appl. Phys.* **6**, 782 (1967)

55. K. Tachikawa, *Proc. Int. Cryogen. Eng. Conf.*, 3rd 339 (1970)

56. M. Suenaga, T. S. Luhman and W. B. Sampson, J. Appl. Phys. 45, 4049 (1974)

57. C. C. Tsuei, J. Appl. Phys. 45, 1385 (1974)

58. J. P. Harbison and J. Bevk, J. Appl. Phys. 48, 5180 (1977)

59. S. Foner, E. J. McNiff, Jr., B. B. Schwartz, R. Roberge and J. L. Fihey, Appl. Phys. Lett. 33, 101 (1978)

60. M. R. Pickus and J. Ling-Fai Wang, Modern Developments in Powder Metallurgy 11, 315 (1977)

61. L. R. Newkirk, F. A. Valencia, A. L. Giorgi, E. G. Szklarz and T. C. Wallace, IEEE Trans. Mag. Mag-11, 221 (1975)

62. S. Ceresara, M. V. Ricci, G. Pasotti, N. Sacchetti and M. Spadoni, IEEE Trans. Mag. Mag-15, 639 (1979)

63. L. Schultz, R. Bormann and H. C. Freyhardt, IEEE Trans. Mag. Mag-15, 94 (1979)

64. R. Flükiger, S. Foner, E. J. McNiff, Jr., and B. B. Schwartz, Appl. Phys. Lett. 34, 763 (1979)

65. K. Lo, J. Bevk and D. Turnbull, J. Appl. Phys. 48, 2597 (1977)

66. R. Akihama, R. J. Murphy and S. Foner, Appl. Phys. Lett. 37, 1107 (1980)

67. R. Bruzzese, N. Sacchetti and M. Spadoni, IEEE Trans. Mag. Mag-23, 653 (1987)

68. P. Johnson, *M.S. Thesis* Dept. Mat. Sci. & Eng. University of California, Berkeley (1987)

69. R. Flükiger, R. Akihama, S. Foner, E. McNiff, Jr., and B. Schwartz, *Adv. Cryg. Eng. Mat.* **26** 337 (1980)

70. J. Hong, I. Wu, J. Holthuis, M. Hong, and J. W. Morris, Jr., Presented at the *International Cryogenic Materials Conference,* San Diego Aug. (1981)

71. W. King, C. Thieme and S. Foner, *IEEE Trans. Mag.* **Mag-21**, 815 (1985)

72. P. Johnson, Y. Im, T. McKnelly and J. W. Morris, Jr., *IEEE Trans. Mag.* **Mag-23**, 1432 (1987)

73. I. Wu, *Ph D. Thesis,* Dept. Mat. Sci. & Eng. University of California, Berkeley (1984)

74. S.Pourrahimi, C. Thieme, S. Foner, and R. Murphy, *Appl. Phys. Lett.* **43** (11), 1070 (1983)

75. *Bulletin of Alloy Phase Diagrams* 2, 75 (1981), C. E. Lundin and A. S. Yamamoto, *Trans. AIME,* **236**, 863 (1966)

76. J. Jorda, R. Flükiger, and J. Muller, *J. Less-Common Metals* **75** 227 (1980)

77. J. Jorda, R. Flükiger, A. Junod, and J. Muller, *IEEE Trans. Mag.* **Mag-17**, 557 (1981)

78. J. Kohr, T. Eager, and R. Rose, *Met. Trans.* **3**, 1177 (1972)

79. J. Woollam, S. Alterovitz, and E. Haugland, *Appl. Phys. Lett.* **36** (8), 706 (1980)

80. K. Lo, J. Bevk, and D. Turnbull, *J. Appl. Phys.* **48** (6) 2597 (1977)

81. S. Singh, S. Lele, and C. Suryanarayana, *J. Mat. Sci. Lett.* **5** 84 (1986)

82. K. Togano, H. Kumakura, Y. Yoshida, and K. Tachikawa, *IEEE Trans. Mag.* **Mag-21**, 463 (1985)

83. R. Wang and S. Dahlgren, *Met. Trans. A* **8A**, 1763 (1977)

84. J. Kwo, R. Hammond, and T. Geballe, *J. Appl. Phys.* **51** 1726 (1980)

85. H. Kumakura, K. Togano, K. Tachikawa, Y. Yamada, S. Murase, E. Nakamura, and M. Sasaki, *Appl. Phys. Lett.* **48** (9), 601 (1986)

86. R. Bormann, H. Krebs, and A. Kent, *Adv. Cryg. Eng. Mat.* **32** 1041 (1986)

87. B. J. Kestel, *Ultramiscroscopy* **9**, 379 (1982)

88. T. Schober and V. Sorajic *Metallography* **6**, 183 (1973)

89. J. C. Bravman and R. Sinclair *J. Elect. Micro. Tech.* **1**, 53 (1984)

90. T. W. Eagar and R. M. Rose *IEEE Trans. Mag.* **Mag-11**, 214 (1975)

91. J. W. Edington *Practical Electron Microscopy in Materials Science* **2**, 15 MacMillan Philips Technical Library (1975)

92. R. Bormann, D. Yu, R. Hammond, A. Marshall, and T. Geballe *Rapid Quenched Metals V* S. Steeb and H. Warlimont, eds., North Holland 879 (1985)

93. L. R. Zheng, L. S. Hung, and J. W. Mayer *J. Vac. Soc. Tech.*, **A 1** 758 (1983)

94. A. E. Morgan, E. K. Broadbent, M. Delfino, B. Coulman, and D.K. Sadana *J. electrochem. Soc.* **134**, 925 (1987)

95. E. G. Colgan *J. Appl. Phys.*, **62** 2269 (1987)

96. E. G. Colgan *J. Appl. Phys.*, **62** 1224 (1987)

97. J. P. Goral and L. Eyring *J. Less-Common Metals*, **116** 63 (1986)

98. H. T. G. Hentzell, R. D. Thomson, and K. N. Tu *J. Appl. Phys.*, **54** (12) 6923 (1983)

99. H. T. G. Hentzell, and K. N. Tu *J. Appl. Phys.*, **54** (12) 6929 (1983)

100. R. M. Walser and R. W. Bene *App. Phys. Lett.*, **28** 624 (1976)

101. Maria Roney *App. Phys. Lett.*, **42** (7) 577 (1983)

102. B. Y. Tsaur, S. S. Lau, J. W. Mayer, and M. A. Nicolet *App. Phys. Lett.*, **38** (11) 922 (1981)

103. J. S. Kirkadly *Can. J. Phys.*, Vol. **36** 917 (1958)

104. J. R. Eifert, D. A. Chatfield, G. W. Powell and J. W. Spretnak *Trans. TMS-AIME*, **242** 66 (1968)

105. R. B. Schwarz and W. L. Johnson *Phys. Rev. Lett.*, **51** 415 (1981)

106. S. Herd, K. N. Tu and K. Y. Ahn *App. Phys. Lett.*, **42** 597 (1983)

107. W. L. Johnson *Prog. Mat. Sci.*, **30** 81 (1986)

108. F. M. d'Heurle and P. Gas *J. Mat. Res.*, **1** 205 (1986)

109. U. Gösele and K. N. Tu *J. Appl. Phys.*, **53** 3252 (1982)

110. W. J. Meng, B. Fultz, E. Ma, and W. L. johnson *App. Phys. Lett.*, **51** 661 (1987)

111. T. Eager and R. Rose *IEEE Trans. Mag.* **Mag-11** 214 (1985)

112. J. Maas, G. Bastin, F. van Loo, and R. Metselaar *Z. Metallkd.* **74**, 294 (1983)

113. E. G. Colgan and J. W. Mayer *J. Mater. Res.* **1**, 786 (1986)

114. G. V. Kidson and G. D. Miller *J. Nucl. Mater.* **1**, 61 (1984)

115. M. Suenaga *Superconductor Material Science* S. Foner and B. Schartz eds. Plenum Press, New York p201 (1981)

116. S. Okuda, M. Suenaga, and R. Sabatini *J. Appl. Phys.* **54**, 289 (1983)

117. C. Thieme, S. Pourrahimi, B. Schwartz, and S. Foner *IEEE Trans. Mag.* **Mag.-21**, 756 (1985)

118. R. Bruzzese, N. Sacchetti, M. Spadoni, G. Barani, G. Donati, and S. Ceresara *IEEE Trans. Mag.* **Mag.-23**, 653 (1987)

X. FIGURE CAPTIONS

Fig. 1 Critical surface of a typical type II superconductor

For a given temperature, the superconductor has a definite critical current density $J_c(T)$ and a critical magnetic field $H_c(T)$; this current density value generally has an inverse dependence on temperature and field.

Fig. 2 Plot of $-4\pi M$, where M is the magnetization, as a function of applied magnetic field B_a, for a type I superconductor. The critical value of the magnetic field $B_{ac} = H_c$. This magnetization curve is for a bulk sample exhibiting a complete Meissner effect, and the temperature is below the critical transition temperature T_c.

Fig. 3 Plot of $-4\pi M$ as a function of applied magnetic field Ba for a type II superconductor. (The sample is assumed to be a long cylinder parallel to the applied field.) The sample is superconducting (B=0) when the applied field is less than the lower critical field Hc1, and is in the mixed or vortex state ($B \neq 0$) when the applied field is between Hc1 and the upper critical field Hc2. For fields larger than Hc2, the superconductivity is destroyed and the sample becomes a normal conductor.

Fig. 4 Origin of the superconducting-normal boundary surface energy. The x axis is distance and the y axis is ΔG.

(a) $\xi > \lambda$, positive surface energy; (b) $\xi < \lambda$, negative surface energy.

Fig. 5 The spatial configuration of $|\psi|^2$ near H_{c2} for a triangular flux array in a type II superconductor. The area density of the dots is approximately proportional to the square of the reduced order parameter[29].

Fig. 6 The variation of the local magnetic field h and the order parameter $|\psi|$ across an isolated flux line in a type II superconductor.

Fig. 7 The BCS energy gap in the excitation spectrum of a superconductor at the Fermi level

Fig. 8 The unit cell of the A15 crystal structure. The dotted lines indicates the orthogonal A-atom chains.

Fig. 9 The grain structure in the reacted layer of a filament of a commercial Nb_3Sn multi-filamentary superconductor. The wire axis is normal to the plane of the paper. Continuous grain-boundary paths exist with components parallel to the Lorentz force (F_L)[37].

Fig. 10 The grain structure of a powder metallurgy processed Nb_3Al wire. The wire axis is parallel to the superconducting Nb_3Al grain layers. The Lorentz force (F_L) is normal to the direction of the grain elongation.

Fig. 11 Illustration of a powder metallurgy technique used to make the Nb/Al superconducting wire.

Fig. 12 Nb-Al binary phase diagram[75] shows that, in the normally chosen heat treatment temperature range (900°C ~ 1100°C), not only superconducting Nb_3Al but also Nb_2Al and $NbAl_3$ phases can be thermodynamically stable.

Fig. 13 Variation of Gibbs free energy ΔG with composition for a hypothetical Nb-X system containing A15 and Nb_aX_b ($\frac{a}{b} < 3$) phases, with differing relative stability[24]. (a) A15 more stable than Nb_aX_b, range of homogeneity of A15 includes 3:1 ratio. (b) A15 less stable than Nb_aX_b, range of homogeneity restricted to high Nb content. (c) A15 so much less stable than Nb_aX_b, its formation is completely suppressed

Fig. 14 Illustration of the cold-rolling technique used to make thick multi-layered samples.

Fig. 15 The Cu disc grid was clamped by a sharp-tipped tweezer, and a coat of enamel was applied on both the grid and the tip of the tweezer except for the wire region so that only the wire would be electropolished during the electro-chemical thinning.

Fig. 16 The beaker method used to thin wire samples: The electrolyte in a beaker was cooled by iced water reservoir while gently stirred magnetically. A 5 mm x 15 mm fine net made by stainless steel was used for the cathode electrode and the anode was directly connected to the tweezer which clamped the Cu grid.

Fig. 17 Preparation prior to mechanical thinning of TEM sample:

Multi-layered samples were glued facing multi-layer sides and placed in a brass tube. The gap between the sample and the tube was filled with epoxy glue. When the epoxy hardened, the brass tube was sliced to 0.5 mm thickness. After this procedure was finished, the sample was mechanically thinned, dimpled and ion-milled to electron-transparency.

Fig. 18 The plot of the dimple-depth vs dimple-diameter of the dimpler. The depth of the dimple was determined by measuring the diameter of the dimple and reading the corresponding depth from the conversion plot instead of using a micrometer attached to the dimpler.

Fig. 19 Differential Scanning Calorimeter data of a powder metallurgy processed wire sample: heat transfer in and out of the sample was monitored as the temperature was raised from 225°C to 725°C, where the temperature was held up to 15 minutes.

Fig. 20 TEM micrograph of an unreacted P/M processed 5 weight % Al wire with R=5000 (Longitudinal view): The darker heavily dislocated layers are Nb and the lighter layers are Al. The Al and Nb filaments formed layers of inhomogeneous thickness and distribution.

Fig. 21 TEM micrograph of an unreacted P/M processed 5 weight % Al wire with R=5000 (Transverse view): Nb and Al powders were severely deformed into irregular filaments or layers.

Fig. 22 TEM micrograph of a P/M processed wire with R=5000, heat treated at 650°C for 2 hrs. (Longitudinal view) All the Al was consumed to form the $NbAl_3$ phase.

Fig. 23 TEM micrograph of a P/M processed wire with R=5000, heat treated at 650°C for 24 hrs. (Longitudinal view) Longer heat treatment time only resulted in coarsening of the $NbAl_3$ grains.

Fig. 24 TEM micrograph of a P/M processed wire with R=5000, heat treated at 700°C for 24 hrs. (Longitudinal view) Nb_3Al and Nb_2Al (not shown here) formed while $NbAl_3$ disappeared.

Fig. 25 TEM micrograph of a P/M processed wire with R=5000, heat treated at 900°C for 20 min. (Longitudinal view) Superlayers of agglomerated Nb remained after the reaction heat treatment.

Fig. 26 TEM micrograph of a P/M processed wire with $R=10^4$, heat treated at 900°C for 20 min. (Longitudinal view) A homogeneous Nb_3Al layer formed thicker than 5000Å without any Nb_2Al formation.

Fig. 27 TEM micrograph of a P/M processed wire with $R=10^4$, heat treated at 900°C for 20 min. followed by 750°C for 2 days (Longitudinal view) A Nb_3Al / Nb_2Al / Nb_3Al layer configuration is shown. This configuration has been frequently observed in similar P/M processed wire samples.

Fig. 28 Longitudinal view of a T.E.M. micrograph of a P/M processed Nb/Al wire reacted at 900°C for 20 min. (5 weight % Al, R = 500) The heavily faulted Nb_2Al grains were found as well as superconducting Nb_3Al.

Fig. 29 TEM micrographs of sputter-deposited Nb/Al multi-layered samples (cross-sectional view): Darker layers are Nb and lighter layers are Al.

a) 20 pairs of 300 Å Nb / 80 Å Al layers on a Nb substrate

b) 10 pairs of 1000 Å Nb / 270 Å Al layers on a Nb substrate

Fig. 30 TEM micrograph of a 1000Å Nb / 270 Å Al multi-layered sample heat treated at 600°C for 100 hrs (Cross-sectional view): The $NbAl_3$ phase was found while the remaining Nb did not contain any detectable Al in solid solution.

Fig. 31 TEM micrograph of a 1000Å Nb / 270Å Al multi-layered sample heat treated at 900°C for 20 min. followed by 750°C for 2 days (cross-sectional view): The multi-layer region reacted to form the superconducting Nb_3Al phase.

Fig. 32 TEM micrograph of a cold-rolled multi-layered sample with 630Å thick Al layers heat treated at 900°C for 20 min. (cross-sectional view): The Nb_3Al / Nb_2Al / Nb_3Al layer configuration was observed.

Fig. 33 SEM micrograph of a cold-rolled multi-layered sample with sufficient Nb and Al supply, heat treated at 600°C for 100 hrs (cross-sectional view): The $NbAl_3$ grains fell out from the Nb/Al interface as they grew larger. New $NbAl_3$ grains grew at the fresh Nb/Al interface.

Fig. 34 SEM micrograph of a cold-rolled thick multi-layered sample with insufficient Nb supply, heat treated at 600°C for 100 hrs (cross-sectional view): The $NbAl_3$ formation continued until all Nb was consumed.

Fig. 35 TEM micrograph of a cold-rolled multi-layered sample heat treated at 900°C / 20 min. (cross-sectional view) A $NbAl_3$ layer is shown to grow over 100 μm thickness.

Fig. 36 Optical micrograph of region I of the Nb-Al bulk sample made by plasma welding. A layer of a Nb-Al solid solution grew from the remaining Nb, and a mixture of the solid solution and Nb_3Al was present above it.

Fig. 37 TEM micrograph of region I of the Nb-Al bulk sample. The superconducting Nb_3Al phase nucleated and grew from the Nb-Al solid solution.

Fig. 38 SEM micrograph of the region II of the Nb-Al bulk sample. A layer of Nb_2Al formed above the remaining Nb, and a $Nb_2Al/NbAl_3$ eutectic grew from the Nb_2Al layer.

Fig. 39 TEM micrograph of the $Nb_2Al/NbAl_3$ eutectic. The dark phase is Nb_2Al and the bright phase is $NbAl_3$.

Fig. 40 X-ray diffraction data of the region I of the bulk sample made by plasma melting technique. Nb peaks are split into two by 0.01Å ~ 0.02Å, which corresponds to a Nb-Al solid solution of approximately 10 atomic % Al[93].

Fig. 41 TEM micrograph of the D.S.C. sample which suffered from a 20°C/min. heat ramp to 700°C. Only $NbAl_3$ was found to form.

Fig. 42 Crystal structures of compound phases in Nb/Al system

a) $NbAl_3$ has the $D0_{22}$ tetragonal structure which is similar to 2 fcc Al unit cells.

b) Nb_3Al has the A15 type cubic structure.

c) Nb_2Al has the sigma type tetragonal structure with 30 atoms in a unit cell.

Fig. 43 Since the activation energy of nucleation of $NbAl_3$ at the Nb/Al interface is relatively smaller than those of Nb_3Al or Nb_2Al, the $NbAl_3$ phase will nucleate at relatively low temperatures (< 700°C) regardless Nb/Al layer configuration.

Fig. 44 The kinetically favorable $NbAl_3$ will grow continuously as long as both Nb and Al remain. The next favorable Nb_3Al will form at the Nb/$NbAl_3$ interface only after all the Al is consumed to form $NbAl_3$.

Fig. 45 When the Nb_3Al grains grow to form a continuous layer, further diffusion is allowed only through the Nb_3Al grain boundaries. The diffusion barrier allows the formation of Nb_2Al kinetically favorable over that of Nb_3Al, resulting in the Nb_3Al/Nb_2Al/Nb_3Al layer configuration.

Fig.46 TEM micrograph of a cold-rolled multi-layered sample heat treated at 900°C for 10min. (Cross-sectional view) Nb_2Al started to grow from the Nb/Nb_3Al interface, where Nb_3Al already formed a continuous layer of 700Å ~ 800Å thickness. Some remaining $NbAl_3$ is seen in the middle of the reacted region.

Fig. 47 Illustration of possible reactions between Nb and $NbAl_3$

A) Al as the primary diffusing element in Nb_3Al

B) Nb as the primary diffusing element in Nb_3Al

Fig. 48 A plot of J_c values vs applied magnetic field for various Nb/Al superconducting wires. It is shown that the average Nb filament thickness, T_{Nb}, can be used to estimate J_c of the wires qualitatively.

XI. FIGURES

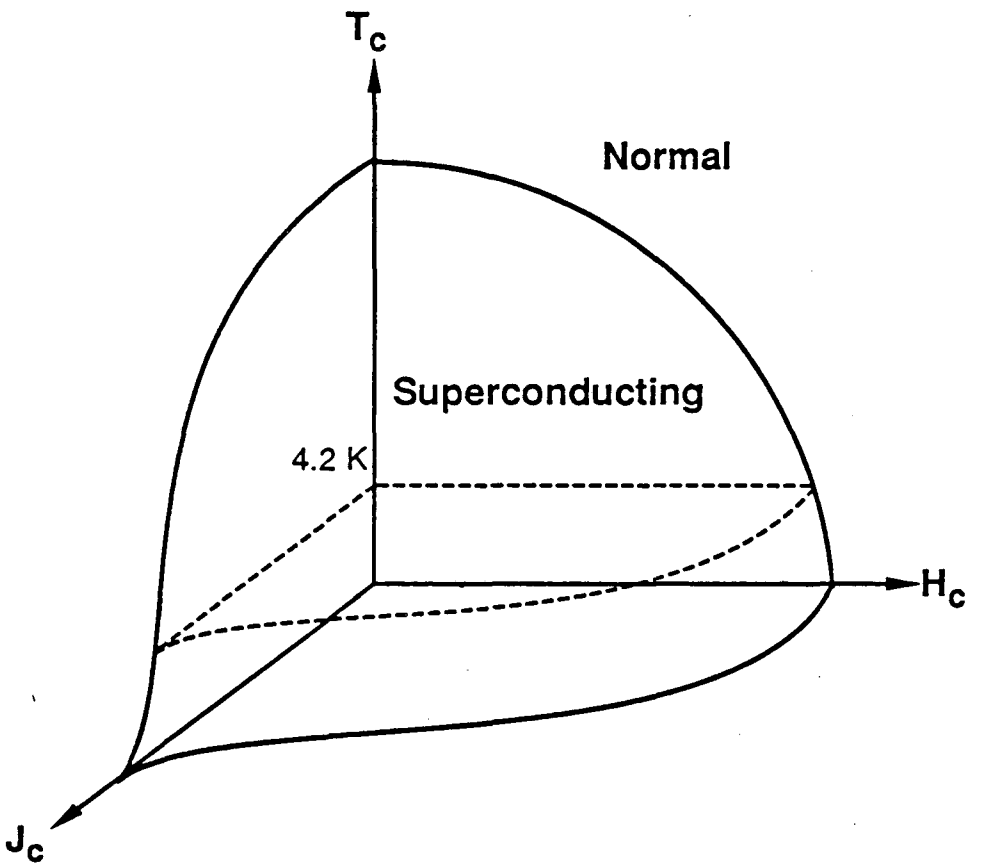

Fig. 1

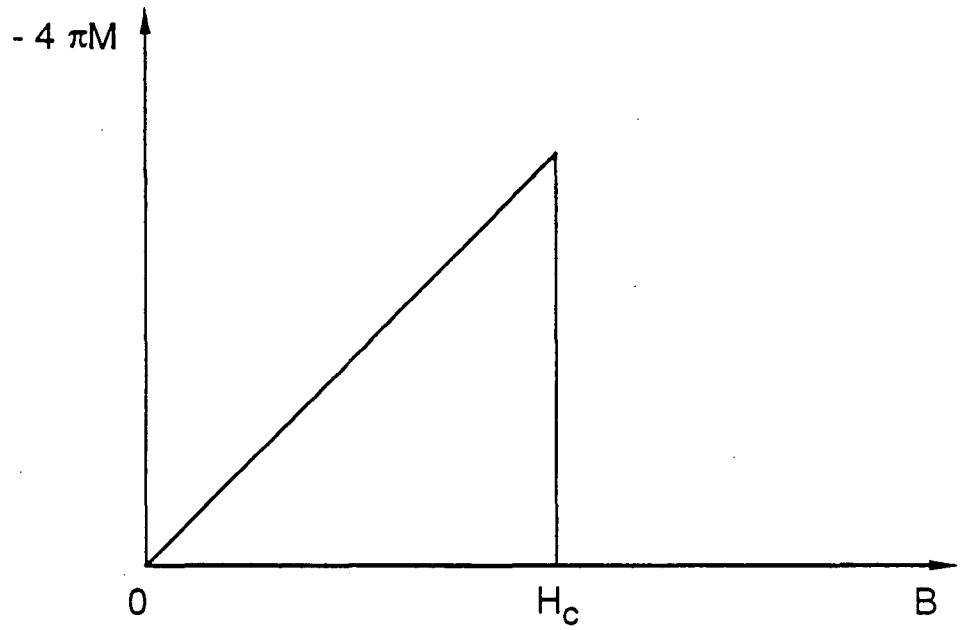

Fig. 2

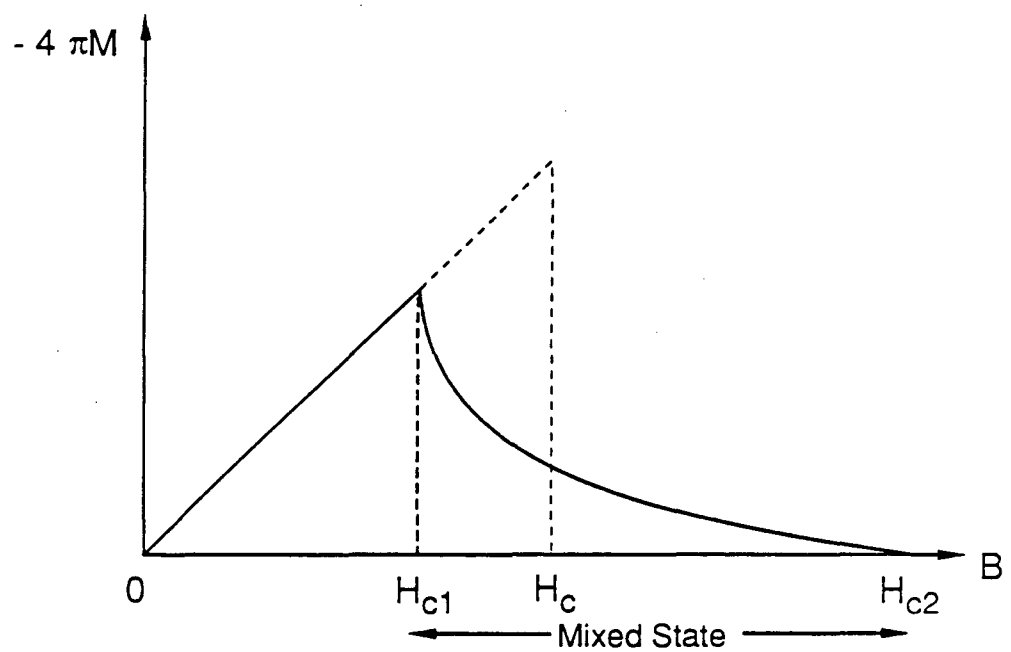

Fig. 3

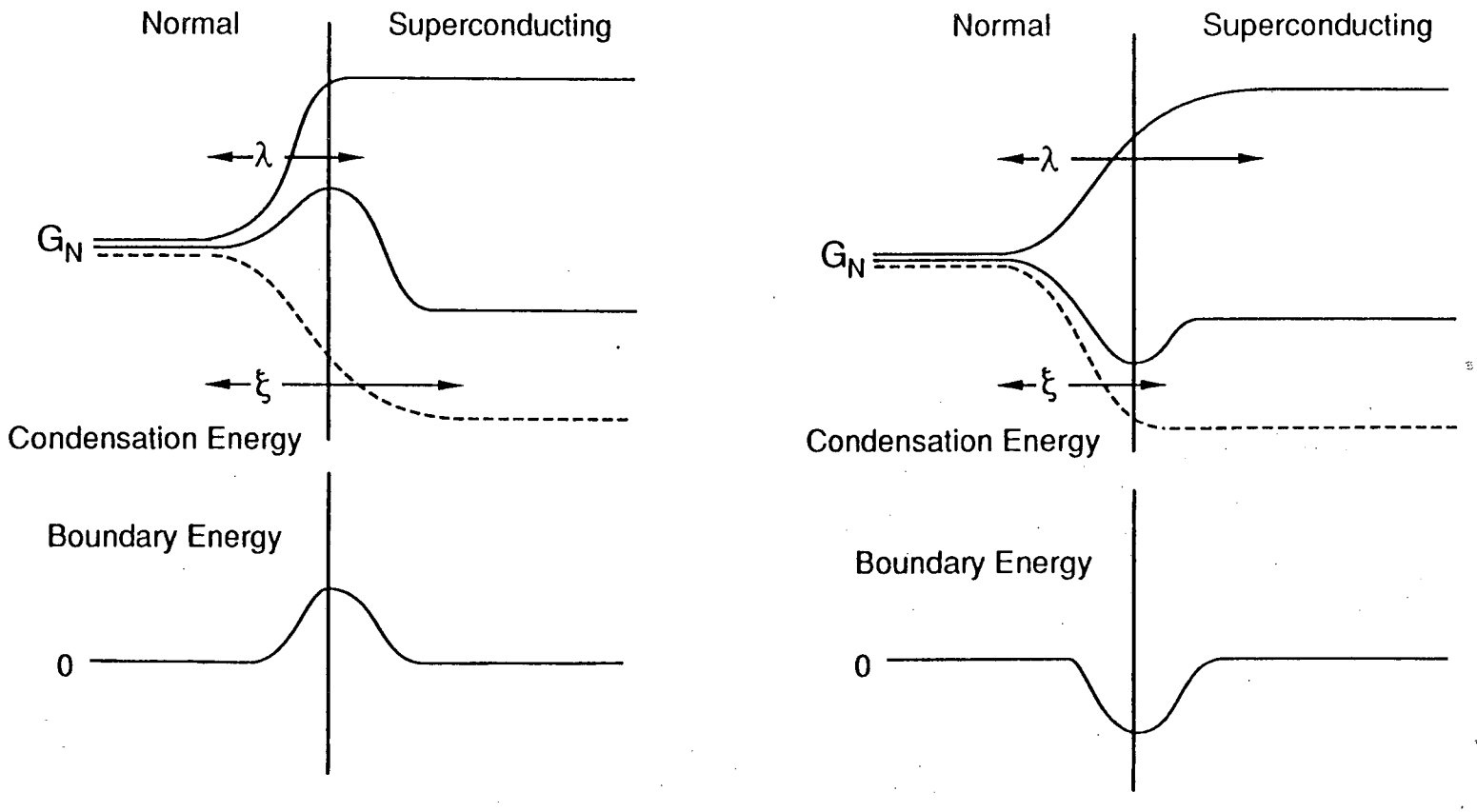

(a) $\xi > \lambda$

(b) $\xi < \lambda$

Fig. 4

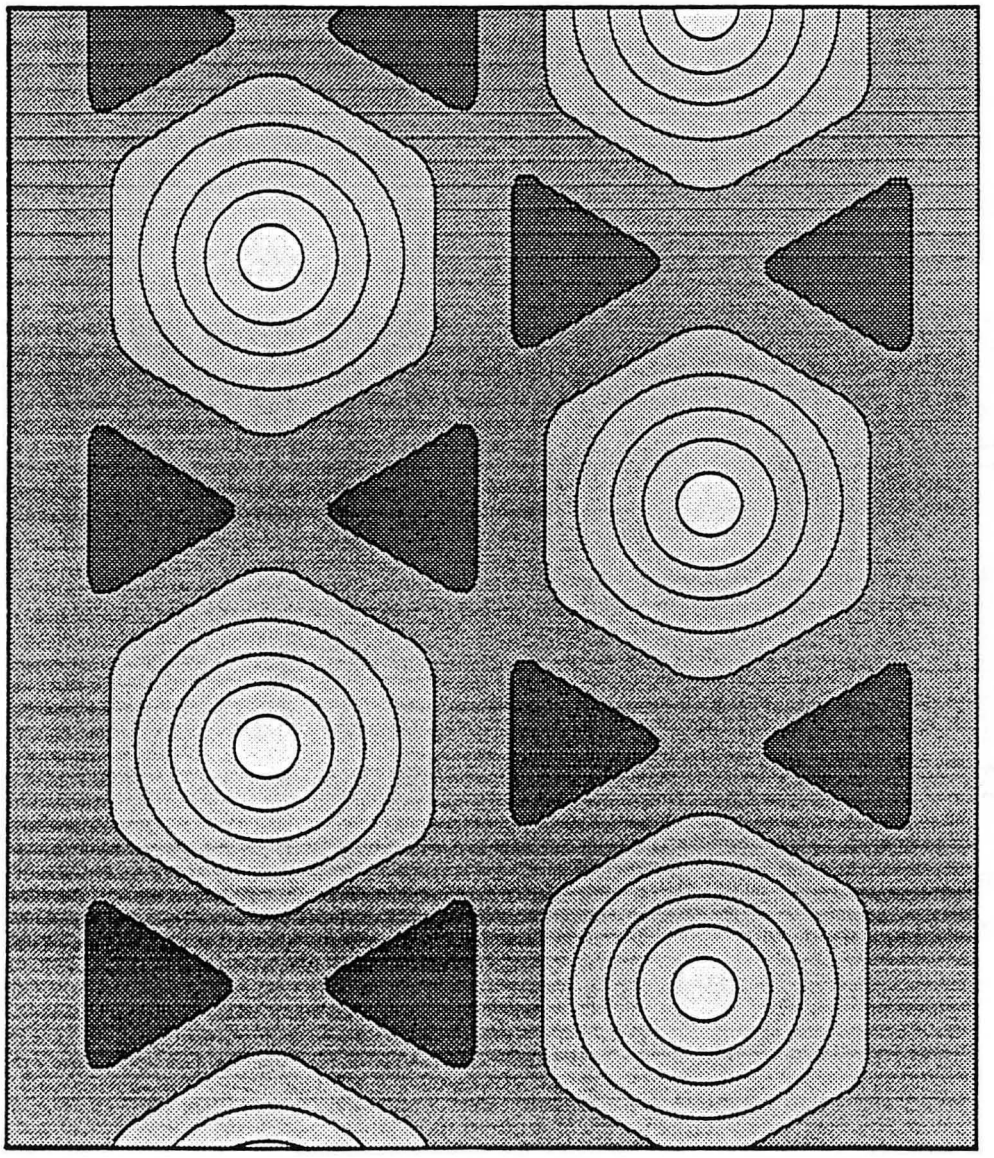

Fig. 5

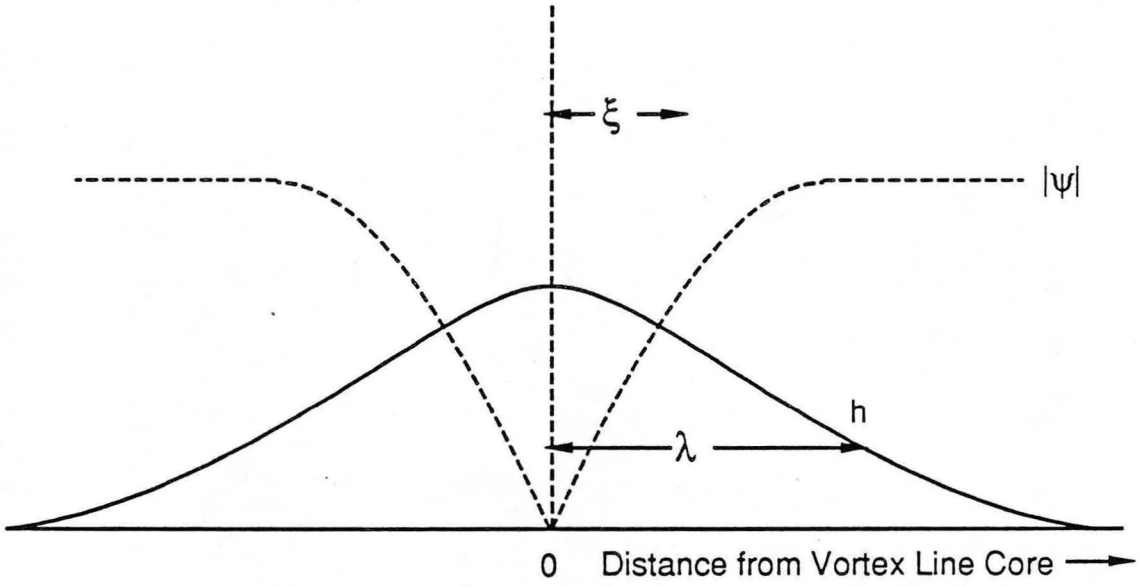

Fig. 6

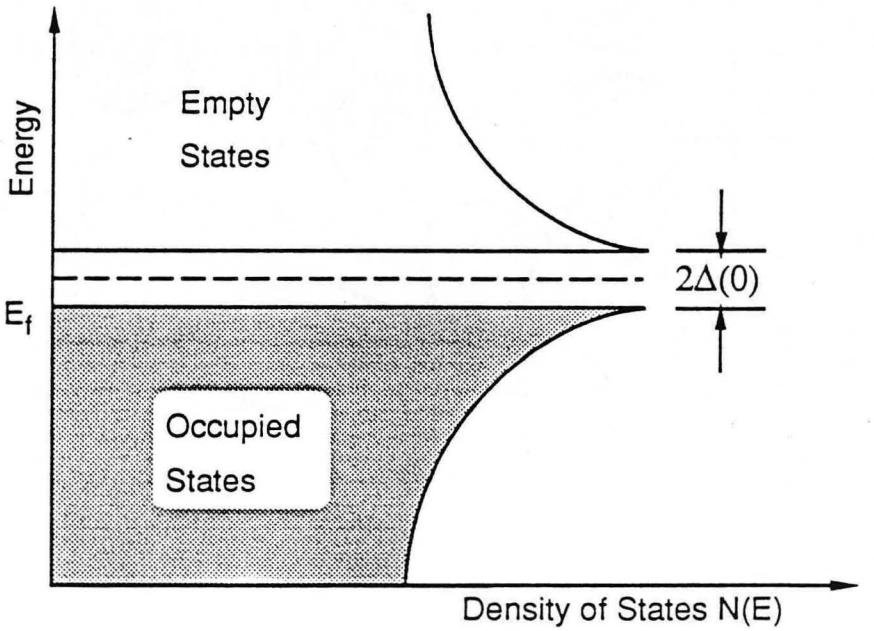
Energy
Empty
States
E_f
$2\Delta(0)$
Occupied
States
Density of States N(E)

Fig.7

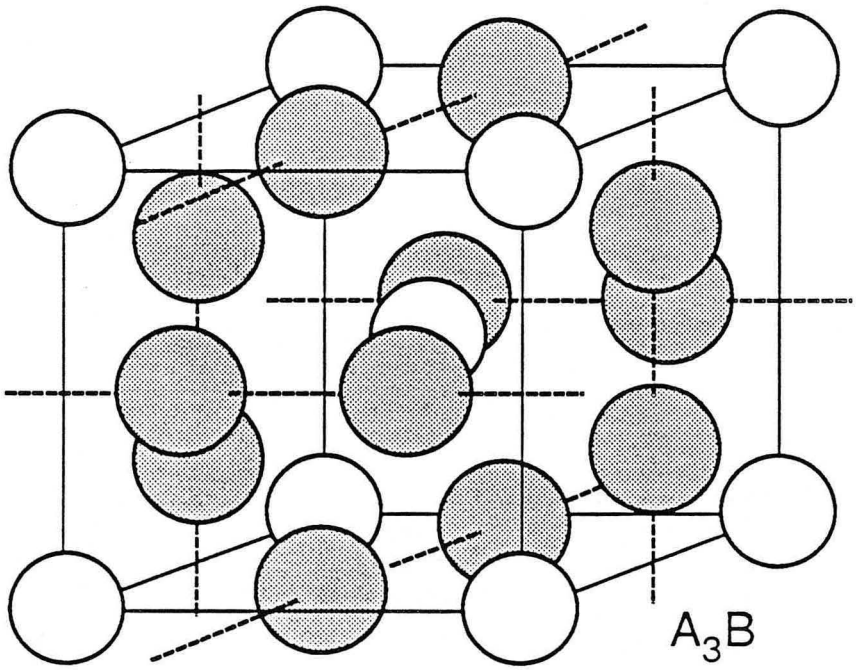

Fig.8

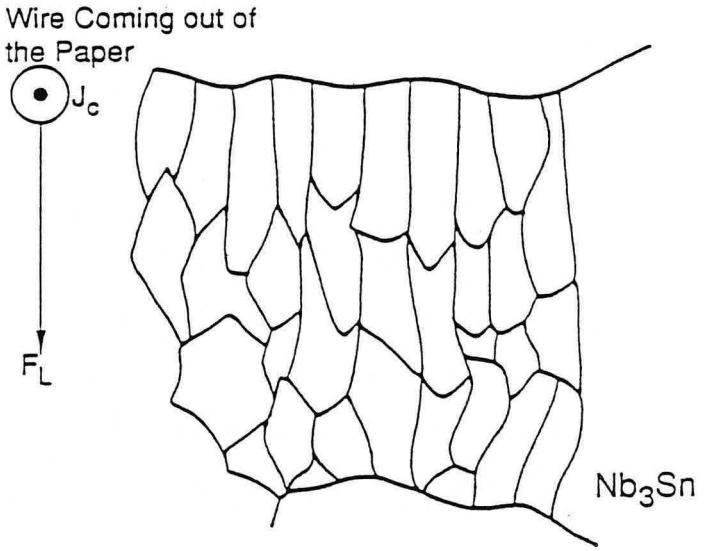
Wire Coming out of
the Paper
J_c
F_L
Nb_3Sn

Fig.9

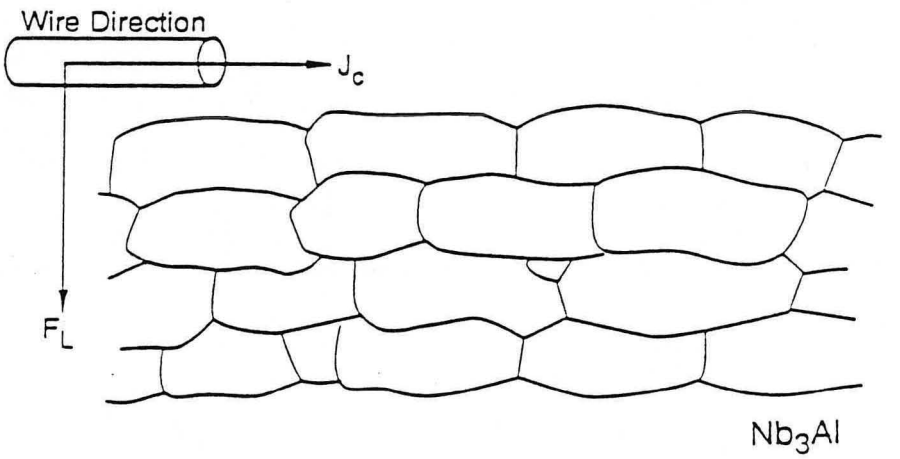
Wire Direction
J_c
F_L
Nb_3Al

Fig. 10

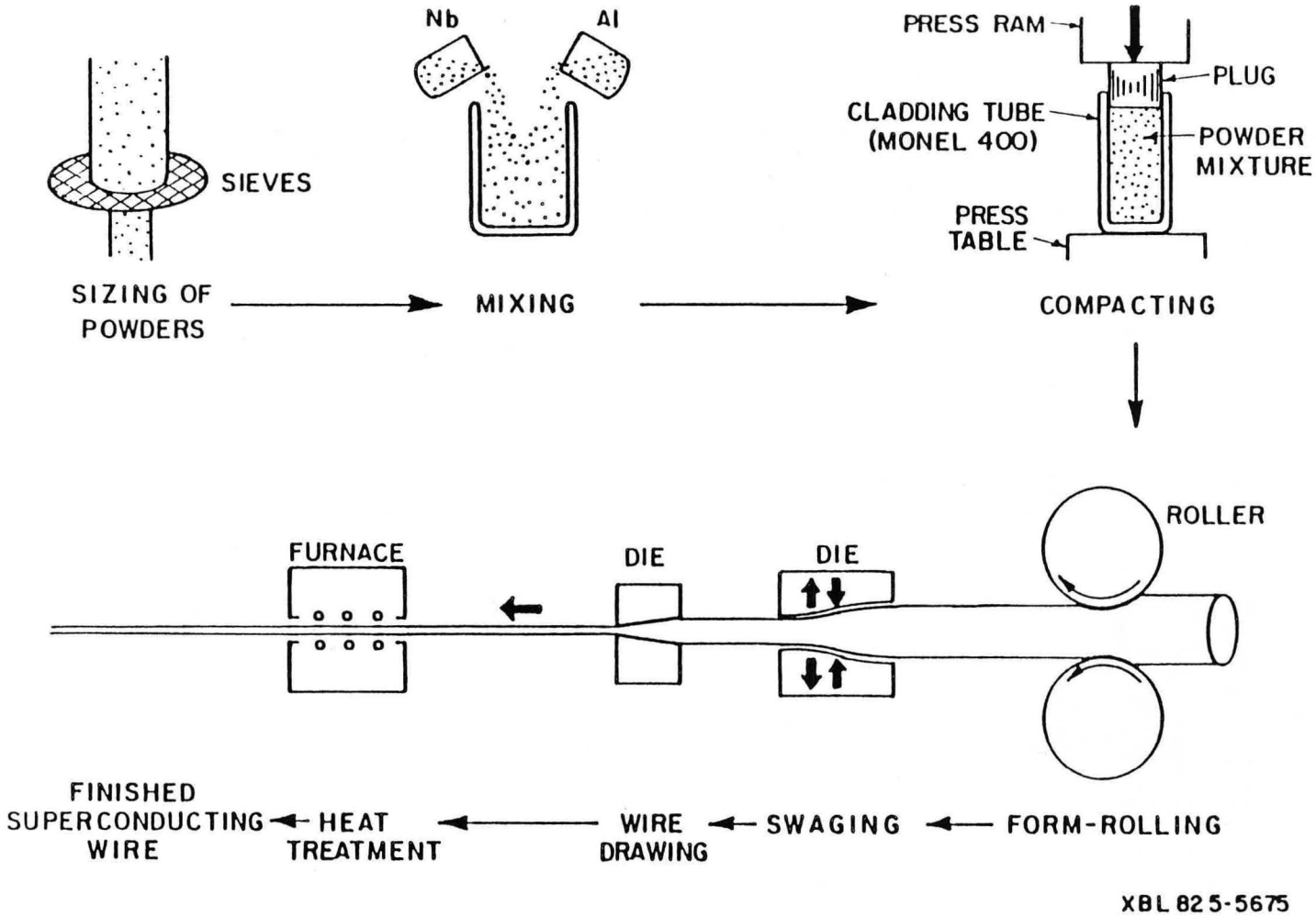
POWDER METALLURGY APPROACH
SIEVES
SIZING OF POWDERS
Nb
Al
MIXING
PRESS RAM
PLUG
CLADDING TUBE (MONEL 400)
POWDER MIXTURE
PRESS TABLE
COMPACTING
ROLLER
FURNACE
DIE
DIE
FINISHED SUPERCONDUCTING WIRE
HEAT TREATMENT
WIRE DRAWING
SWAGING
FORM-ROLLING
XBL 825-5675

Fig. 11

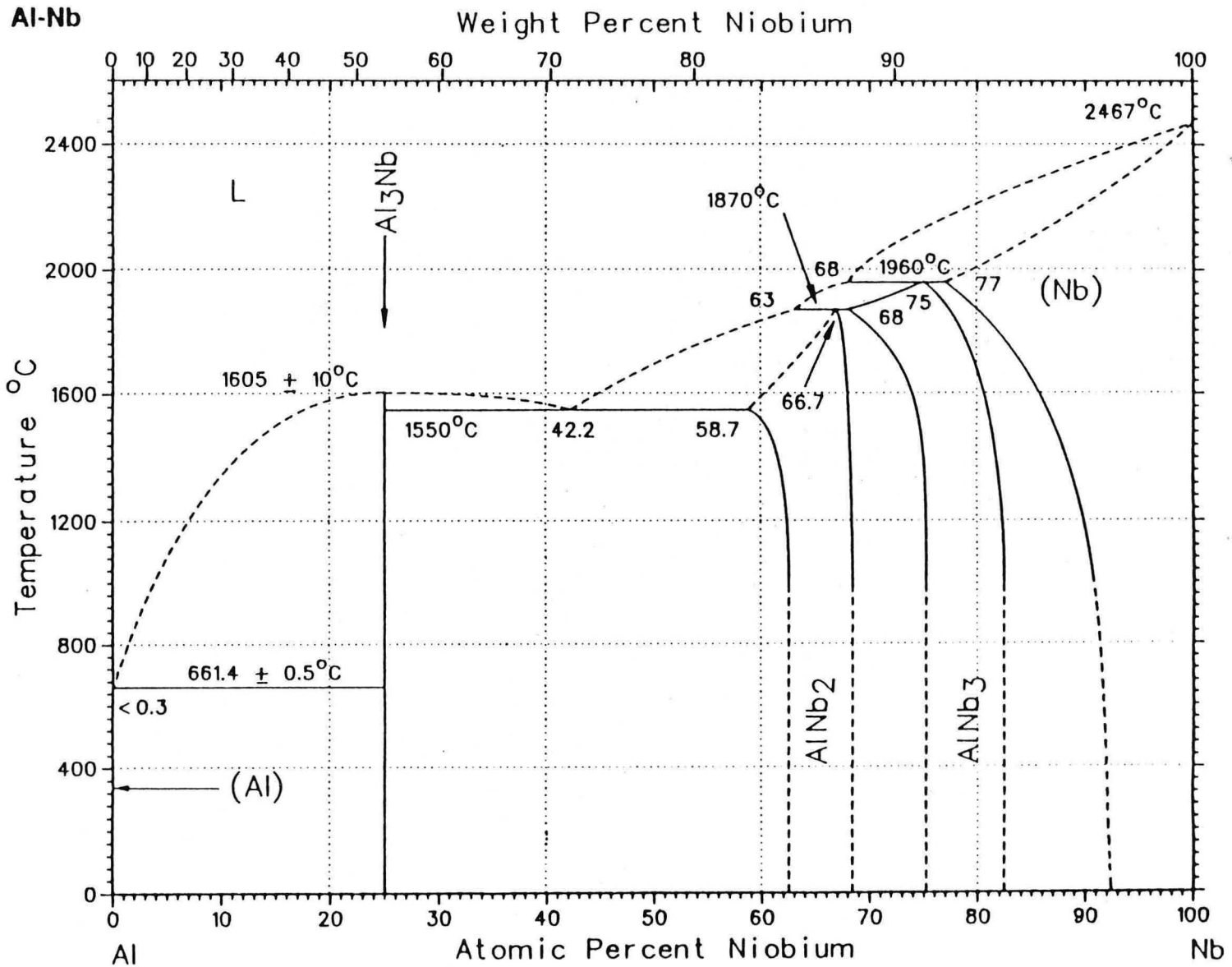
Al-Nb
Weight Percent Niobium
0 10 20 30 40 50 60 70 80 90 100
2467°C
L
Al3Nb
1870°C
68
1960°C
77
(Nb)
63
75
68
66.7
1605 ± 10°C
1550°C
42.2
58.7
Temperature °C
2400
2000
1600
1200
800
400
0
661.4 ± 0.5°C
< 0.3
(Al)
AlNb2
AlNb3
0 10 20 30 40 50 60 70 80 90 100
Al
Atomic Percent Niobium
Nb

Fig. 12

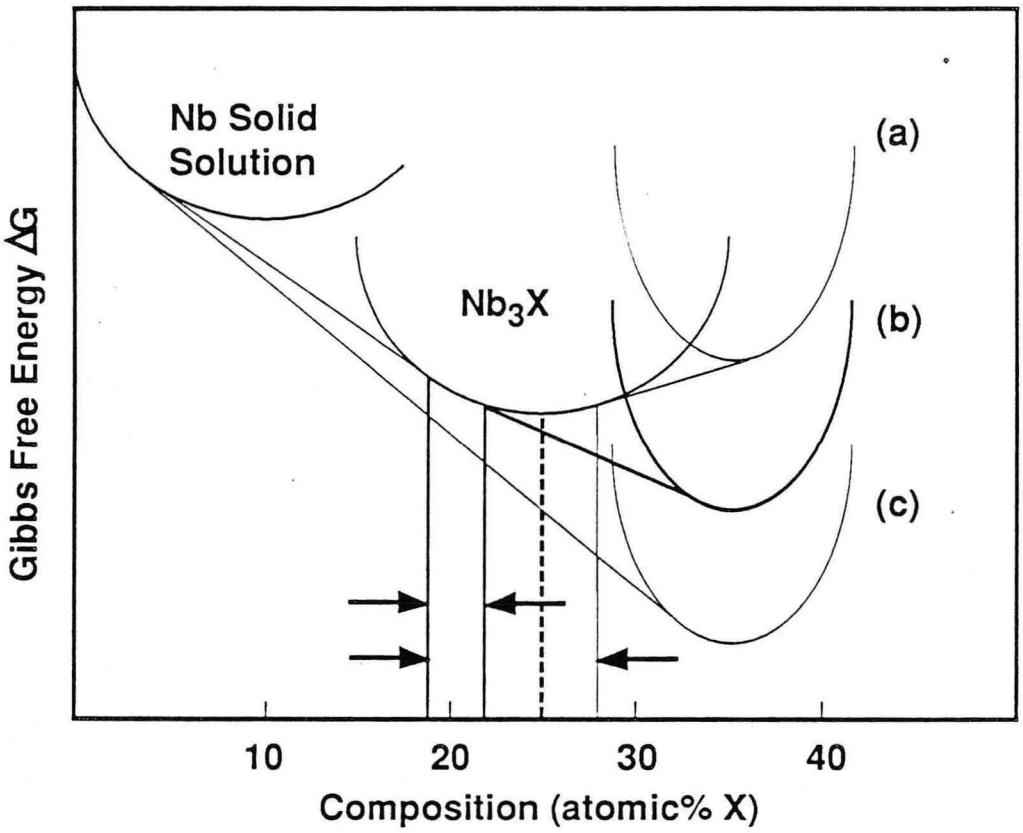
Nb Solid
Solution
(a)
Nb3X
(b)
(c)
Gibbs Free Energy ΔG
10
20
30
40
Composition (atomic% X)

Fig. 13

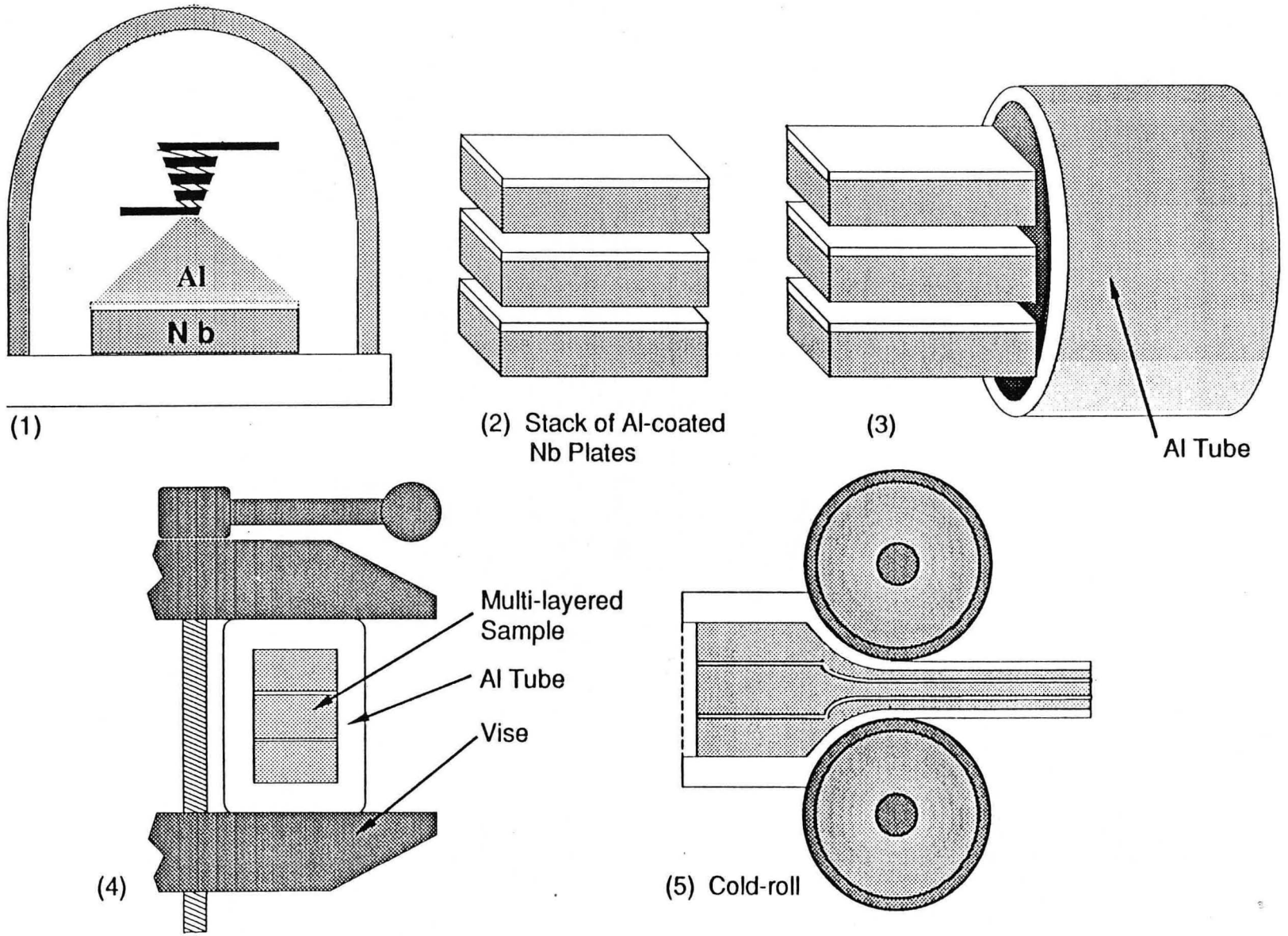
Al
Nb
(1)
(2) Stack of Al-coated
Nb Plates
(3)
Al Tube
Multi-layered
Sample
Al Tube
Vise
(4)
(5) Cold-roll

Fig. 14

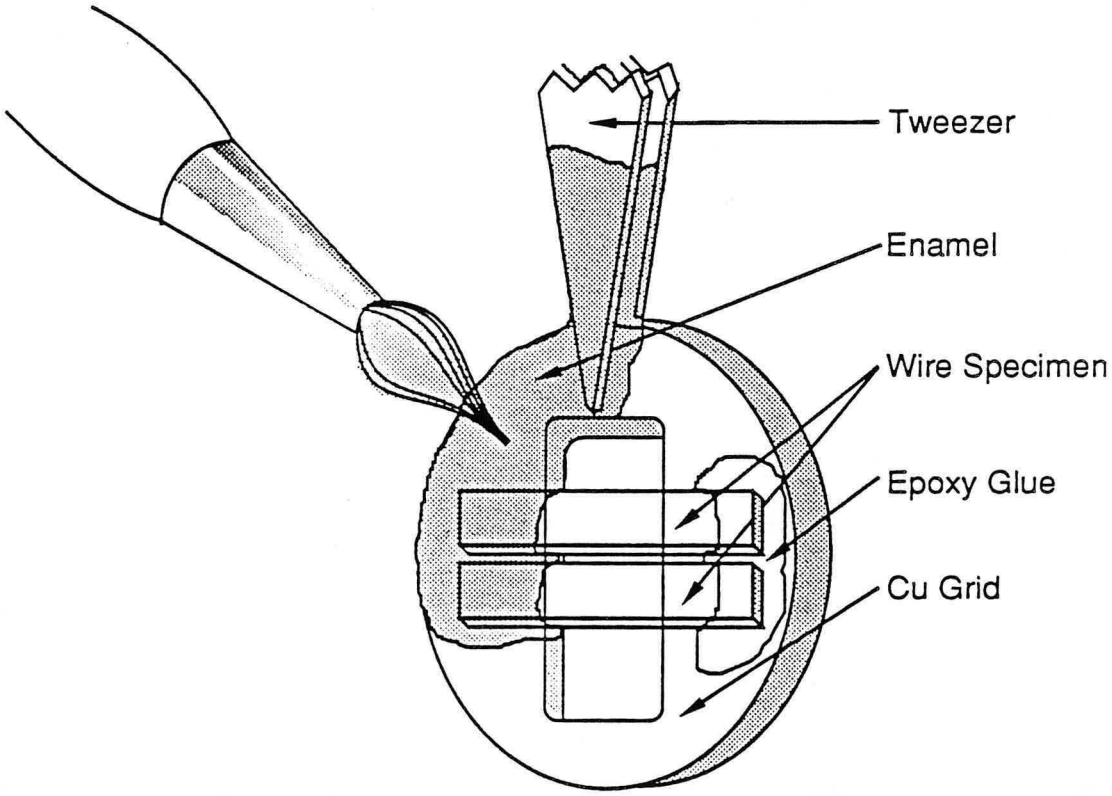

Fig. 15

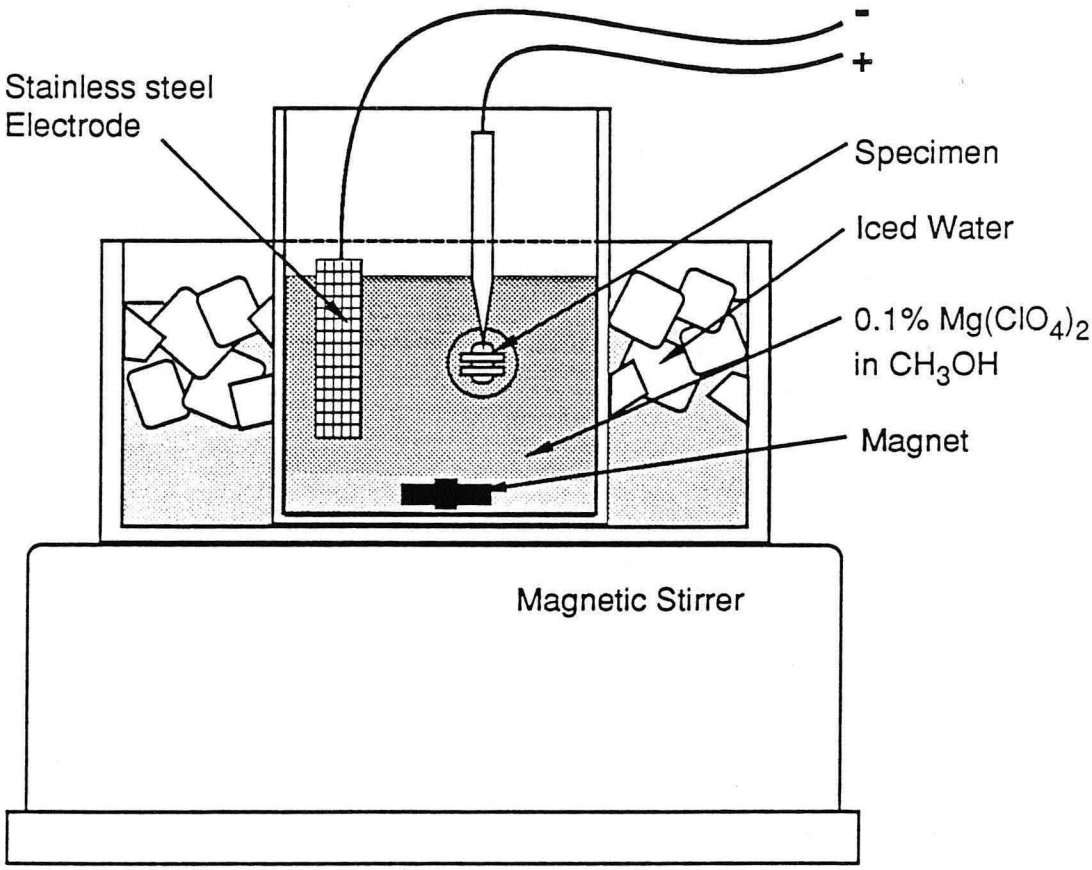
-
+
Stainless steel
Electrode
Specimen
Iced Water
0.1% $Mg(ClO_4)_2$
in CH_3OH
Magnet
Magnetic Stirrer

Fig. 16

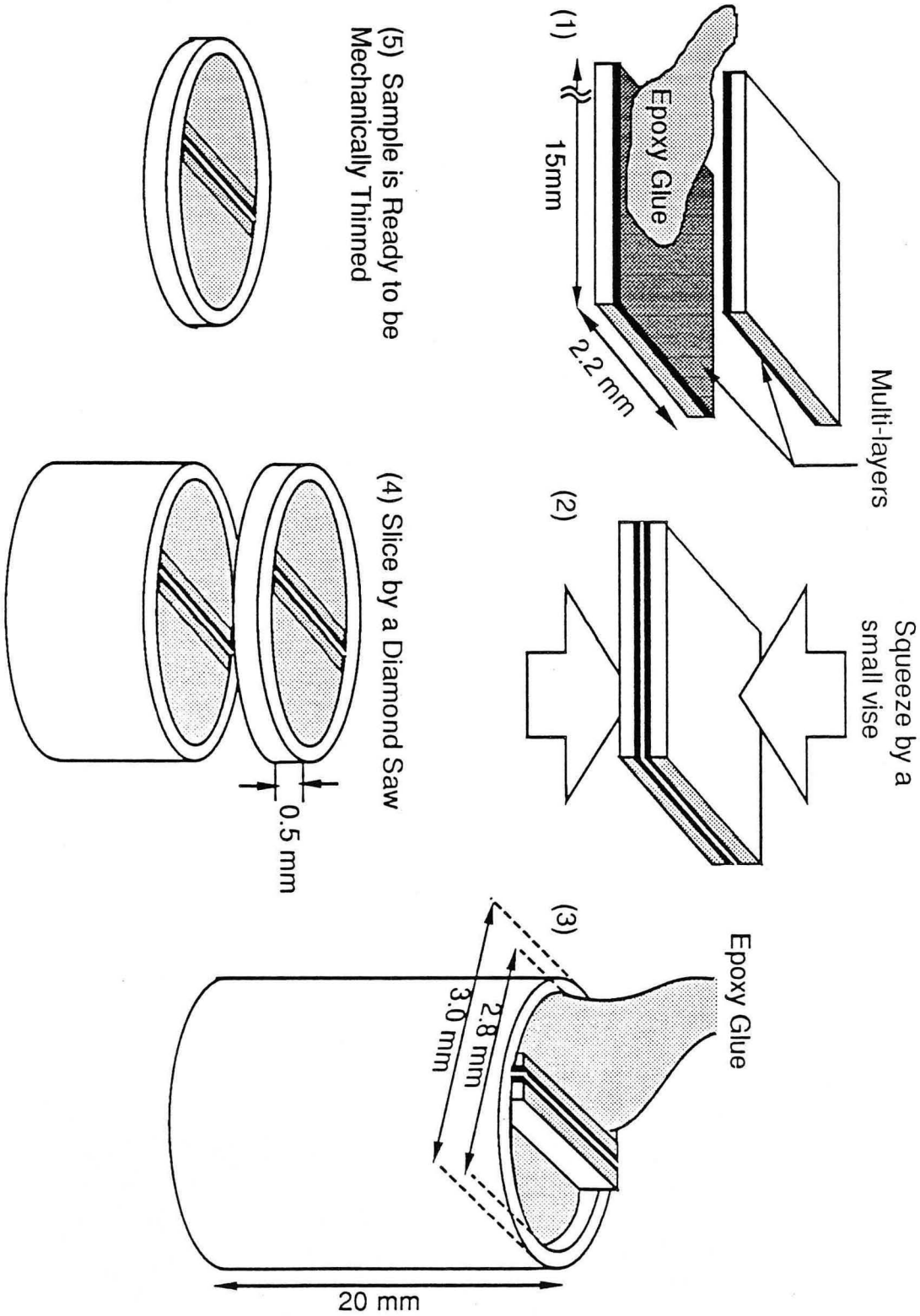
Multi-layers
Epoxy Glue
(1)
15mm
2.2 mm
Squeeze by a small vise
(2)
Epoxy Glue
(3)
2.8 mm
3.0 mm
20 mm
(4) Slice by a Diamond Saw
0.5 mm
(5) Sample is Ready to be Mechanically Thinned

Fig. 17

Dimple Diameter (mm)	Dimple Depth (μm) R=6.5mm	R=7.0mm	R=7.5mm
1.0	19.26	17.88	16.69
1.1	23.31	21.64	20.19
1.2	27.75	25.76	24.04
1.3	32.58	30.24	28.22
1.4	37.80	35.09	32.74
1.5	43.41	40.29	37.59
1.6	49.42	45.86	42.79
1.7	55.82	51.80	48.32
1.8	62.61	58.10	54.20
1.9	69.80	64.76	60.41
2.0	77.38	71.80	66.97
2.1	85.37	79.20	73.86
2.2	93.75	87.00	81.11
2.3	102.54	95.11	88.69
2.4	111.73	103.62	96.62
2.5	121.32	112.51	104.90
2.6	131.33	121.77	113.53
2.7	141.74	131.41	122.50
2.8	152.56	141.43	131.83
2.9	163.79	151.83	141.50
3.0	175.44	162.60	151.53

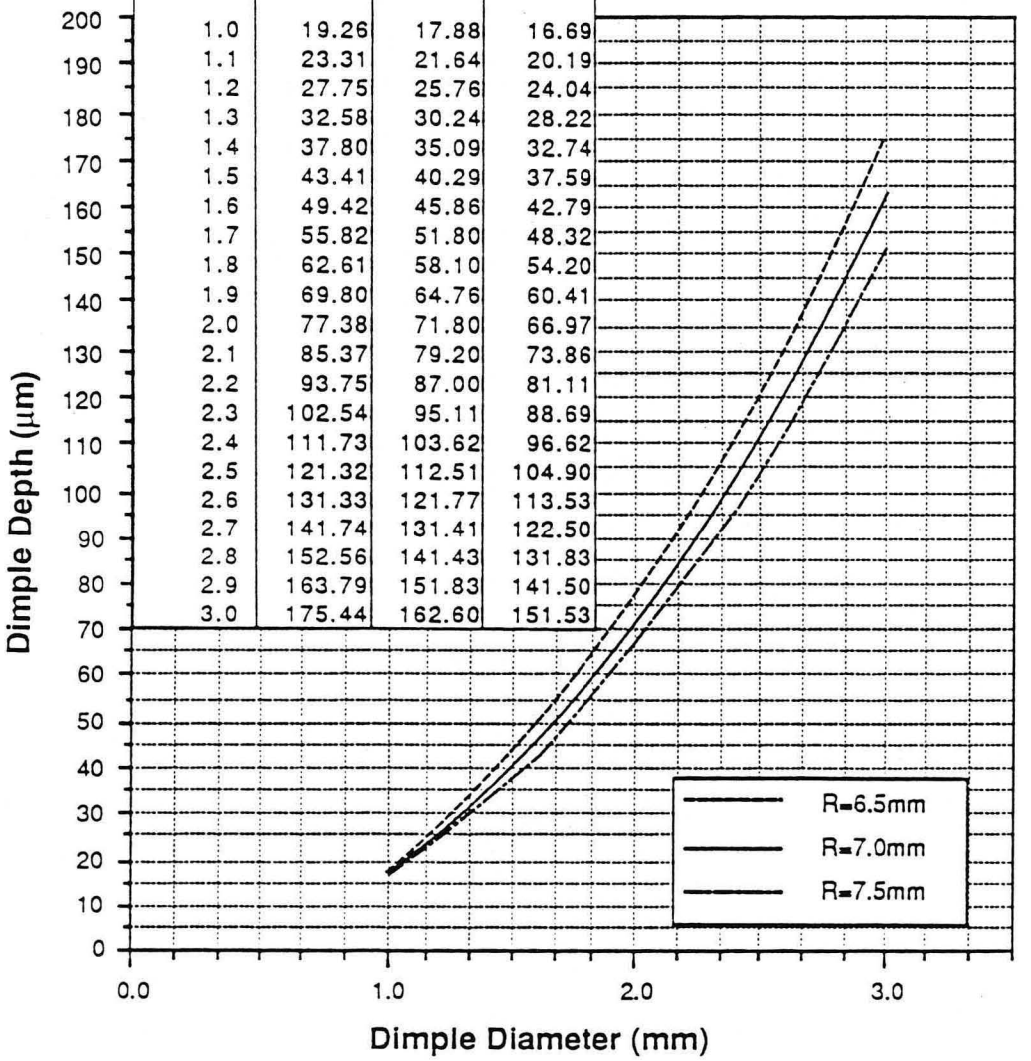

Fig. 18

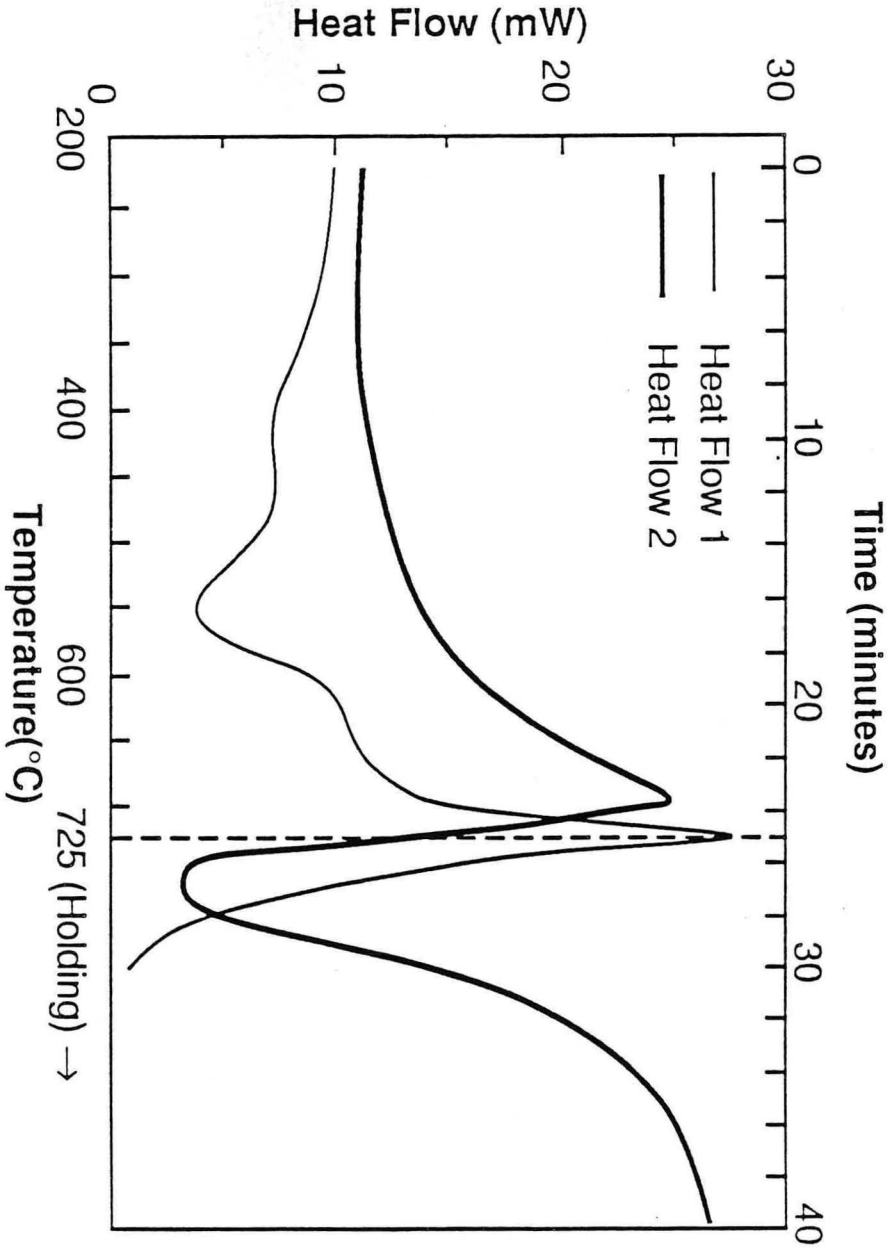
Time (minutes)
0
10
20
30
40
Heat Flow 1
Heat Flow 2
Heat Flow (mW)
0
10
20
30
0
200
400
600
725 (Holding) →
Temperature(°C)

Fig. 19

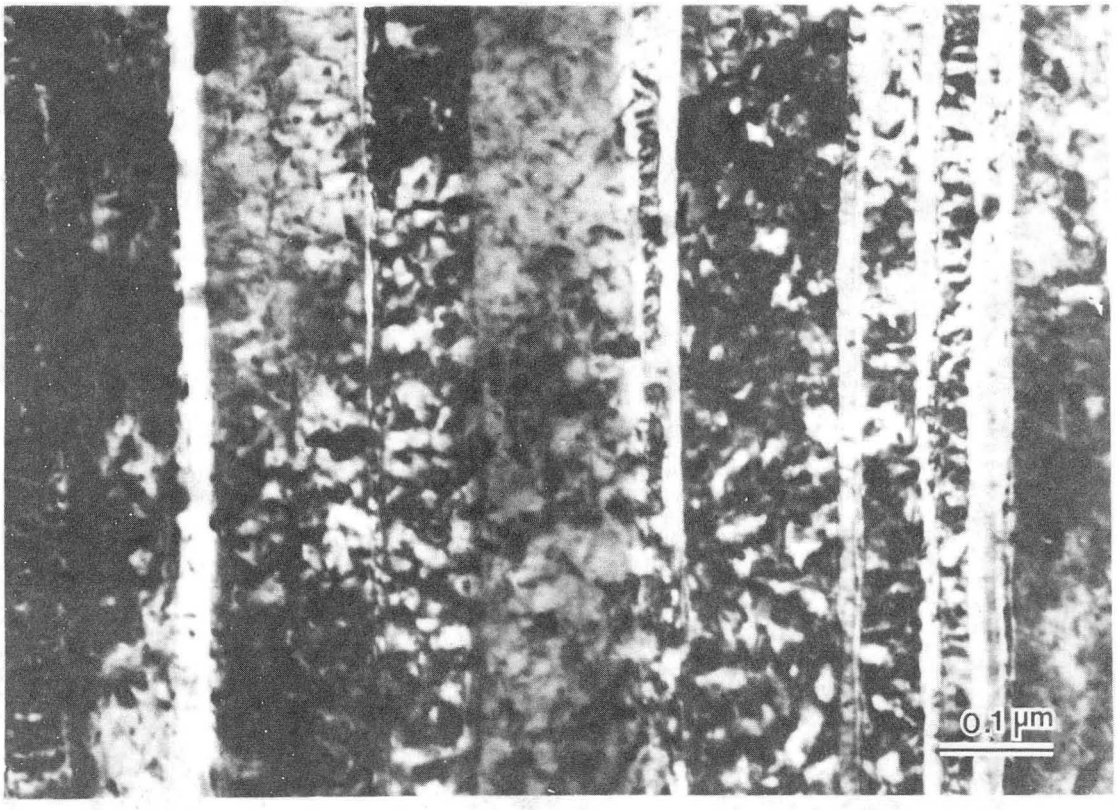

XBB 872-1279

Figure 20

XBB 872-1279

Figure 21

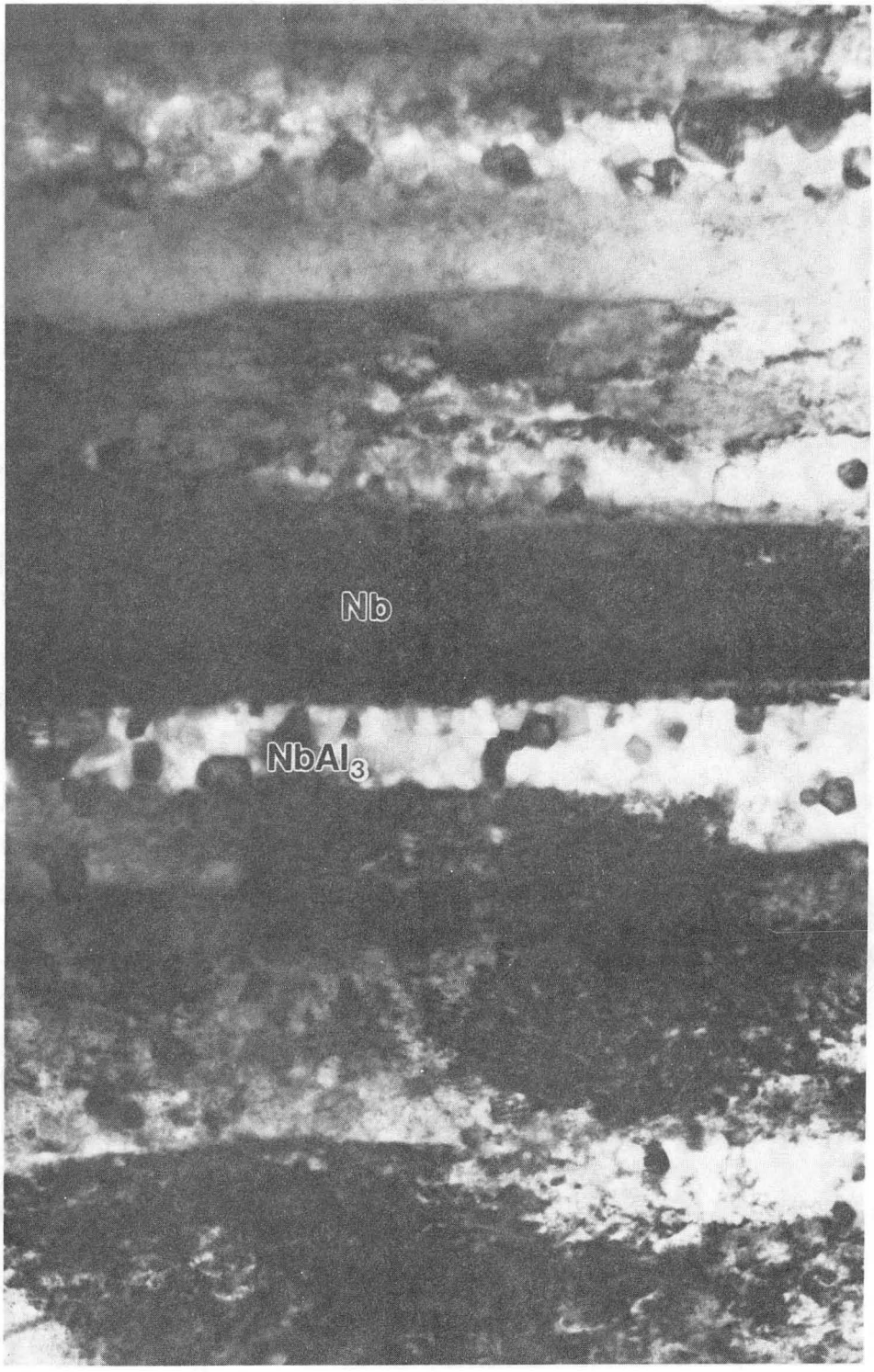

XBB 880-9427

Figure 22

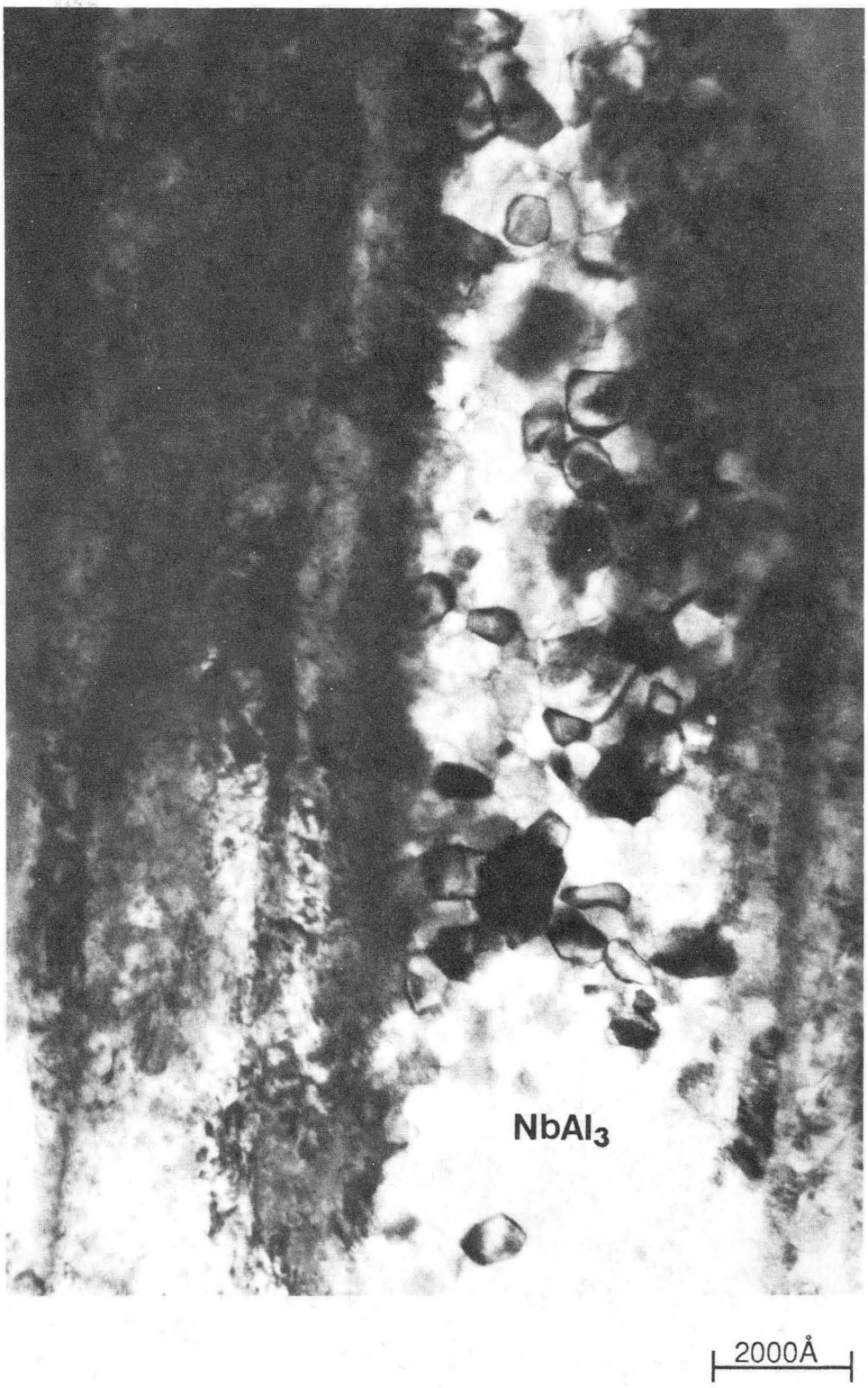

XBB 880-9431

Figure 23

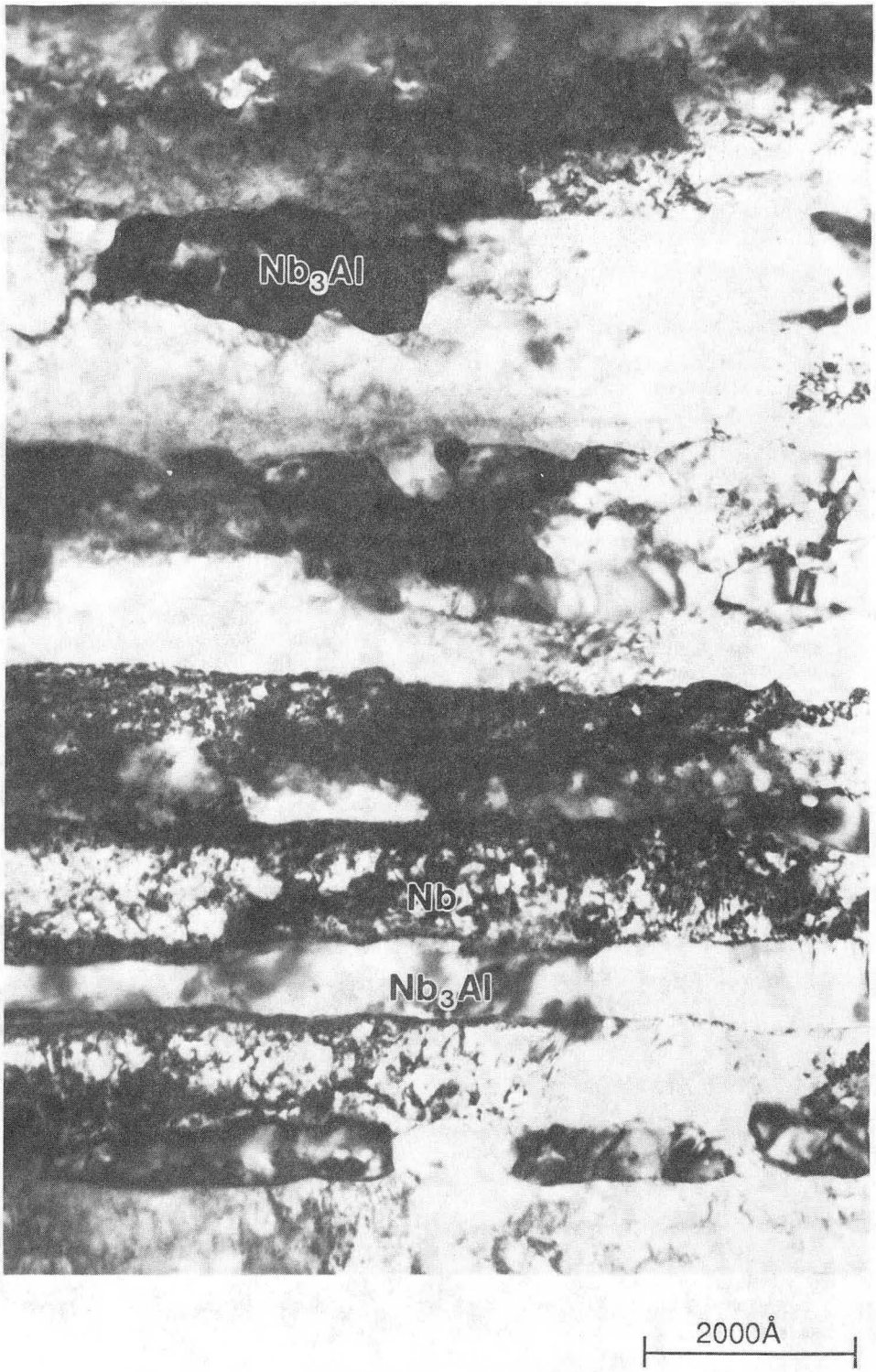

XBB 880-9432

Figure 24

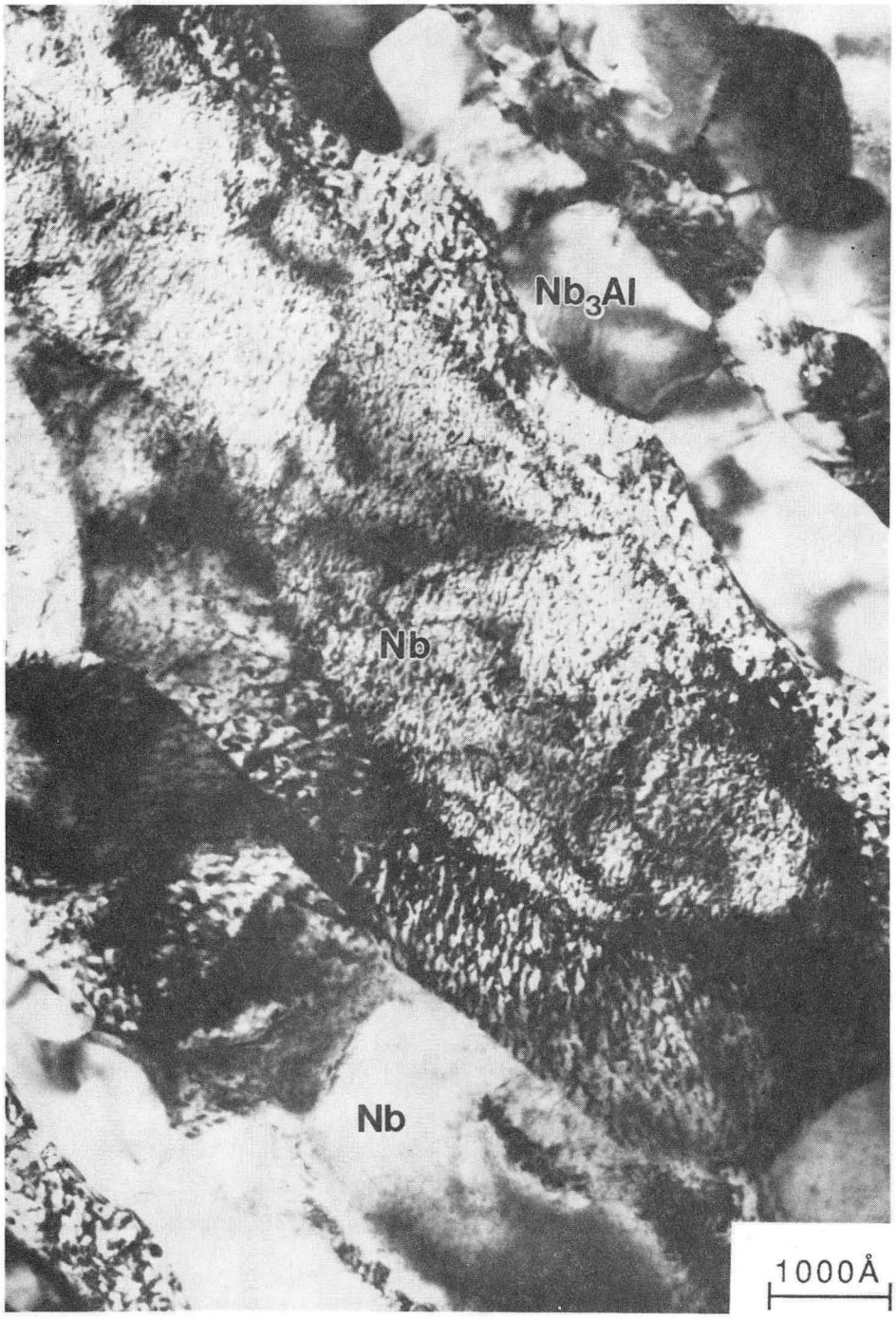

XBB 880-9428

Figure 25

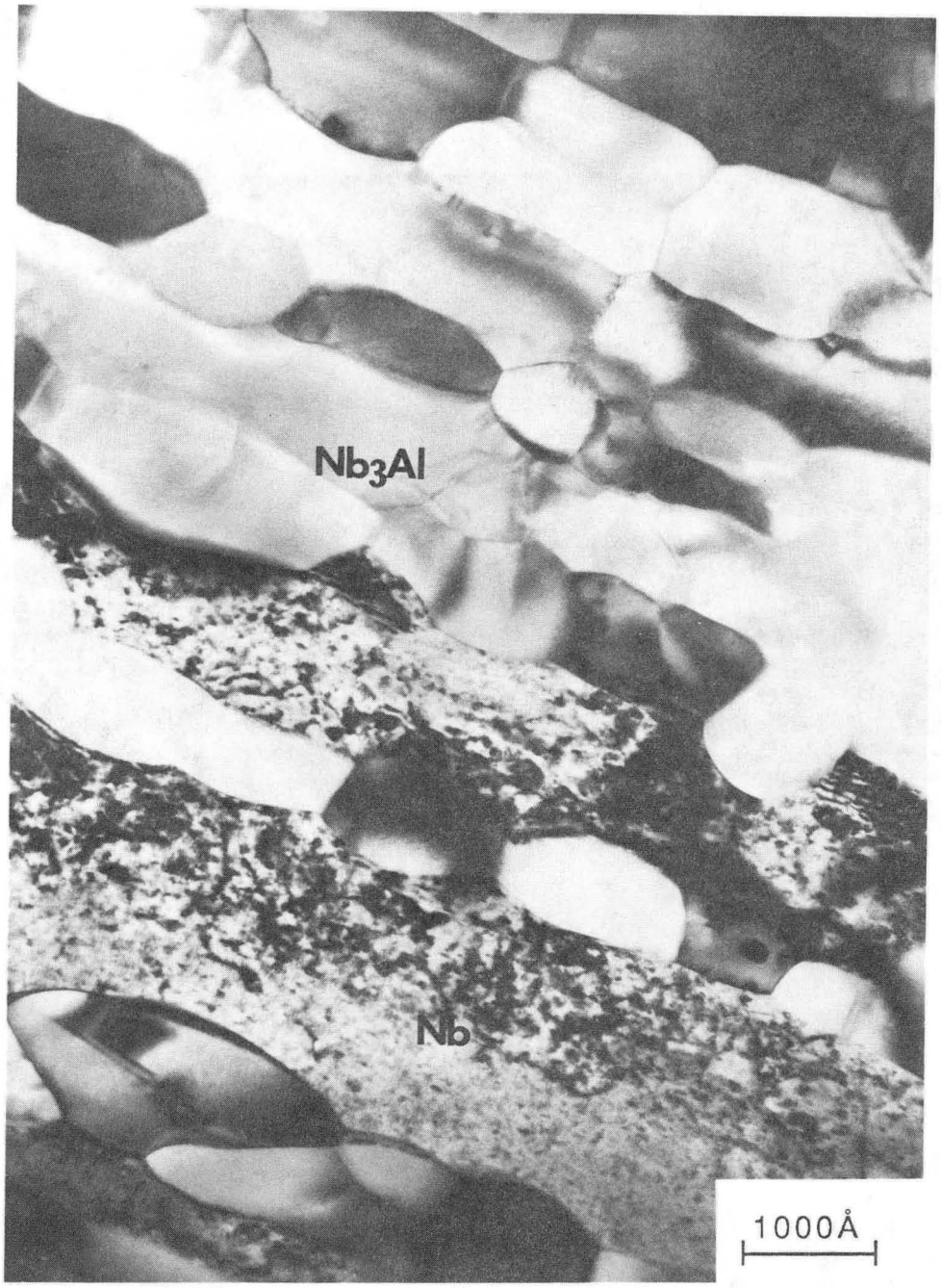

XBB 880-9426

Figure 26

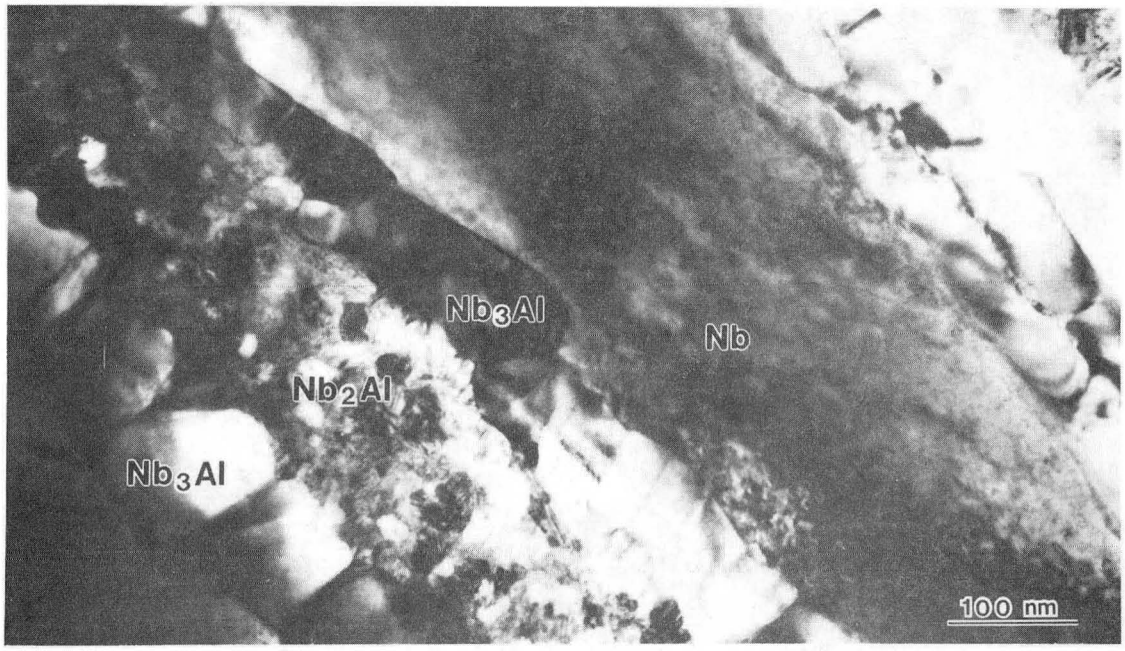

XBB 875-4179

Figure 27

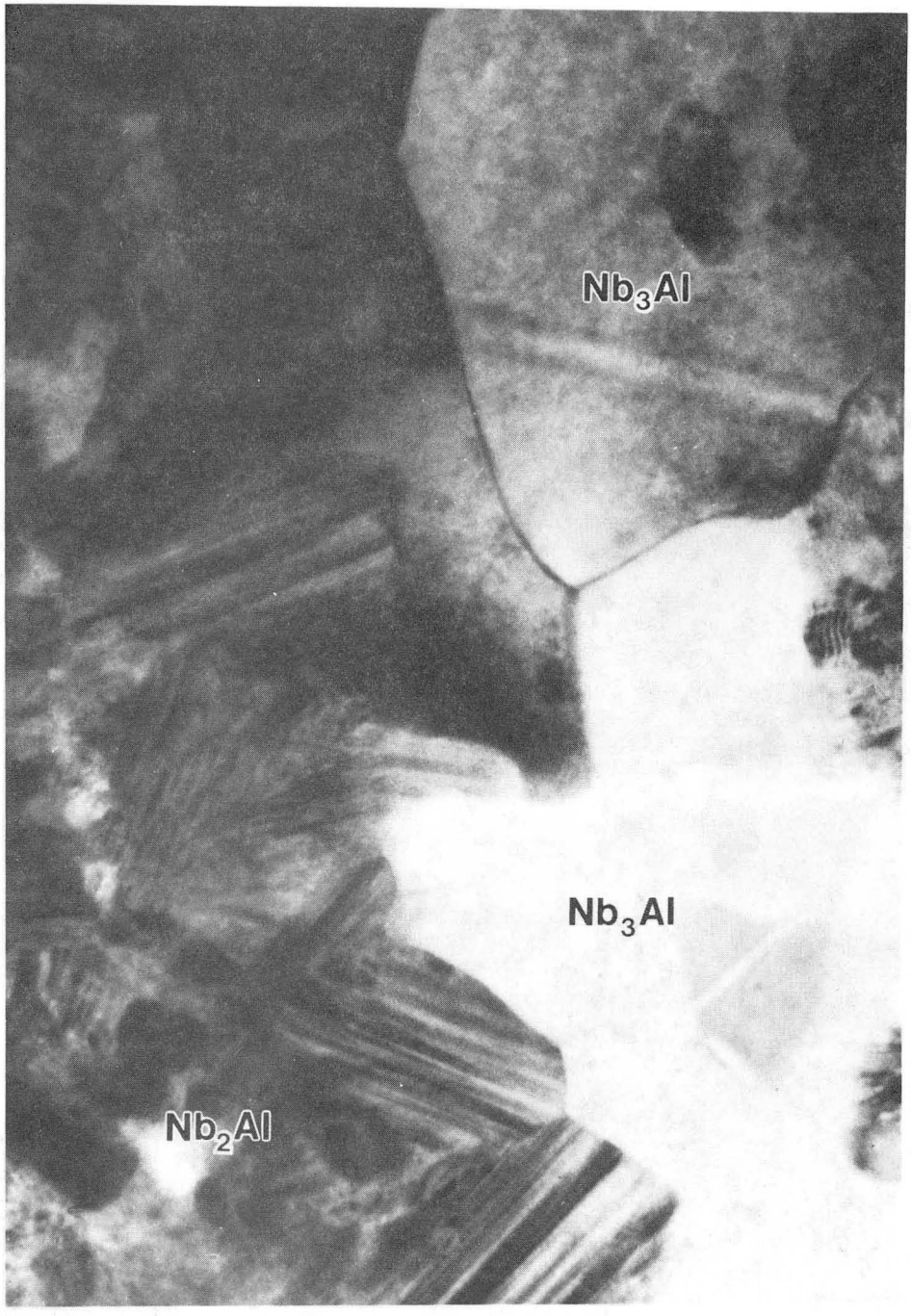

500Å

XBB 880-9430

Figure 28

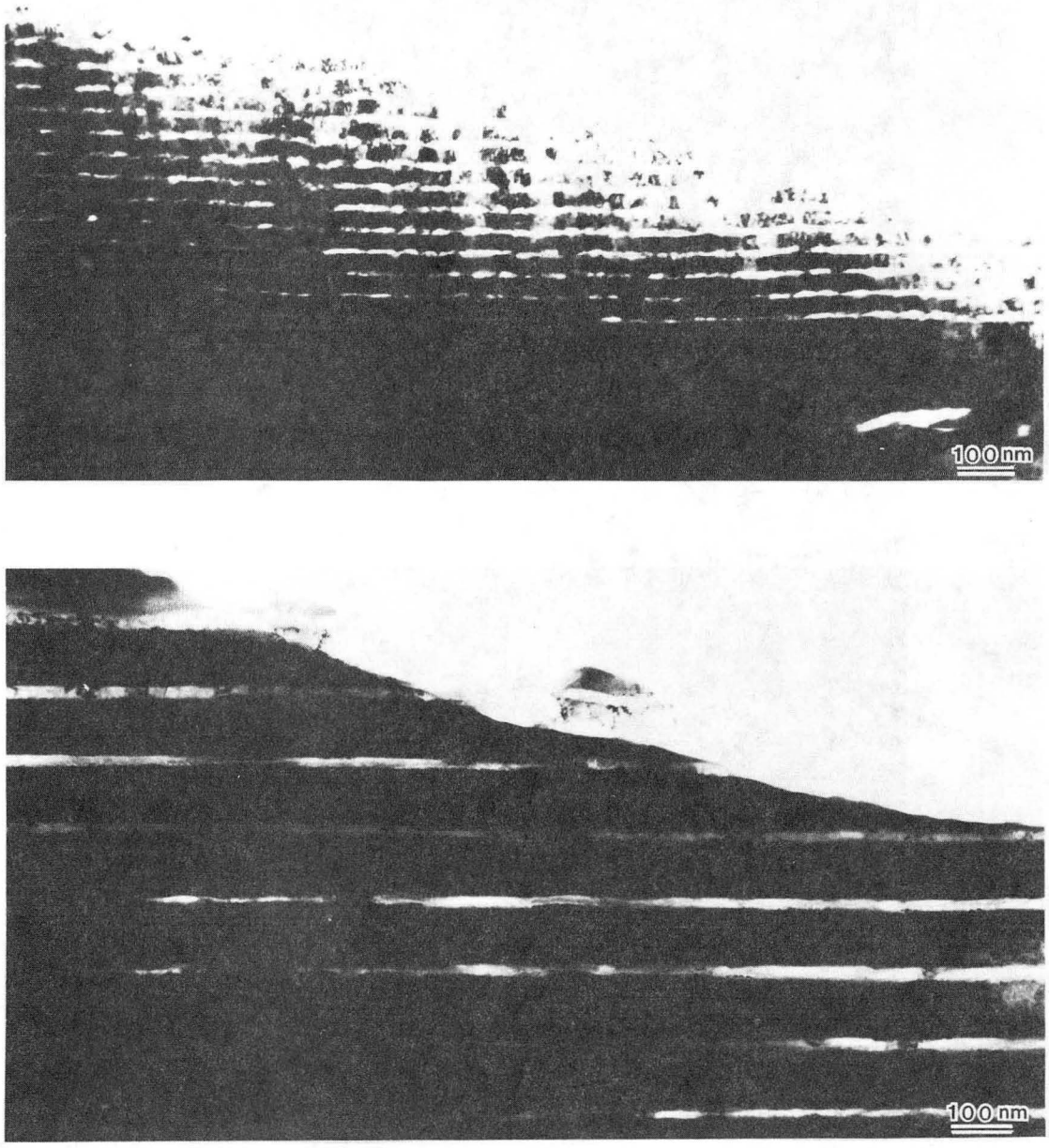

XBB 872-1281

Figure 29

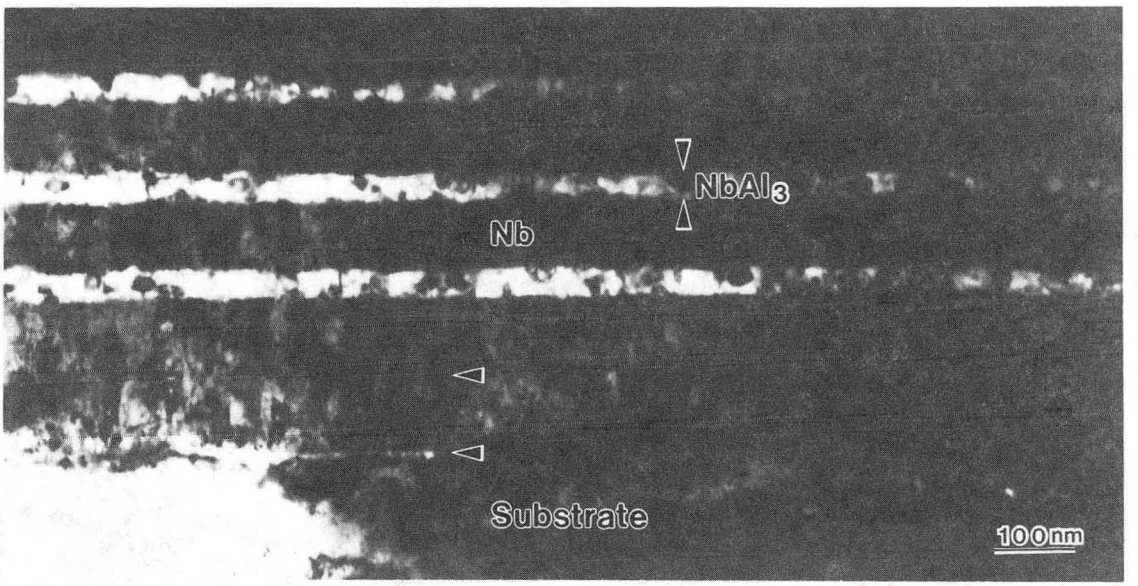

XBB 875-4176

Figure 30

XI. FIGURES

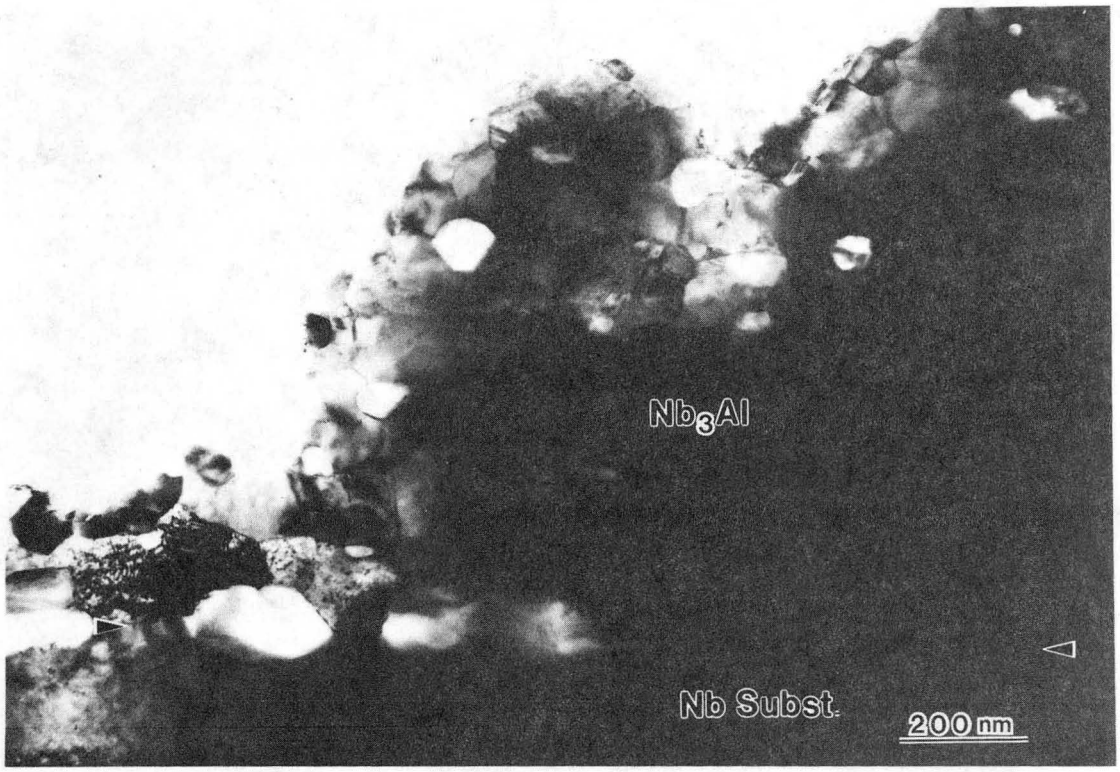

XBB 875-4177

Figure 31

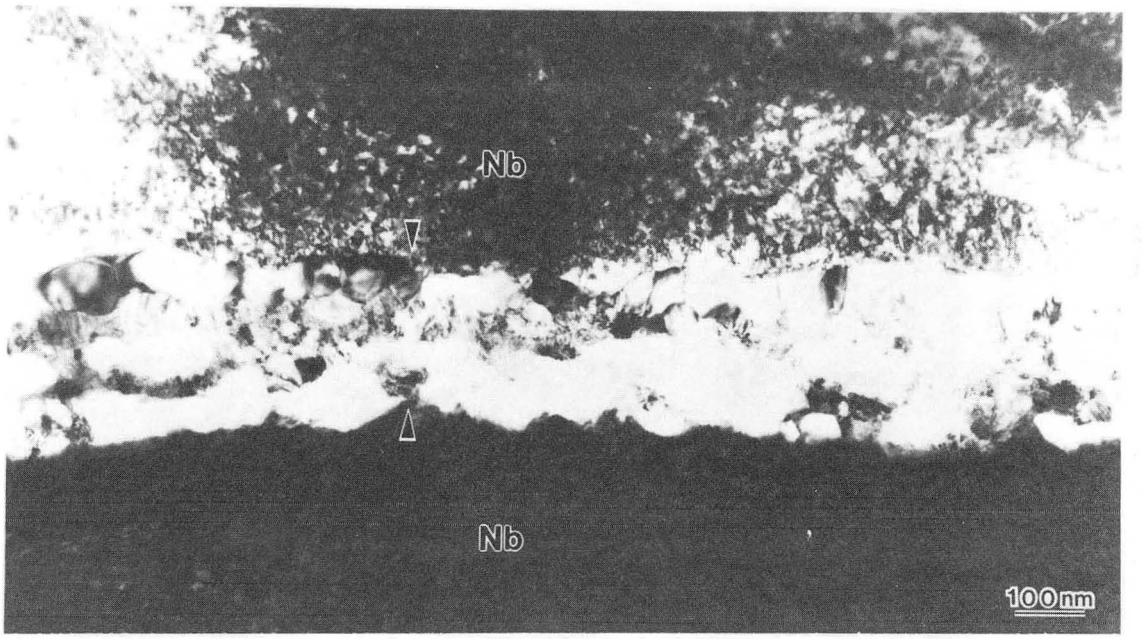

XBB 875-4178

Figure 32

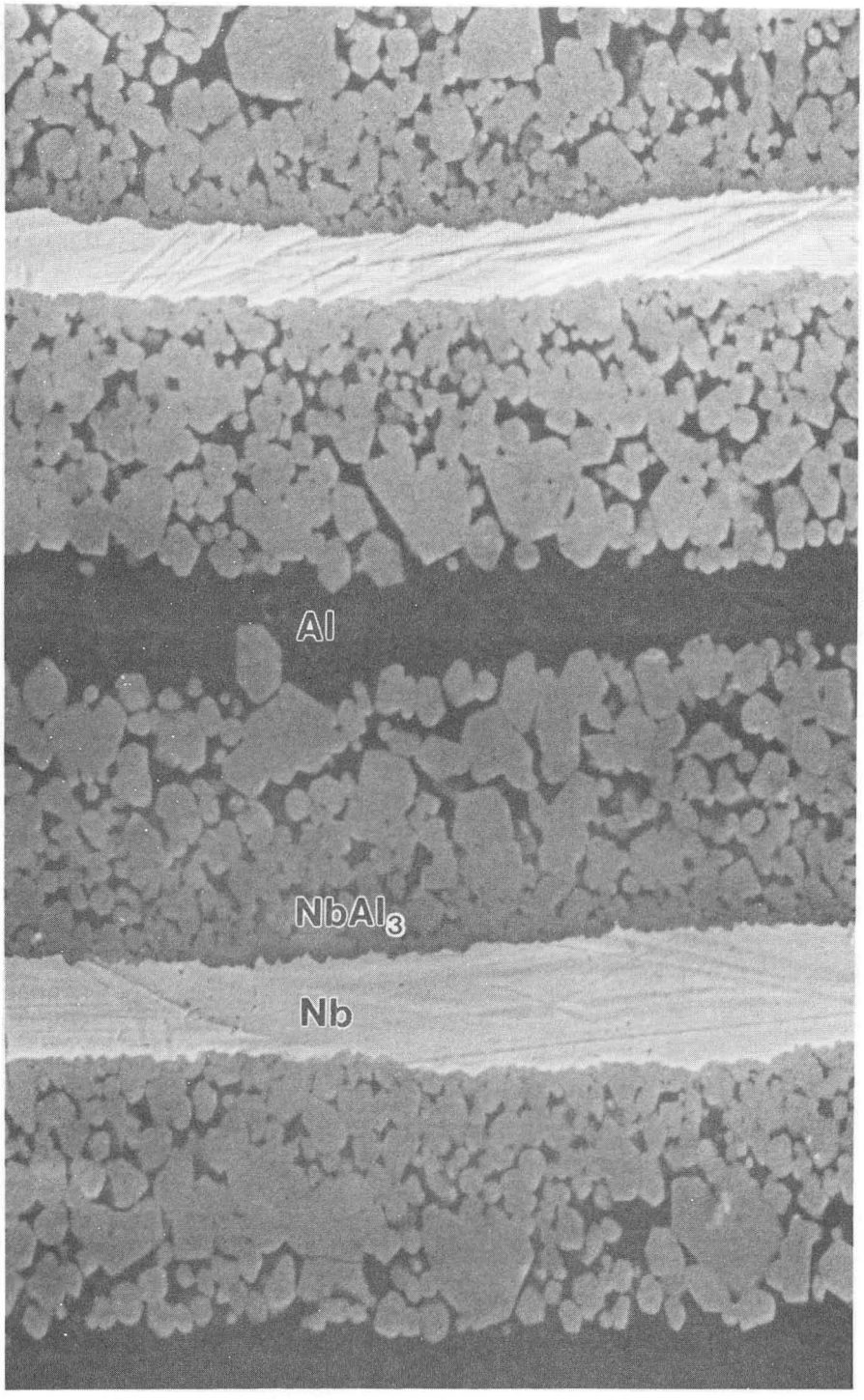

20 μm

XBB 880-9425

Figure 33

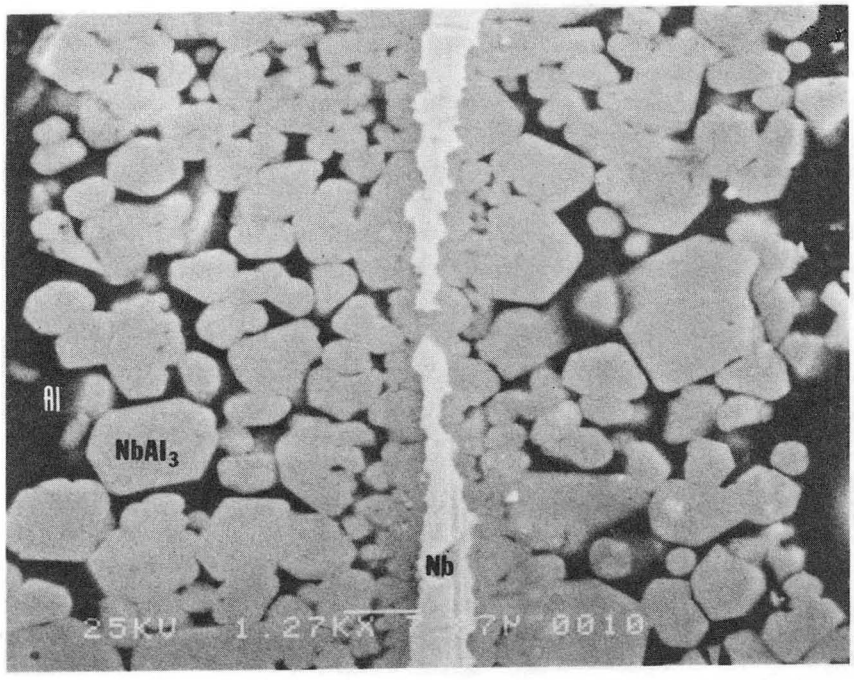

XBB 880-9422

Figure 34

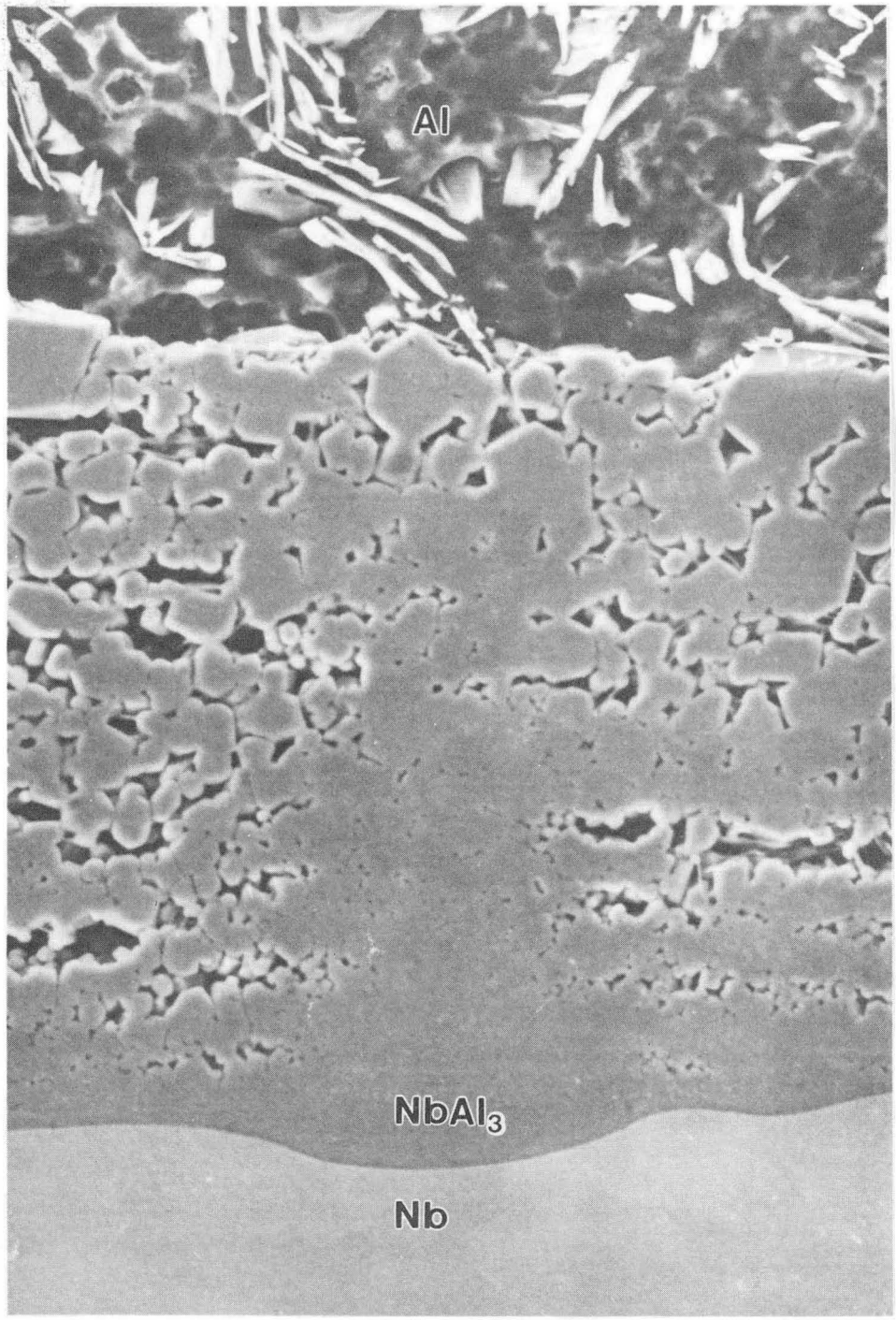

20 μm

XXB 880-9424

Figure 35

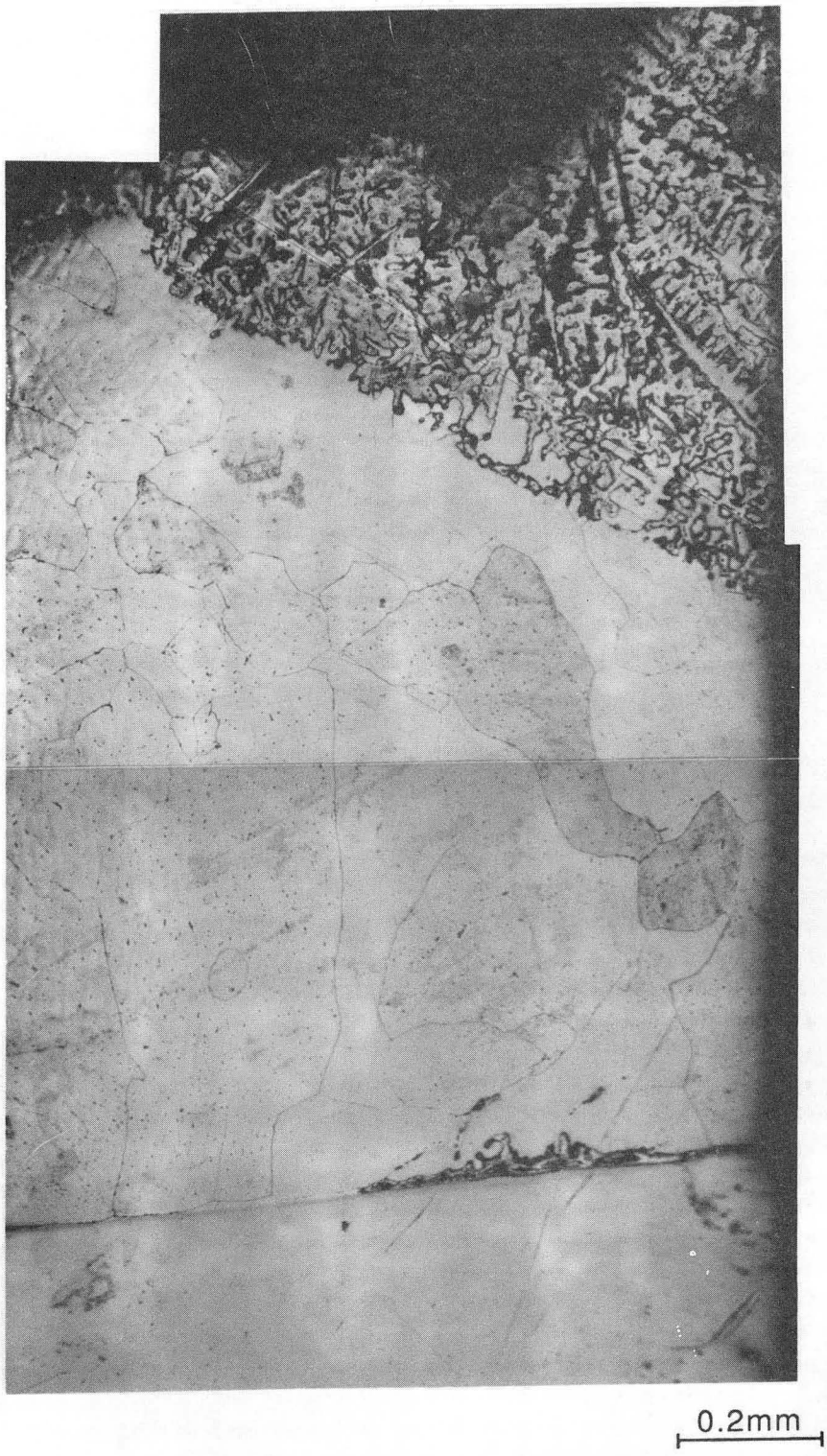

XBB 870-10262

Figure 36

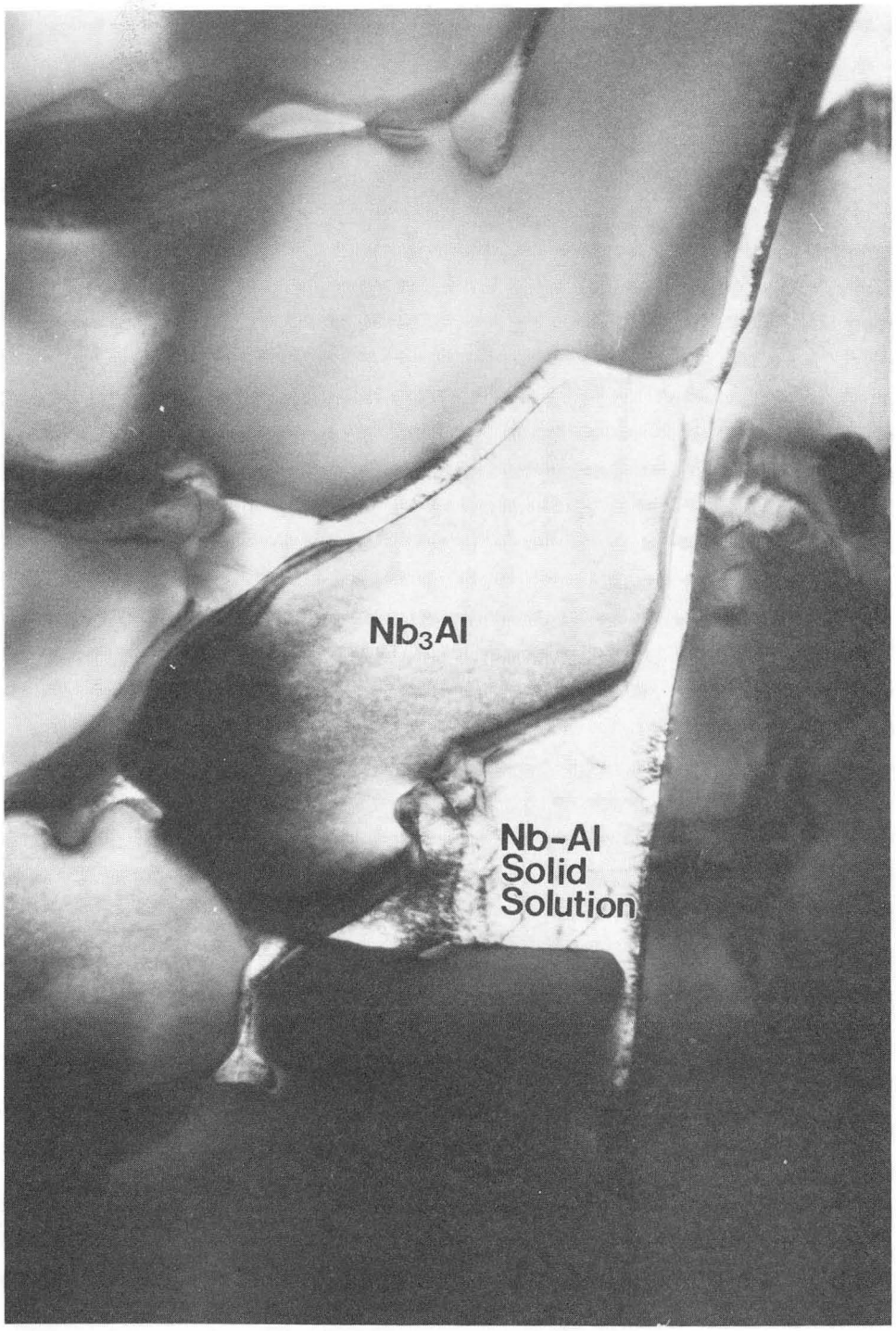

5000Å

XBB 880-9437

Figure 37

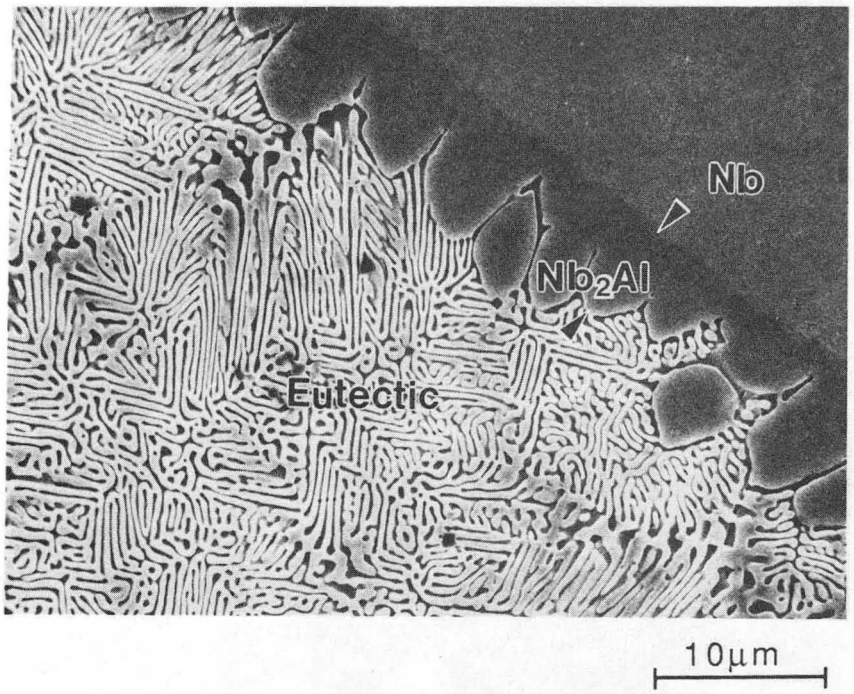

XBB 880-9423

Figure 38

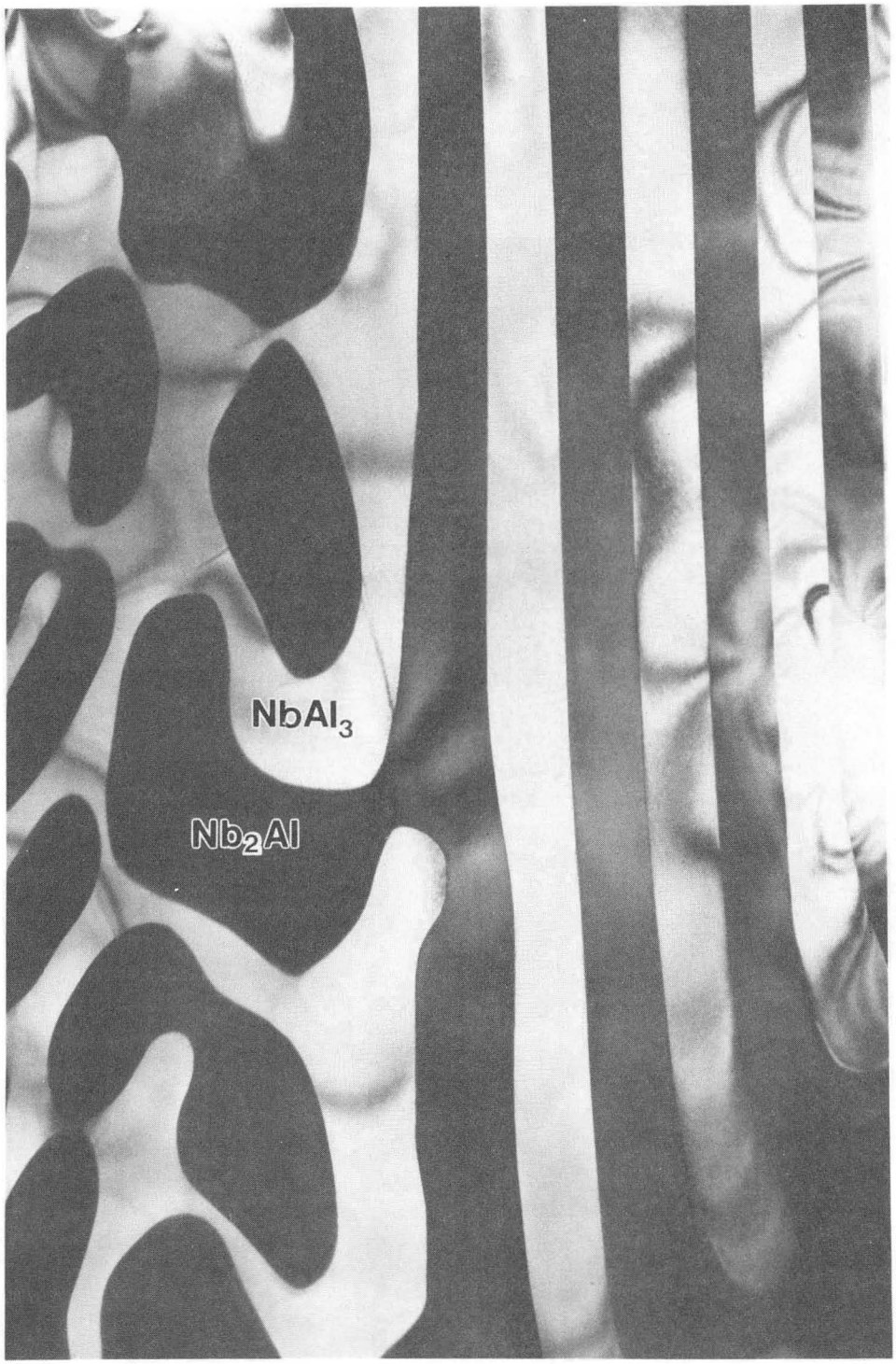

2000Å

XBB 880-9433

Figure 39

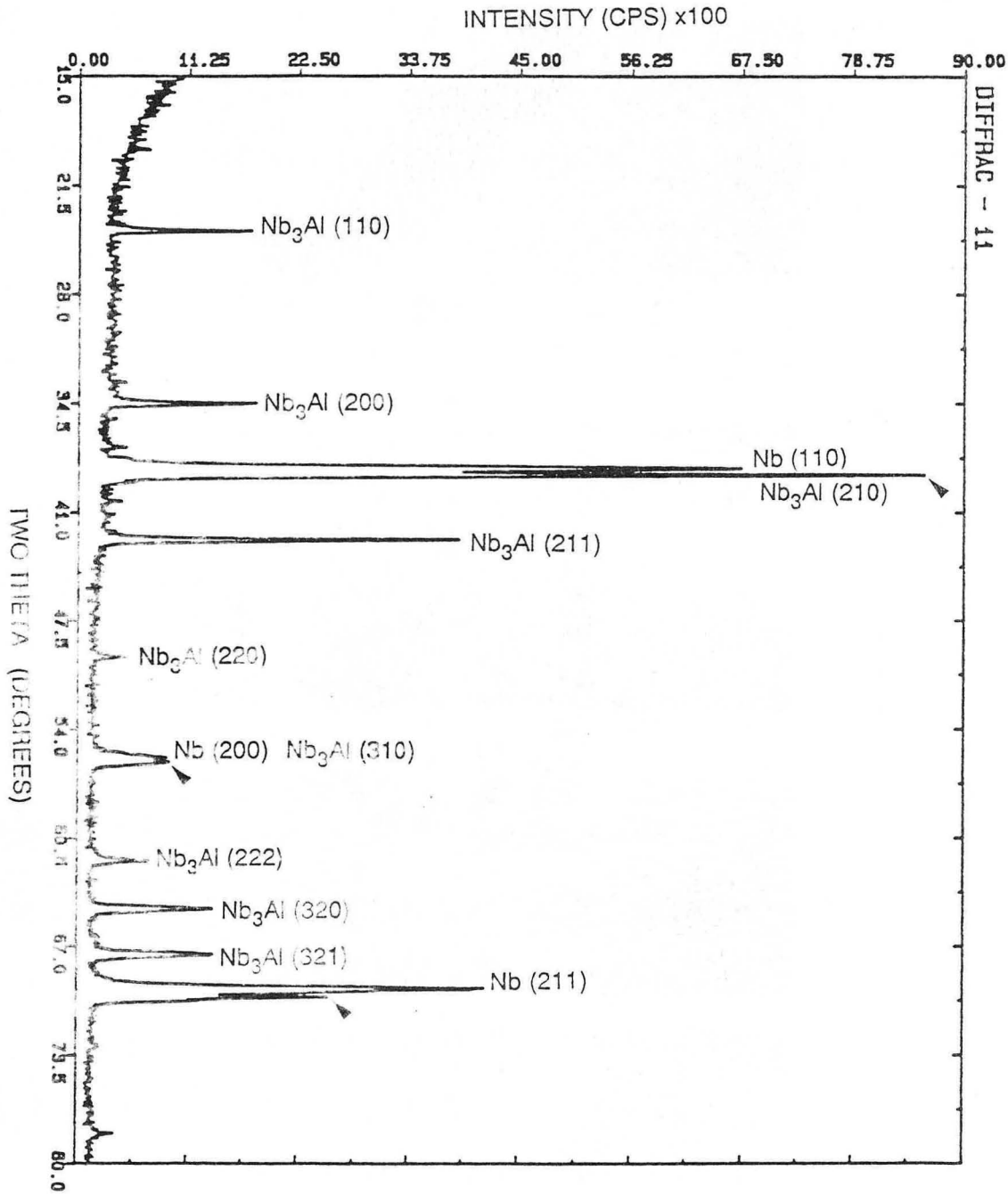
INTENSITY (CPS) x100
0.00
11.25
22.50
33.75
45.00
56.25
67.50
78.75
90.00
DIFFRAC - 11
Nb3Al (110)
Nb3Al (200)
Nb (110)
Nb3Al (210)
Nb3Al (211)
Nb3Al (220)
Nb (200) Nb3Al (310)
Nb3Al (222)
Nb3Al (320)
Nb3Al (321)
Nb (211)
TWO THETA (DEGREES)
15.0
21.5
28.0
34.5
41.0
47.5
54.0
60.5
67.0
73.5
80.0

Fig. 40

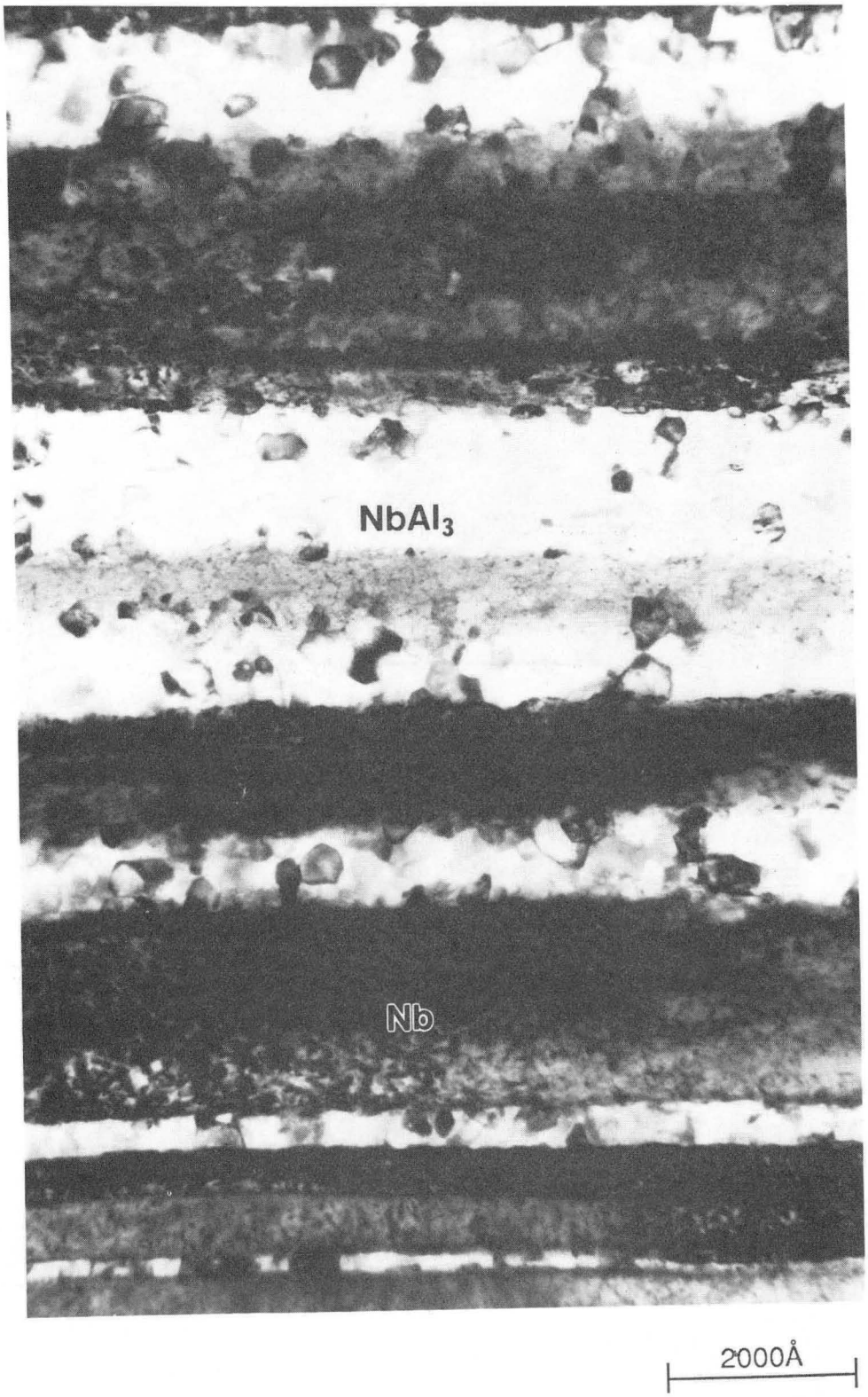

XBB 880-9429

Figure 41

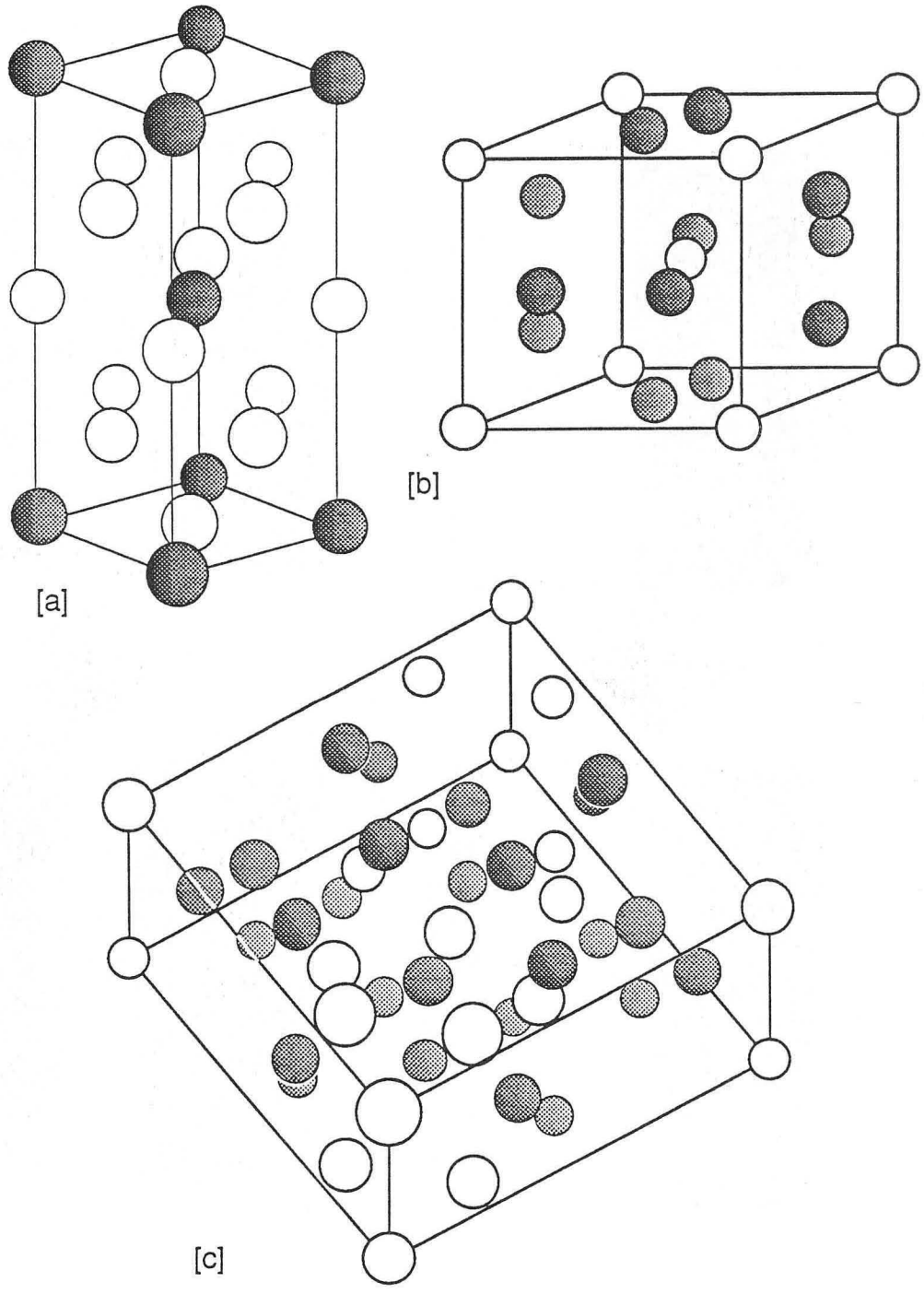

Fig. 42

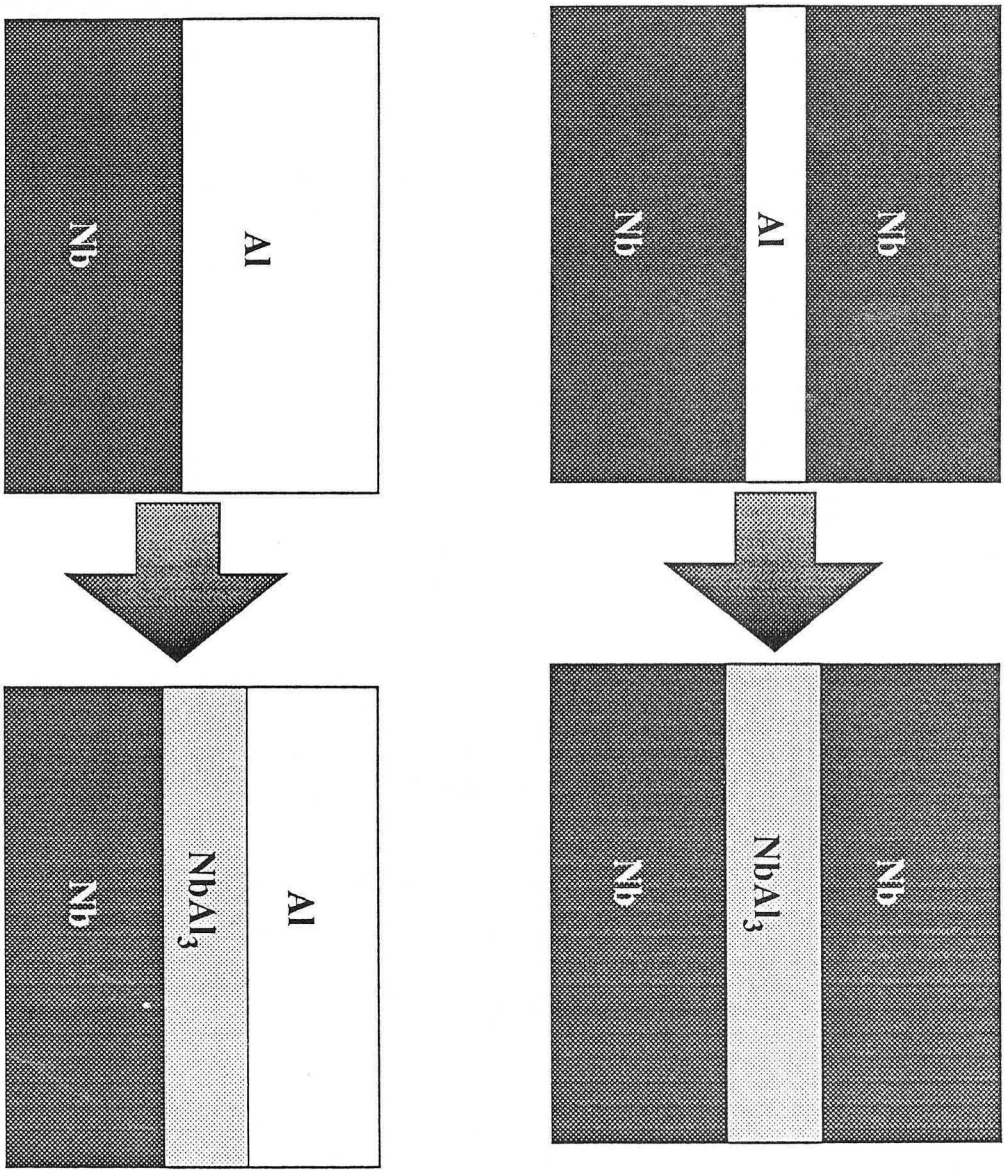

Fig. 43

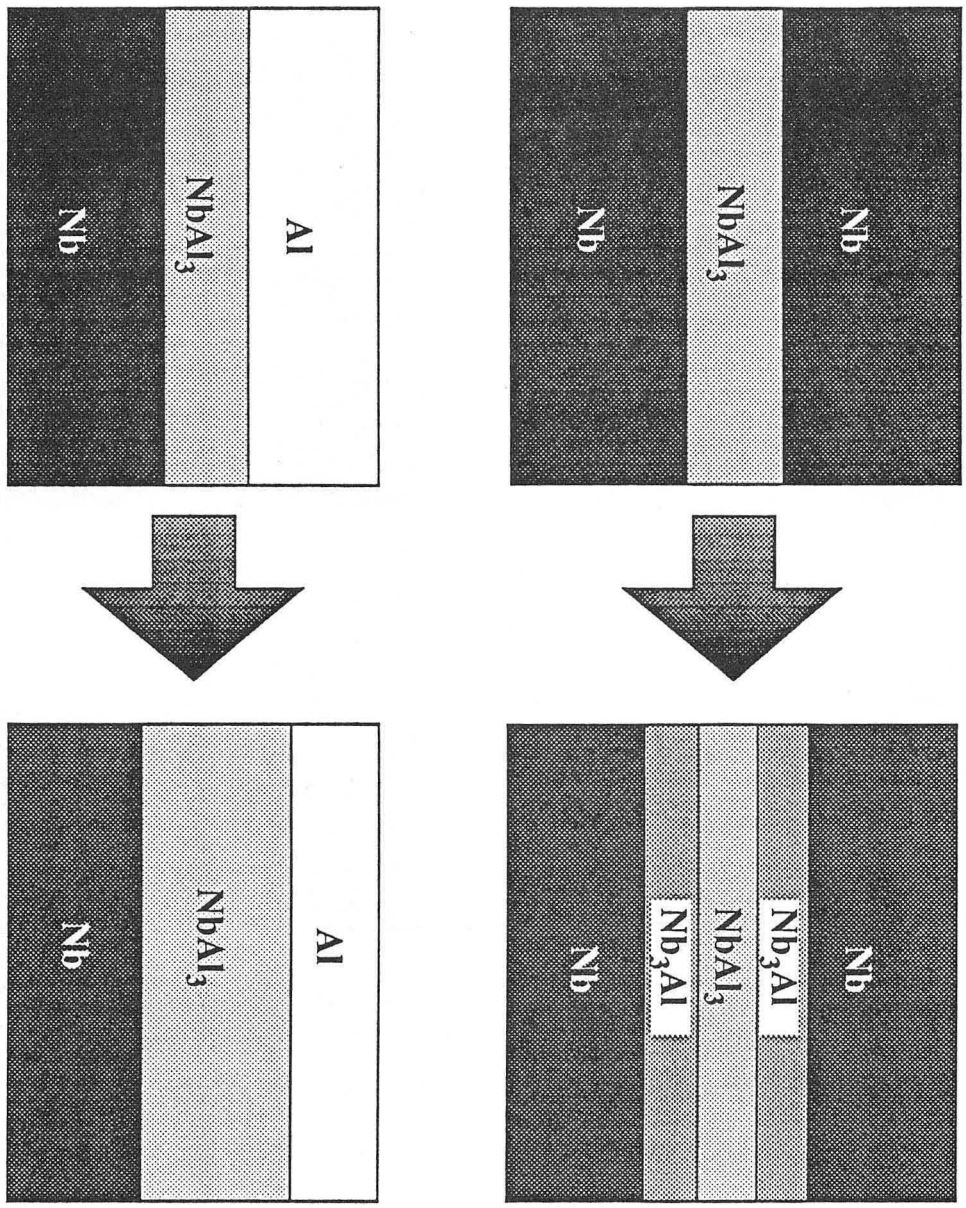

Fig. 44

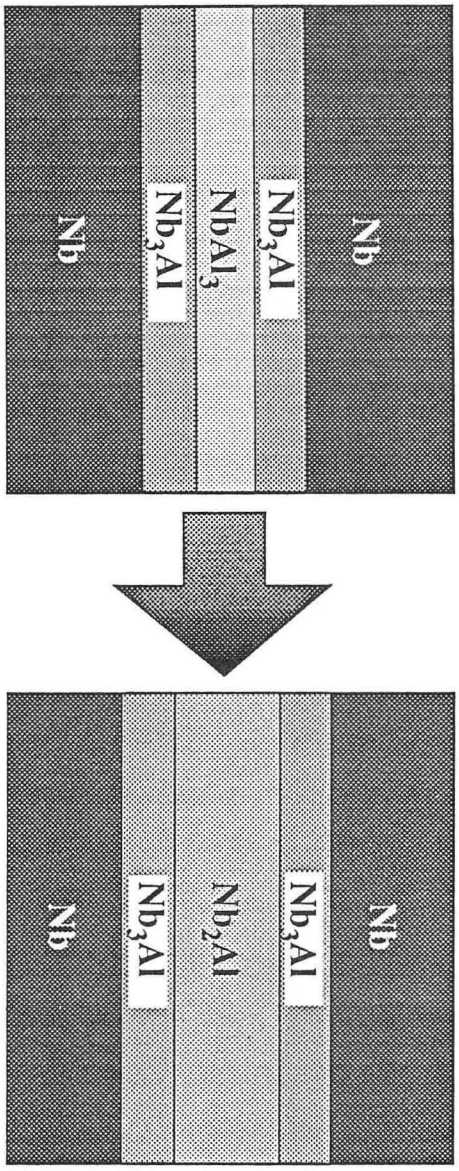

Fig. 45

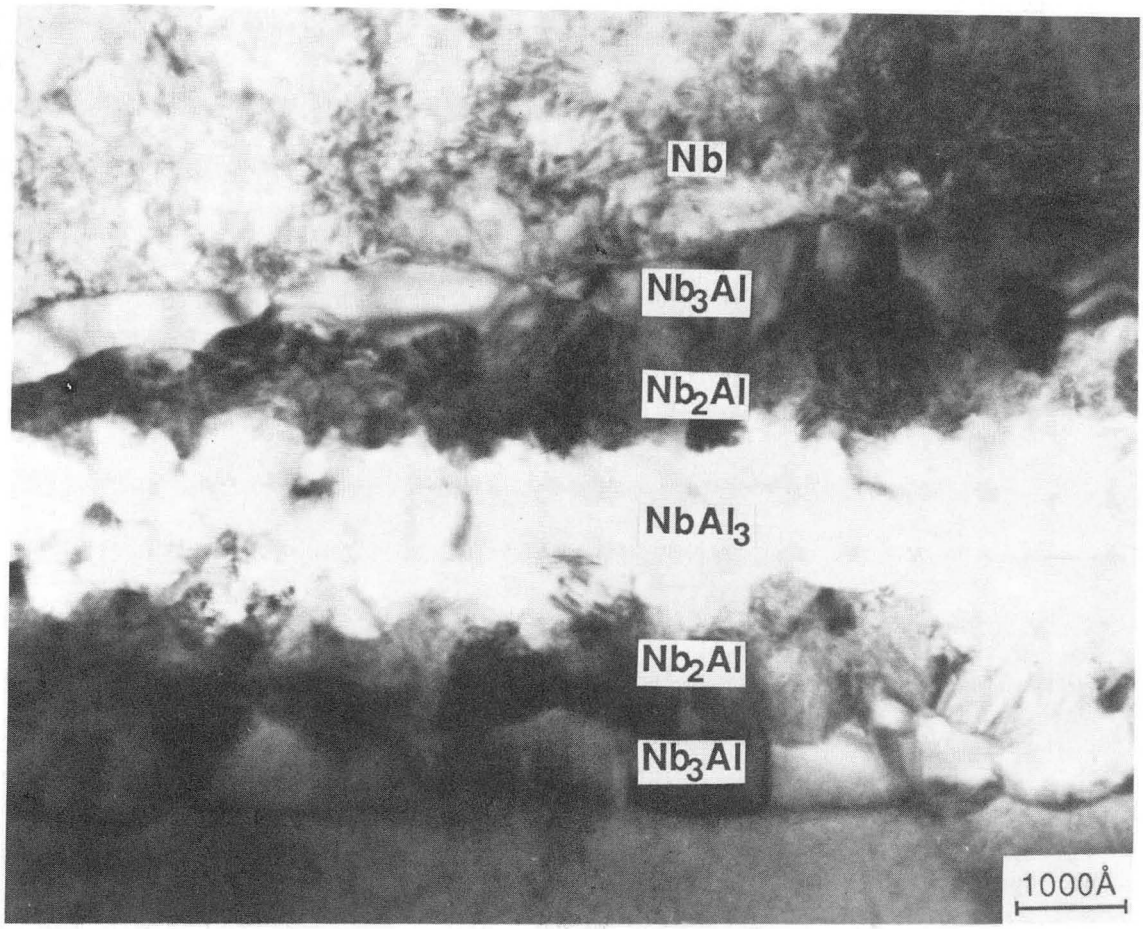

XBB 881-670

Figure 46

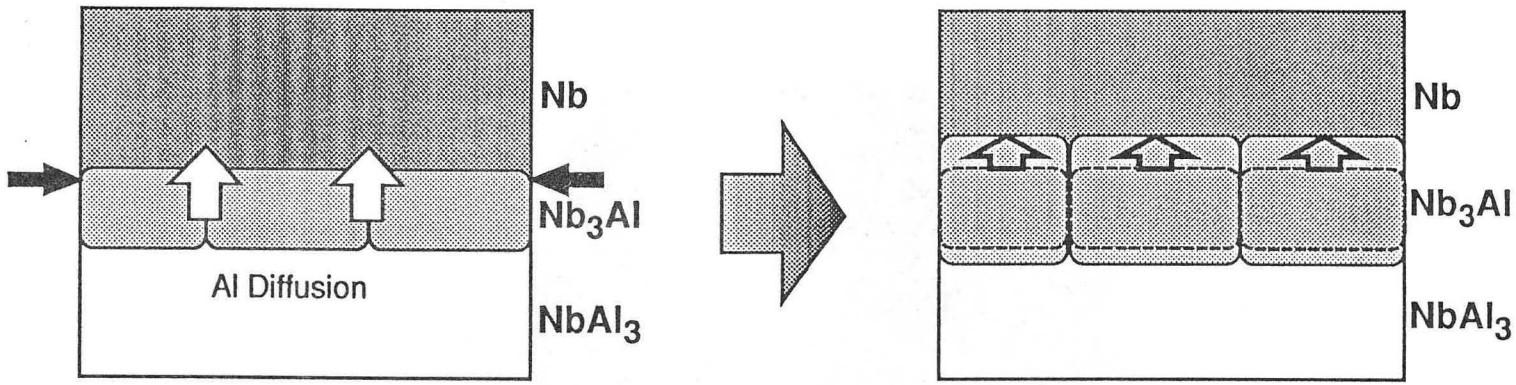

A) If Al is the primary diffuser, then further reaction will occur at the Nb/Nb_3Al interface.

Nb_3Al grain coarsening is expected.

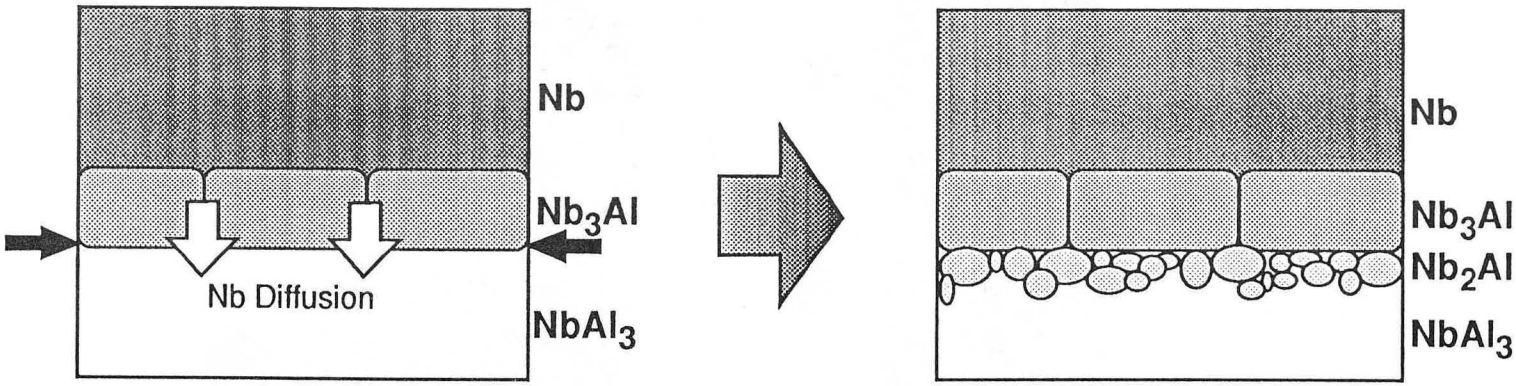

B) If Nb is the primary diffuser, then further reaction will occur at the $Nb_3Al/NbAl_3$ interface.

Nb_2Al will form at the $Nb_3Al/NbAl_3$ interface.

Fig. 47

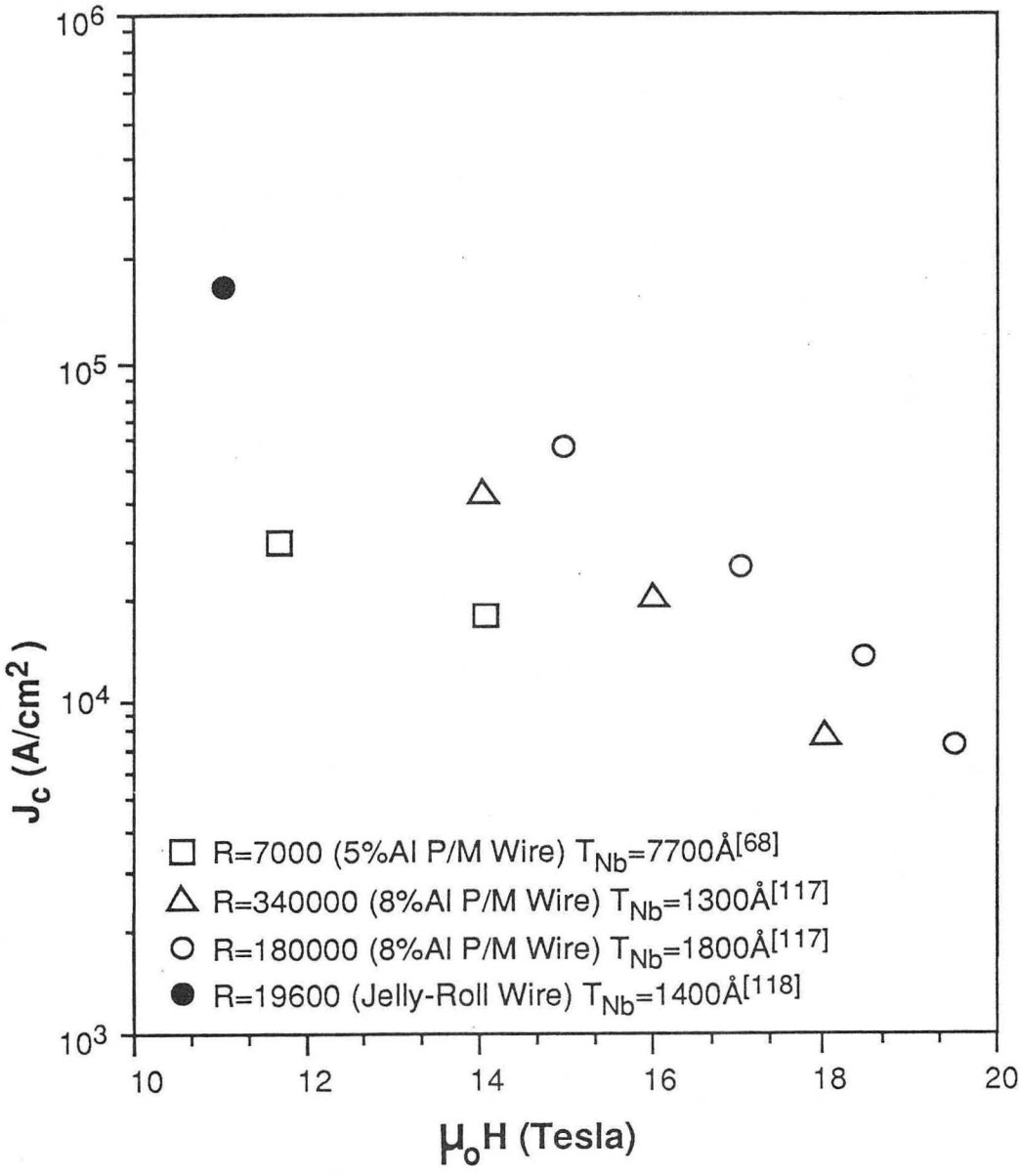
10^6
10^5
10^4
10^3
J_c (A/cm^2)
10
12
14
16
18
20
μ_oH (Tesla)
R=7000 (5%Al P/M Wire) T_{Nb}=7700Å[68]
R=340000 (8%Al P/M Wire) T_{Nb}=1300Å[117]
R=180000 (8%Al P/M Wire) T_{Nb}=1800Å[117]
R=19600 (Jelly-Roll Wire) T_{Nb}=1400Å[118]

Fig. 48

LAWRENCE BERKELEY LABORATORY
CENTER FOR ADVANCED MATERIALS
1 CYCLOTRON ROAD
BERKELEY, CALIFORNIA 94720